East Asian Summer Monsoon Simulations: Dynamical Downscaling and Seasonal Prediction

A Dissertation

Submitted in Partial Fulfilment of the Requirements

for the Degree of Doctor rerum naturalium (Dr. rer. nat.)

to the Department of Earth Sciences

of the Freie Universität Berlin

by

Bo Huang

Berlin, April 2017

Supervisor: Prof. Dr. Ulrich Cubasch
Freie Universität Berlin

Second examiner: Prof. Dr. Klaus Dethloff
Alfred Wegener Institute, Potsdam

Date of the viva voce/defense: 23.06.2017

Declaration

I hereby declare that except where specific reference is made to the work of others, the contents of this dissertation are original and have not been submitted in whole or in part for consideration for any other degree or qualification in this, or any other university. This dissertation is my own work and contains nothing which is the outcome of work done in collaboration with others, except as specified in the text and Acknowledgements. This dissertation contains fewer than 50,000 words including appendices, bibliography, footnotes, tables and equations and has fewer than 50 figures.

Bo Huang
April 2017

Abstract

The East Asian summer monsoon (EASM) is an important part of the global climate system and plays a vital role in the Asian climate. It influences the livelihood and the socio-economic status of over a billion residents who live in the EASM dominated region. Accurate predictions of the EASM can provide enormous socio-economic advantages. This study employs multi-prediction systems to investigate the seasonal predictability of EASM. Six prediction systems consisting of coupled atmosphere-ocean general circulation models (AOGCMs: BCC-CSM1-1, CanCM4, GFDL-CM2p1, HadCM3, MIROC5 and MPI-ESM-LR) were applied in initialised experiments. Applying full-field and anomaly initialisation, these six prediction systems show significant improvement in predicting the zonal winds (850 hPa) as compared to a non-initialised forecast. Two of the prediction systems (GFDL-CM2p1 and MIROC5) increase the forecast skill of the EASM index substantially in the initialisation. The variability of EASM is evaluated in the eight re-analysis datasets (*i.e.* 20CR, CFSR, ERA-20C, ERA-Interim, JRA-55, MERRA, NCEPI and NCEPII). There is no significant difference of EASM index which has been calculated by the eight re-analyses. However, the spread of the EASM index is larger in the prediction systems than in the re-analysis datasets. One possible reason is the different depiction of EASM-ENSO coupled mode in the prediction systems. Because of the coarse resolution of the prediction systems, there is a spatial scale gap between them and the input needed for applications at high resolution. This study employs regional climate models to downscale the AOGCMs output. Five regional climate models (RCMs: COSMO-CLM, HadGEM3-RA, RegCM4, SNU-MM5 and YSU-RSM) contribute to this study. They follow a world-wide regional downscaling framework in East Asia (*i.e.* CORDEX-East Asia). These five RCMs have been assessed in their ability in representing the EASM. The five models are able to capture the major characteristics of monsoon precipitation. There is significant difference between models in presenting the monsoon precipitation features (*e.g.* mean state, inter-annual variability, monsoon precipitation intensity *etc*.). In general, the set up of the five RCMs can be used for dynamical downscaling in East Asia. One particular prediction system (MPI-ESM-LR) and one RCM (COSMO-CLM) are selected for studying the further dynamical downscaling in detail. Although both the simulations capture the monsoon precipitation and its associated general circulation, the RCM shows more details. The simulating skill of EASM index by the RCM strongly depends on the prediction system' s driving data. Overall, the prediction systems combined with dynamical downscaling provide a perspective for a skilful seasonal prediction of EASM.

Zusammenfassung

Der Ostasiatische Sommermonsun (EASM) ist ein wichtiger Bestandteil des globalen Klimasystems und spielt eine wichtige Rolle im asiatischen Klima. Er beeinflusst den Lebensunterhalt und den sozioökonomischen Status über 1 Milliarde Einwohner, die in der EASM dominierten Region leben. Genaue Vorhersagen des EASM können diese Verluste entscheidend mindern. Diese Studie stellt Multi-Vorhersage-Systeme vor, um die saisonale Vorhersagbarkeit des EASM zu untersuchen. In initialisierten Experimenten wurden sechs Vorhersagesysteme angewendet, die aus gekoppelten Atmosphäre-Ozean-Zirkulationsmodellen bestehen (AOGCMs: BCC-CSM1-1, CanCM4, GFDL-CM2p1, HadCM3, MIROC5 und MPI-ESM-LR). Bei der Anwendung der Absolut -und Anomalie-Initialisierung zeigen die sechs Vorhersagesysteme eine signifikante Verbesserung bei der Vorhersage der Zonalwinde (850 hPa) im Vergleich zur nicht-initialisierten Vorhersage. Zwei der Vorhersagesysteme (GFDL-CM2p1 und MIROC5) verbessern durch eine Initialisierung die Prognose des EASM-Indexes. Die Variabilität des EASM in verschiedenen Analysen wird in acht Reanalyse-Datensätzen (20CR, CFSR, ERA-20C, ERA-Interim, JRA-55, MERRA, NCEPI und NCEPII) betrachtet. Die verschiedenen Reanalysen weisen keinen signifikanten Unterschied bei der Reparäsentation des EASM-Index auf. Die Variationsbreite des EASM ist mit den Vorhersagesystemen größer als bei den Reanalysen. Ein möglicher Grund ist die unterschiedliche Simulation der EASM-ENSO-Kopplung in den Vorhersagesysteme. Bedingt durch die grobe Auflösung der verwendeten Modelle gibt es eine räumliche Skalenlücke zwischen den Vorhersagesystemen und den für Klimafolge-Modelle bentigen Antriebsdaten. In dieser Studie werden regionale Klimamodelle verwendet, um ein dynamisches Downscaling mit den AOGCM-Ergebnissen durchzuführen. Fünf regionale Klimamodelle (COSMO-CLM, HadGEM3-RA, RegCM4, SNU-MM5 und YSU-RSM) werden dabei ausgewertet. Die RCMs, die alle innerhalb eines internationalen Verbunds (CORDEX-Ostasien) zum regionalen Downscaling in Ostasien beitragen, wurden bezüglich ihrer Simulationsgüte des EASMs bewertet. Die fünf CORDEX-Modelle sind in der Lage, die Hauptmerkmale des Monsun-Niederschlags zu erfassen. Im Allgemeinen können diese regionalen Klimamodelle für das dynamische Downscaling in Ostasien genutzt werden. Es gibt allerdings signifikante Unterschiede zwischen den Modellen bei der Simulation des Niederschlags (mittlerer Zustand, mehrjährige Variabilität, Monsun-Niederschlagsintensität). Ein spezielles Vorhersagesystem (MPI-ESM-LR) und ein RCM (COSMO-CLM) wurden ausgewählt, um das dynamische Downscaling weiter im Detail zu untersuchen. Beide Simulationen erfassen den Monsun-Niederschlag und die damit verbundene allgemeine Zirkulation, das RCM zeigt jedoch mehr Details. Die Simulationsfähigkeit des EASM-Index durch das RCM hängt stark von den Antriebsdaten der Vorhersagesystem ab. Insgesamt bieten die Vorhersagesysteme gekoppelt mit dynamischem Downscaling eine Perspektive für eine realistische saisonale Vorhersage des EASM.

Table of contents

List of figures

List of tables

Chapter 1

Introduction

Monsoon has long been the focus of scientific investigations. Sir Edmund Halley (1686) first proposed that the monsoon is caused by the differential heating of the land and oceans. Subsequently, his hypothesis was modified by Hadley (1735) to include the effect of earth's rotation that deflects the winds from cold oceans to warmer land. In the 20th century, climatologists discovered that the monsoon is associated with a seasonal reversal of surface wind field (Hann, 1908; Khromov, 1957). Ramage (1971) summarised the definition of monsoon as 1) the prevailing wind direction shifts at least 120 degrees between January and July; 2) average frequencies of the prevailing wind direction in January and July is $>$40 per cent. In general, monsoons are driven by the annual cycle of solar heating and the land-sea surface temperature contrast, leading to seasonal reversal of surface winds as well as contrasting wet summers and dry winters, accompanied by a global-scale atmospheric overturning circulation (Trenberth *et al.*, 2000; Wang and Ding, 2008).

There are eight sub-monsoon systems in the world (Wang *et al.*, 2012; Fig. 1.1). The East Asian summer monsoon (EASM) plays an important role in the global monsoon system. It affects approximately one-third of the global population, influencing the climate of Japan (including Okinawa), Korea, Taiwan, Hong Kong, Macau, the Philippines, Indochina, and much of mainland China (Ding and Chan, 2005). The EASM is an essential component of the Asian climate system (Chen and Chang, 1980; Ding, 1992; Lau *et al.*, 1988; Tao and Chen, 1987), and interacts with other components of the Asian monsoon system (*i.e.* the South Asian summer monsoon and the Australian monsoon). However, the EASM cannot be regarded as a simple eastward extension of the South Asian summer monsoon as it has its own general circulation patterns and independent climate behaviour (Ding and Chan, 2005; Ding, 1994; Tao and Chen, 1987; Fig. 1.2). It is composed of Australian High, cross-equatorial jet, south-west monsoon, monsoon trough (Inter Tropical Convergence Zone−ITCZ), trade winds, western Pacific subtropical high, Meiyu/Baiu/Changma and mid-

latitudinal turbulence (Tao and Chen, 1987). The EASM exhibits strong internal variability (Chang *et al.*, 2000*a*,*b*; Ding and Chan, 2005; Jiang *et al.*, 2008; Ju *et al.*, 2005; Lau *et al.*, 1988; Wang *et al.*, 2001; Zhang *et al.*, 2003) and is closely associated with the internal forcing, *i.e.* El Niño−Southern Oscillation (ENSO; Chang *et al.*, 2000*a*; Ding and Chan, 2005; Wang *et al.*, 2000), North Atlantic Oscillation (NAO; Wu *et al.*, 2009) and Indian Ocean dipole (IOD; Ding *et al.*, 2009; Guan and Yamagata, 2003). Therefore, accurate simulation and prediction of the EASM is a long-standing challenge for climate scientists (Lee *et al.*, 2013*b*, 2008*a*,*b*; Wang *et al.*, 2007, 2009; Wu *et al.*, 2009).

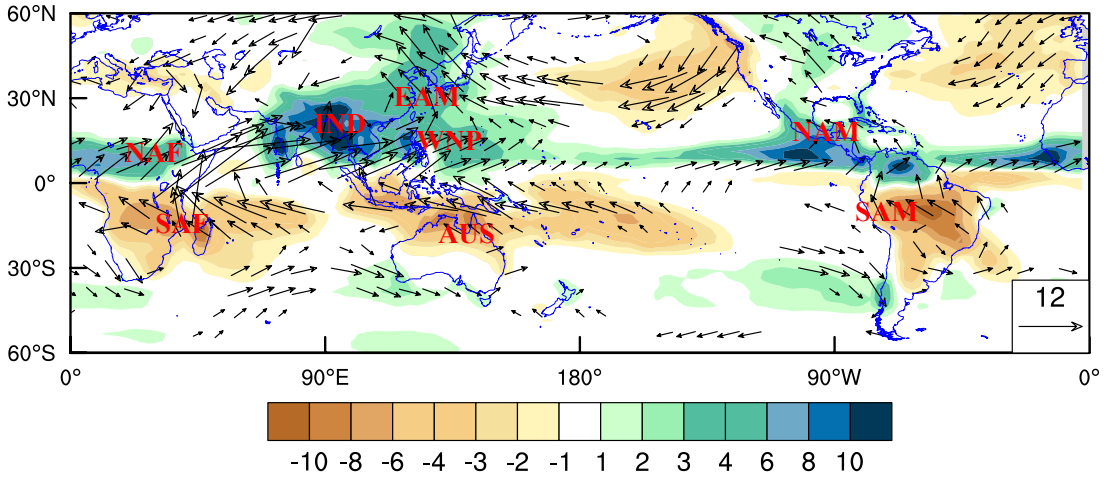

Figure 1.1 Global monsoon system and its local components, illustrated by the differences between mean 850 hPa winds and mean precipitation between the June-July-August and December-January-February months, modified from Wang *et al.* (2008*a*). The regional monsoon systems are the North African monsoon (NAF), the South African monsoon (SAF), the Indian/South Asian monsoon (IND), the East Asian monsoon (EAS), the Western North Pacific monsoon (WNP), the Australian monsoon (AUS), the North American monsoon (NAM), and the South American monsoon (SAM).

There are two approaches to predict the EASM: statistical prediction and dynamical prediction. The statistical method seeks the relationship between the EASM and a strong climate signal (*e.g.* ENSO, NAO; Wang *et al.*, 2015; Wu *et al.*, 2009; Yim *et al.*, 2014). This method is, however, limited by the strength of the climate signal. The other method is dynamical prediction which employs climate model to predict the EASM (Kang and Shukla, 2006; Kim *et al.*, 2012; Lee *et al.*, 2010; Sperber *et al.*, 2001; Wang *et al.*, 2009; Yang *et al.*, 2008). Two kinds of climate models have been developed in the past few decades, the atmosphere general circulation model (AGCM) and the coupled atmosphere-ocean general circulation model (AOGCM). Both the models have been used to predict the EASM (Kang *et al.*, 2004; Wang *et al.*, 2005, 2007, 2009; Zhou *et al.*, 2009). For AGCMs, the lower

boundary conditions (*i.e.* SST: sea surface temperature) are required. An additional ocean model is applied to predict the SST. Subsequently, the prescribed SST is employed as the lower boundary condition to force the AGCMs. This predictive method is a "tier 2" method. It has been developed as an application tool to predict climate. For example, the International Research Institute for Climate and Society (IRI) employs 4 AGCMs (ECHAM4.5, CCM3.6, COLA and GFDL-AM2p1) to predict global climate at seasonal time-scale (Barnston *et al.*, 2010). However, this method shows low prediction success over East Asia, especially in the monsoon season (Barnston *et al.*, 2010; Wang *et al.*, 2005) because the AGCMs fail to produce realistic SST-rainfall relationships in the monsoon season (Wang *et al.*, 2005). Therefore, the monsoon community endeavours to predict the EASM with AOGCMs (Jiang *et al.*, 2013*b*; Kim *et al.*, 2012; Wang *et al.*, 2009; Zhou *et al.*, 2009).

AOGCMs have proved to be the most valuable tools in predicting the EASM (Jiang *et al.*, 2013*b*; Kim *et al.*, 2012; Wang *et al.*, 2009; Zhou *et al.*, 2009). Though the horizontal resolution of most present-day AOGCMs is still coarse (Meehl *et al.*, 2007), there has been significant progress in these models in the past two decades due to an improved representation of earth sub-systems (*e.g.* atmospheric and earth surface processes, *etc.*) and enhanced computational capabilities. The coarse resolution prevents them from capturing the regional effects and limits their application in the monsoon regions (Fu *et al.*, 2005; Huang *et al.*, 2015*b*). A fundamental spatial scale gap still exists between the climate information provided by AOGCMs and the input needed for impact assessment work (Giorgi *et al.*, 2009). Dynamical downscaling (or regional climate downscaling) is an important method to address the spatial scale gap problem (Giorgi *et al.*, 2001; Giorgi and Mearns, 1991). It uses regional climate models (RCMs) to downscale the AOGCMs. The RCMs could capture local-scale climate information (Giorgi and Gutowski, 2015; Laprise, 2008; Rummukainen, 2010) and show potential to add value to the AOGCMs (Feser *et al.*, 2011; Flato *et al.*, 2013; Rummukainen, 2016). This also has been found to be true in the EASM region (Gao *et al.*, 2011; Lee *et al.*, 2014; Oh *et al.*, 2014; Wang *et al.*, 2013*b*).

The RCM success in reproducing regional climate is strongly dependent upon the physical parametrisation (Hong and Kanamitsu, 2014; Lee *et al.*, 2013*a*, 2014), the boundary conditions (Laprise, 2008; Rummukainen, 2010; Staniforth, 1997), its domain size (Leduc and Laprise, 2009), and its horizontal resolutions (Gao *et al.*, 2006), especially in steeply orographic regions, in order to capture sub-grid scale processes (Hong and Kanamitsu, 2014; Nikulin *et al.*, 2012). Following a common framework can reduce the model's uncertainty and is also an advantage in inter-comparison of model performances (Gates, 1992). For regional climate modelling, Giorgi *et al.* (2009) set up a common framework with the aim of obtaining comprehensive RCM data to study regional climate change, *i.e.* the Coordinated Regional

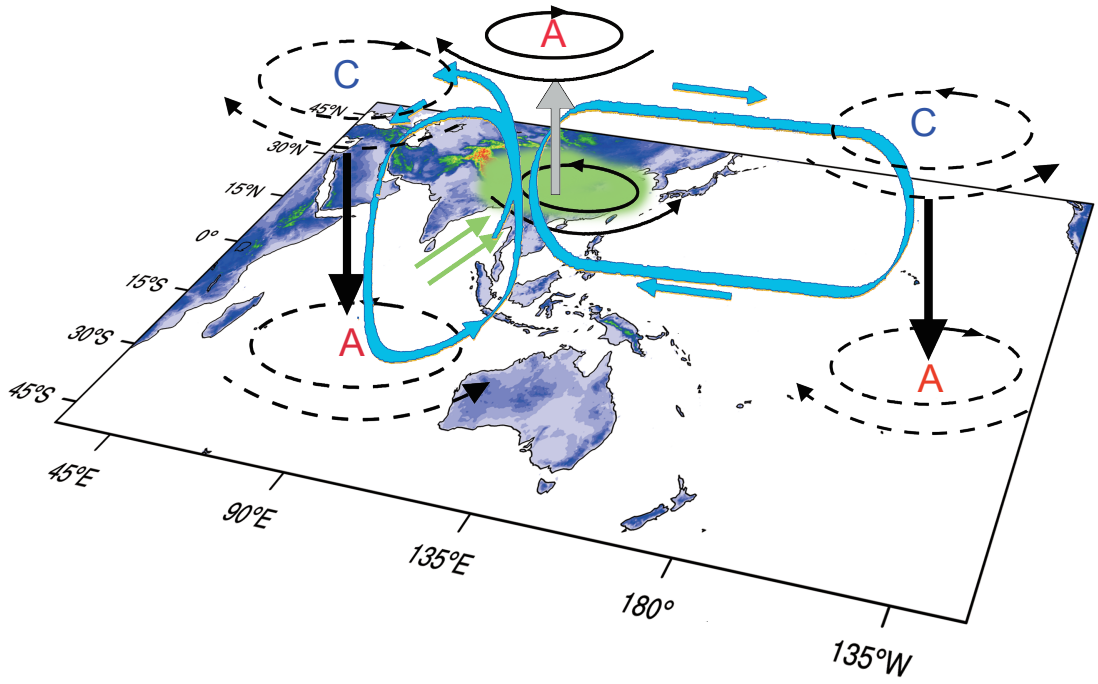

Figure 1.2 The dominant summer general circulations for East Asian summer monsoon, modified from Chang (2004).

Climate Downscaling Experiment (CORDEX). This study will follow the guidelines of CORDEX to set up the regional modelling experiment and evaluate the model performance in capturing monsoon characteristics.

The RCMs have ability to present high resolution climate information. But they cannot be directly used to predict the climate for which the boundary condition is required. Given observed initial condition, the AOGCMs can predict the climate on seasonal-to-yearly time-scale (Goddard *et al.*, 2001; Shukla *et al.*, 2000). Therefore, employing the initialised AOGCMs output to drive the RCMs can predict the climate at high resolution. The initial conditions are the dominating factor in predicting the climate at seasonal time-scale (Kirtman *et al.*, 2013; Meehl *et al.*, 2009). Different initialisation strategies lead to different prediction skills. Inter-comparison between different initialisation strategies in various models can test the predictability of EASM, and also help in understanding the mechanism of seasonal prediction for EASM.

The main objective of this study is seasonal prediction the EASM at high resolution. Multi-datasets and various statistical methods have been used to address this objective. It has been discussed in four separate chapters (Chapter 2 to 5). Figure 1.3 shows the framework of downscaling and prediction for EASM.

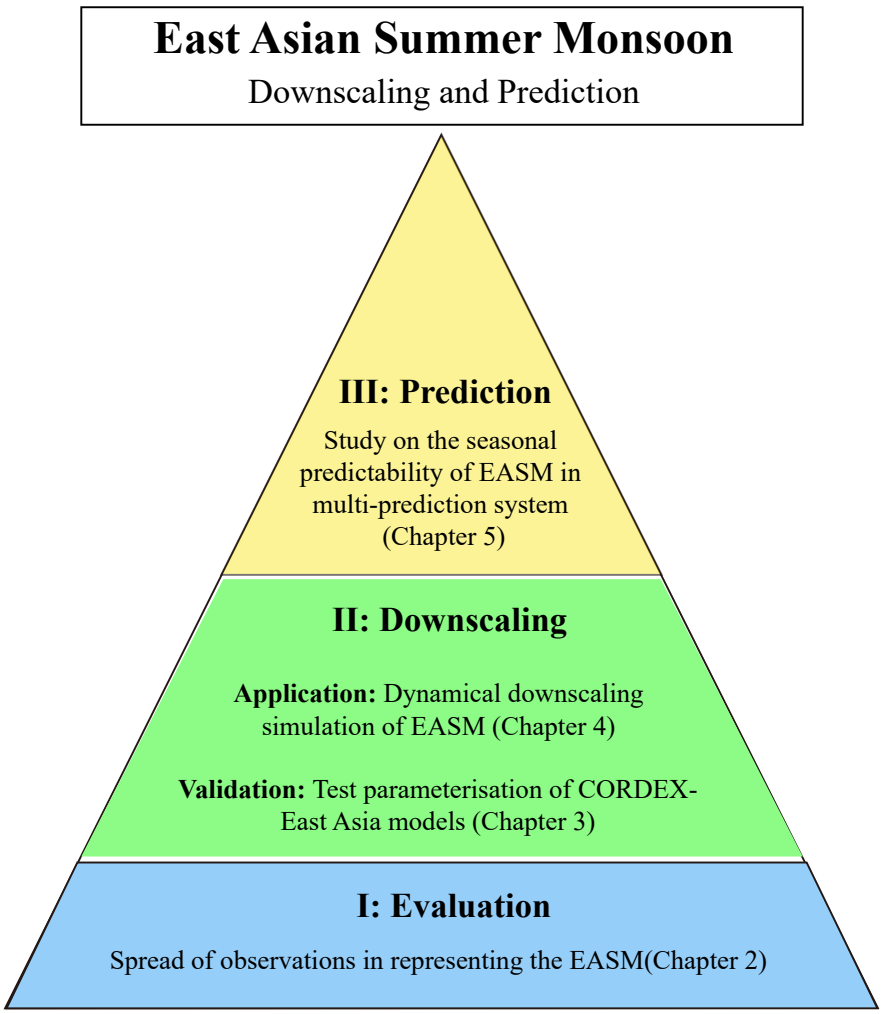

Figure 1.3 The structure of dynamical downscaling and seasonal prediction project for East Asian summer monsoon.

Chapter 2 analyses the spread in the representation of the EASM in different re-analysis datasets. Re-analysis datasets have been widely used in climate science. They have been applied as reference data to evaluate the model output (Flato *et al.*, 2013), drive RCM (Giorgi *et al.*, 2009), and provide initial condition for climate prediction (Meehl *et al.*, 2014). Since 1990s, four generations of re-analysis have been developed by different organisations. The re-analyses employ different observations and data assimilation methods. Previous studies show that significant differences have been found between re-analyses in representing precipitation (Bosilovich *et al.*, 2008; Lin *et al.*, 2014; Newman *et al.*, 2000), wind diurnal cycle (Chen *et al.*, 2014) and temperature (Wang and Zeng, 2012). However, there is no work dedicated to assessing the EASM characteristics in re-analysis datasets. It is important to describe the

differences between re-analyses, as they are used as the reference data for RCM's output, especially for investigating the monsoon system in East Asia. Therefore, evaluation of the re-analyses in capturing the EASM addresses the question:

(I) How large is the spread of the re-analysis datasets in representing the EASM?

This chapter has been submitted to an international journal (Huang and Cubasch, 2017, *Advance in Meteorology*, under review)

Chapter 3 addresses the regional dynamical downscaling in the EASM region. Several papers have been published on the topic of regional climate downscaling in East Asia (Gao *et al.*, 2011, 2008, 2012; Hong *et al.*, 2013; Lee *et al.*, 2014; Liu *et al.*, 1994; Oh *et al.*, 2014; and many others). The studies are based upon a single RCM and have different resolution and research domain. For example, Gao *et al.* (2011) employed the Abdus Salam International Centre for Theoretical Physics (ICTP) Regional Climate Model (RegCM3) with 20-km grid spacing to research climate change over China whereas Lee *et al.* (2014) selected the Global/Regional Integrated Model system−Regional Model Program (RMP) with 50-km horizontal resolution to investigate the climate change over East Asia. There are limitations to the model performance that preclude derivation of accurate climate information. Therefore, a world-wide inter-model comparison project was launched to guide the regional climate downscaling study (Giorgi *et al.*, 2009). It set up a common framework to evaluate the RCM performance. There are more than 12 domains contributing to the project. In East Asia, it is CORDEX-East Asia (https://cordex-ea.climate.go.kr/). Following the evaluation framework of CORDEX-East Asia, this chapter set up a regional climate downscaling experiment which employs the COSMO-CLM (COSMO: the Consortium for Small-scale Modelling; CLM: Climate Limited-area Modelling or climate version of "Lokalmodell") regional climate model. The simulation participates in the CORDEX-East Asia as well as the other four RCMs. Therefore, an inter-comparison of the performance of five RCMs in representing the precipitation climatology over East Asia was undertaken to answer the questions:

(II) What is the difference between CORDEX-East Asia models in representing the precipitation climatology?

(III) How good are the CORDEX-East Asia models in capturing the EASM?

This chapter has been published in Climate Research (Huang *et al.*, 2015*b*).

Chapter 4 extends the analysis of regionalisation undertaken in Chapter 3. The main goal of regional climate community is applying the RCM output for impact and adaptation studies. To address this aim, the lateral and boundary conditions are provided by AOGCMs which

could simulate present and future climate (Giorgi *et al.*, 2009). Under the joint effort of global climate model community, many global model simulations have been produced to support the Fifth Assessment Report of the Intergovernmental Panel on Climate Change (IPCC AR5). The simulations include a large number of experiments to investigate present climate variability (*i.e.* historical experiments), future climate change under new greenhouse-gas scenario simulations for the 21st century (*i.e.* Representative Concentration Pathways−RCPs experiments), climate prediction (*i.e.* decadal prediction experiments), carbon cycle, and individual feedback mechanisms to climate change (Taylor *et al.*, 2012). It provides a large number of datasets as forcing data to the regional climate community working on different research topics. The historical experiment data is the reference data for model evaluation, for the baseline of climate prediction and for the calculation of climate changes. Based upon the historical simulation, a new downscaling experiment has been set up. Following the climate projection framework of CORDEX-East Asia, the COSMO-CLM was driven by the MPI-ESM-LR in 1979-2005. The following question will be answered:

(IV) Is the downscaling method improving the model performance in representing the EASM?

Chapter 5 evaluates the predictive skill of AOGCMs to predict the EASM on a seasonal time-scale. Research on EASM prediction began in the early 2000s with "state-of-the-art model predictability studies" and focused on the predictability of EASM rainfall on seasonal time-scale (Kang *et al.*, 2004; Wang *et al.*, 2005). As mentioned, the AGCMs are unable to predict the EASM rainfall due to the incorrect rainfall-SST relationship (Wang *et al.*, 2005). However, the AOGCMs are a valuable tool to study the predictability and prediction skill of the EASM (Wang *et al.*, 2005). In the coupled model inter-comparison project phase 5 (CMIP5) era, the AOGCMs show significant improvement in capturing the EASM (Sperber *et al.*, 2013). They have the ability to simulate the mean state of EASM (Sperber *et al.*, 2013), but cannot capture its year-to-year variations (Huang *et al.*, 2013; Song and Zhou, 2014). The CMIP5 models accurately represent the relationship between EASM and ENSO at inter-annual time-scale (Sperber *et al.*, 2013). Previous studies show that the EASM-ENSO relationship is the determining factor in predicting EASM in climate model (Lee *et al.*, 2010; Wang *et al.*, 2015; Wu *et al.*, 2009). Additionally, given observed initial conditions, the CMIP5 models add skill to predict the ENSO on seasonal-to-decadal time-scale (Choi *et al.*, 2016; Meehl *et al.*, 2014; Meehl and Teng, 2012). This extended prediction skill of the ENSO suggests that the EASM can be predicted on a seasonal time-scale if the dynamic link between the ENSO and the monsoon circulations is well represented in the CMIP5 models. For this purpose, six prediction systems which participate in the CMIP5 will be

inter-compared to test their ability to predict the EASM on seasonal time-scale. The main research questions of this chapter are:

(V) How are the six prediction systems capturing the EASM under forcing by observed initial conditions?

(VI) What is the difference between the six systems in predicting the EASM on seasonal time-scale?

This chapter has been submitted to an international journal (Huang *et al*, 2017, *Earth System Dynamics*, under review)

Chapter 6 summarises the main results, and suggests possible directions for future research.

Chapter 2

EASM Representation in Re-analysis Datasets

2.1 Introduction

In the past decades, extensive research has been conducted to increase our knowledge of monsoon variability and predictability, and to improve projections of the impact of human activities on monsoonal systems over East Asia (Wang *et al.*, 2012). The extensive work strongly depends on observations. A global observation network was built up in 20th century (Peterson and Vose, 1997). The observation network collects data from in-situ stations, ships, buoys, satellite and aircraft *etc*. It provides the best estimate of the state of the atmosphere, land and ocean. However, the data is inhomogeneous due to the fact that there are gaps in spatial and temporal coverage. Global atmospheric assimilated datasets, called re-analysis, have been developed, which combine observation and geophysical fluid-dynamical models (Kalnay *et al.*, 1996). Because of the parametrisation for important physical processes (*e.g.* radiative transfer, convection, turbulent transfer *etc*.), the model has its own uncertainty and biases to the real atmosphere. The re-analysis uses observations to constrain the model output to optimise the spatial&temporal coverage and accuracy.

Since the early 1990s, several generations of atmospheric re-analyses have been produced at different organisations. The National Centers for Environmental Predictions (NCEP)/National Center for Atmospheric Research (NCAR) Reanalysis (NCEPI; Kalnay *et al.*, 1996) is the original re-analysis effort. Then NCEP/Department of Energy (DOE) updated the forecast model with better physical parametrisations and fixed the data assimilation errors (*e.g.* assorted data assimilation errors) to produce a new version of re-analysis (*i.e.* NCEPII; Kanamitsu *et al.*, 2002). Both the NCEPI and the NCEPII belong to the

first-generation re-analysis. The European Centre for Medium Range Weather Forecasts (ECMWF) 45-year Reanalysis (ERA-40; Uppala *et al.*, 2005) and the Japanese 25-year Reanalysis (JRA-25; Onogi *et al.*, 2007) are the second-generation re-analysis. These re-analysis datasets have the same data assimilation approach (*i.e.* 3D-Var; three-dimensional variational data assimilation) as in the first-generation re-analysis. The second-generation re-analyses show some errors in climate study, *e.g.* the JRA-25 illustrates a clod bias in the lower stratosphere (Onogi *et al.*, 2007) and a dry bias in the Amazon basin (Bosilovich *et al.*, 2008). Therefore, a third-generation re-analysis datasets have been developed, which include the Climate Forecast System Re-analysis (CFSR; Saha *et al.*, 2010, 2006), the ECMWF Interim Reanalysis (ERA-Interim; Dee *et al.*, 2011), the Japanese 55-year Reanalysis (JRA-55; Kobayashi *et al.*, 2015), and the Modern Era Retrospective-Analysis for Research and Applications (MERRA; Rienecker *et al.*, 2011). The new generation re-analyses apply a more advanced data assimilation method (*e.g.* analysis increments and 4D-Var) and models and addressed issues discovered in the second-generation re-analysis efforts. Sequential, the ECMWF and the National Oceanic and Atmospheric Administration (NOAA) developed a new generation re-analysis to provide a long time cover observational validation dataset to assess climate model simulations of the 20th century, the ECMWF's first atmospheric re-analysis of the 20th century (ERA-20C; Stickler *et al.*, 2014) and the Twentieth Century Reanalysis v2 (20CR; Compo *et al.*, 2011), respectively.

The re-analysis datasets have been widely used in studying climate variability and climate change. It is a reference data for climate model output (Flato *et al.*, 2013) and a driving data for RCMs in simulating present climate (Giorgi *et al.*, 2009; Huang *et al.*, 2015*b*). As mentioned, the re-analyses are produced by different organisations, employ various forecast models and data assimilation approaches. There is a discrimination between each re-analysis. Newman *et al.* (2000) firstly described the difference between the ECMWF, NCEP and NASA (National Aeronautics and Space Administration's Goddard Laboratory for Atmospheres) re-analysis. Then, Betts *et al.* (2006) described the strengths, weaknesses, and usefulness of re-analysis datasets. Several works assess precipitation in re-analyses due to it is a "forecast" variable from the forecast model (Bosilovich *et al.*, 2008; Lin *et al.*, 2014). Both the Bosilovich *et al.* (2008) and the Lin *et al.* (2014) compared the re-analysis performance in reproducing precipitation on large scale. Bosilovich *et al.* (2008) assessed precipitation climatology of five re-analyses in nine sub-regions (North Pacific, Eurasia, Indian monsoon region *etc.*). Lin *et al.* (2014) evaluated five re-analyses performance in capturing global monsoon metrics. The monsoon metrics include climatology of global monsoon modes, inter-annual variability, and long-term trend of global monsoon precipitation. Then, Chen *et al.* (2014) found that four re-analyses (*i.e.* JRA-55, ERA-Interim, CFSR and MERRA)

exhibit similar structure and summer progress of mean wind diurnal cycle, but illustrate some differences in the low-level meridional wind. Wang and Zeng (2012) analysed six re-analysis products in representing observational precipitation, temperature and radiation over Tibetan Plateau where is the surrounding area of EASM. However, there is little work focusing on the re-analysis performance in capturing the EASM.

Based on the relative dependence of the model and the assimilated observational data, Kalnay *et al.* (1996) classified the output variables into four classes. The precipitation is categorised into "C" variable due to it is completely determined by the model during the data assimilation. Because of the zonal and meridional wind, and geopotential height are directly assimilated from observational data, they are the most reliable variable in the first, second and third-generation re-analysis. These data are categorised into "A" variable. However, the extended generation re-analysis (20CR and ERA-20C) only takes surface data (*e.g.* pressures and winds) into data assimilation. Therefore, pressure level variables (*e.g.* wind fields and geopotential height) in extended generation reanalysis are classified into "C" class. These variables should be compared to the observations when they are used for scientific research, especially for studying the EASM.

2.2 Re-analysis datasets and methods

In this study, eight re-analyses are evaluated and inter-comparison. The concise information of the eight re-analyses is presented in Table 2.1. Because of the spatial (EASM region) and temporal (1979-2010) coverage, monthly data of the eight re-analyses will be selected to analyse. They are the first-generation re-analysis (*i.e.* NCEPI and NCEPII), the third-generation re-analysis (*i.e.* CFSR, ERA-Interim, MERRA, and JRA-55), and the extended-generation re-analysis (*i.e.* 20CR and ERA-20C). Table 2.1 shows a brief summary of each re-analysis datasets focusing on their main strength and limitation. The detailed description of each re-analysis datasets can be found from Climate Data Guide website https://climatedataguide.ucar.edu/climate-data.

The Global Precipitation Climatology Project (GPCP; Adler *et al.*, 2003) has been employed as the precipitation observational data. Reference dataset of the mean sea level pressure is the extended Hadley Centre's monthly historical mean sea level pressure dataset (HadSLP2r; Allan and Ansell, 2006). The Integrated Global Radiosonde Archive (IGRA; Durre *et al.*, 2006) is applied to evaluate the uncertainty of multi-pressure level wind fields in re-analysis datasets. Over 1500 global distributed stations contribute to the IGRA which consists of radiosonde and pilot balloon observations (Durre *et al.*, 2006). More than 150 stations locate in our study area (Fig. 2.1). The station data is interpolated to grid dataset

Table 2.1 Basic information of re-analyses investigated in Chapter 2.

Name	Standard Name	Orangisation	Resolution	Data assimilation method	Reference
20CR	Twentieth Century Reanalysis v2	NOAA ESRL/PSD and CIRES	T62L28	Ensemble Kalman Filter	Compo *et al.* (2011)
CFSR	Climate Forecast System Reanalysis	NCEP	T382L64	3D-VAR	Saha *et al.* (2010)
ERA-20C	ECMWFs first atmospheric reanalysis of the 20th century	ECMWF	T159 L91 and N80 reduced Gaussian	4D-VAR	Stickler *et al.* (2014)
ERA-Interim	ECMWF re-analysis	ECMWF	T255 L60 and N128 reduced Gaussian	4D-VAR	Dee *et al.* (2011)
JRA-55	Japanese 55-year Reanalysis	JMA	T319 L60	4D-VAR	Kobayashi *et al.* (2015)
MERRA	NASA Modern Era Reanalysis for Research and Applications	NASA GMAO	1/2 lat x 2/3 lon; 72 sigma levels	3D-VAR, with incremental analysis update	Rienecker *et al.* (2011)
NCEPI	NCEP/NCAR Reanalysis	NCEP/NCAR	T62L28	3D-VAR	Kalnay *et al.* (1996)
NCEPII	NCEP/DOE Reanalysis	NCEP/DOE	T62L28	3D-VAR	Kanamitsu *et al.* (2002)

Table 2.2 Brief summary of the eight re-analysis datasets in Chapter 2 with their strength and limitation.

Name	Temporal coverage	Strength	Limitation	Internet
20CR	1850-2014	The longest re-analysis record	Data assimilation with a few observations	https://www.esrl.noaa.gov/psd/data/20thC_Rean/
CFSR	1979-2011	Improved and finer resolution model, and advanced assimilation schemes (4D-Var)	Few comparisons	https://rda.ucar.edu/pub/cfsr.html
ERA-20C	1900-2010	Higher horizontal and vertical resolution than 20CR	Shorter than 20CR and a few observations for data assimilation	www.ecmwf.int/en/research/climate/reanalysis/era-20C
ERA-Interim	1979-to-present	High horizontal and vertical resolution; improved low-frequency variability and stratospheric circulation than ERA40	Large intensity of a water cycling over the oceans, positive biases in temperature and humidity at the lower troposphere (below 850 hPa) and not capture low-level inversions in the Arctic	www.ecmwf.int/en/research/climate-reanalysis/era-interim
JRA-55	1958-to-present	The longest third-generation re-analysis with full observations	Dry bias in upper and middle troposphere and in regions deep convection, time-varying warm bias in the upper troposphere	www.jra.kishou.go.jp/JRA-55/index_en.html
MERRA	1979-to-present	Improved the precipitation and water vapour climatology	Assimilation routine is frozen and will not be updated for new satellite instruments	https://gmao.gsfc.nasa.gov/reanalysis/MERRA/
NCEPI	1948-to-present	First effort of re-analysis and the longest running re-analysis that uses rawindsonde data	Low spatial and temporal moisture variability over oceans and a relatively poor climate state in Southern Hemisphere	https://www.esrl.noaa.gov/psd/data/gridded/data.ncep.reanalysis.html
NCEPII	1979-to-present	Improvement of surface flux files, hydrological budget, short wave radiation flux	Drawbacks in the outgoing long-wave radiation over tropical warm pool and upper-level tropical moisture	https://www.esrl.noaa.gov/psd/data/gridded/data.ncep.reanalysis.html

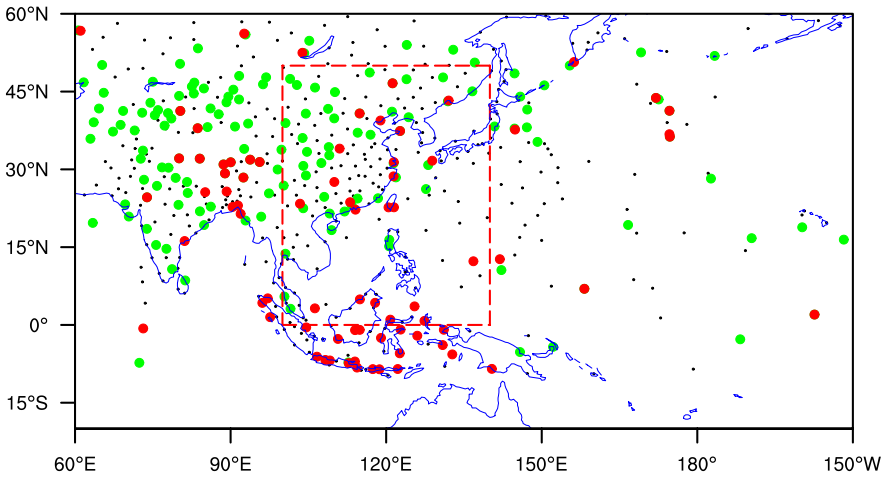

Figure 2.1 Geographic distributions of the Integrated Global Radiosonde Archive stations. Black dots mark all stations, green dots denote deleted stations, and red dots indicate added stations. The red dashed box illustrates the east Asian summer monsoon region (0°-50°N, 100°-140°E).

by iterative improvement objective analysis. To eliminate the uncertainty associated with different data resolution, the validation data and the re-analyses are remapped onto a common gird of 2.5°x2.5° by bi-linear interpolation. All the abbreviation of each meteorological variable is following the guide of CMIP5, *i.e.* pr for precipitation, psl for mean sea level pressure, ua850 for zonal wind at 850 hPa and va850 for meridional wind at 850 hPa.

The quality of re-analysis data is measured by anomaly correlation coefficient (ACC), root-mean-square error (RMSE) and BIAS. The PCC statistic method is the un-centred statistical measure which is without removal of the global mean. Appendix B presents the detail for all the methods.

2.3 Results

2.3.1 Inter-annual variability

Taylor diagram is a valuable tool in evaluating the model data performance regarding the matching of temporal variability using temporal correlation and standard deviation (Taylor, 2001). This section shows the temporal correlations from summer (June-July-August) mean precipitation and associated three meteorological fields averaged over the EASM region (0°-50°N, 100°-140°E) for all the re-analyses versus the reference data (Fig. 2.2). Compared to the GPCP, the re-analyses show a large spread with the normalised standard deviations

(NSD) range from 0.87 to 1.52 and the correlation range from 0.37 to 0.66. The JRA-55 has the highest correlation (0.66), while the ERA-Interim illustrates the lowest correlation (0.37) to the observed precipitation. The JRA-55 and the NCEPI demonstrates a small inter-annual variation than the reference data with the NSD <1. The other six re-analyses exhibit a larger year-to-year variation in precipitation than that in the GPCP, especially the CFSR and the MERRA with the NSD, 1.52 and 1.50, respectively.

The re-analysis datasets illustrate high consistency in the psl and the ua850. The range of psl's correlation is 0.71 to 0.81, and NSD is 0.95 to 1.17. We can find the re-analyses have the same performance in representing the ua850 as the psl, with a high correlation (0.88-0.93) and an approximate inter-annual variation (NSD: 1.05-1.29) to the IGRA. Obviously, the va850 presents a lower year-to-year variation than that in the reference data. To our notice, the CFSR and the MERRA have a worse performance in capture the va850 variation than the other six re-analyses with NSD, 1.48 and 1.58, respectively.

A further evaluation is focusing on the re-analysis datasets and their ensemble mean in representing the inter-annual variability of the three variables over land (Fig. 2.2b) and ocean (Fig. 2.2c). In general, the pr and the va850 exhibit better performance (with higher correlation coefficient) over land than over oceans, while the psl and the ua850 show a versus performance. We find that the CFSR and the NCEPII have a lower correlation and a higher NSD than the other re-analysis datasets. The re-analysis mean captures a more realistic year-to-year variation of the four variables. It shows a higher correlation coefficient than an individual re-analysis dataset.

2.3.2 Spatial difference in re-analysis datasets

Figure 2.3 presents the ensemble standard deviation (ESD) of the eight re-analyses for the four meteorological variables. It shows the inter-reanalysis difference. The precipitation's spread reduces with the latitude increasing. A large ESD (3 mm day^{-1}) occurs in the low latitudes, especially in the western Indo-China Peninsula where the ESD is >5 mm day^{-1}. There is no prominent difference among the re-analyses in representing the psl over ocean. However, we can find a large ESD of psl over land, especially in the western EASM region (*i.e.* the Tibetan Plateau; ESD >3 hPa). For the ua850 and the va850, the re-analyses show high consistency with ESD 1 mm s^{-1} in the entire EASM region.

For specific variable (*e.g.* pr and psl) and region, the re-analysis members show significant disagreement to each other. This study employed the BIAS analysis to quantify their magnitude of deviation from observation (Fig. 2.4 and 2.5). In monsoon season, the inter-tropical convergence zone (ITCZ) reaches its northernmost location. The water moisture is transported by northward wind from ocean to land. Two precipitation belts are located in the

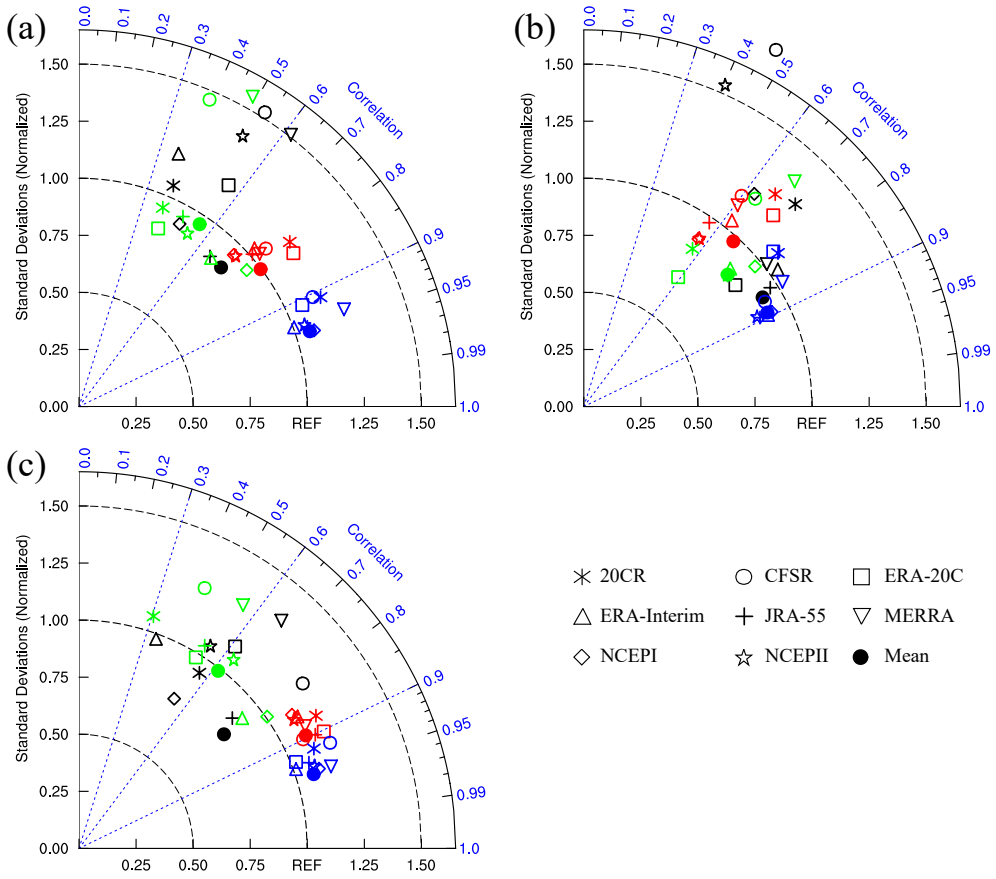

Figure 2.2 Temporal statistics describing inter-annual variability of the re-analysis datasets and the multi-datasets ensemble mean in terms of June-July-August (JJA) mean precipitation (black), zonal winds (blue) and meridional winds (green) at 850 hPa, and mean sea level pressure (red) over the East Asian summer monsoon (EASM) region (0°-50°N, 100°-140°E; a), the EASM land (b), and the EASM ocean (c) from 1979 to 2010.

East Asia, the south branch stretches from the Bay of Bengal, the Indo-China Peninsula and the Philippine Sea; and the north branch occurs from the east of China, the Korean peninsula and the south of Japan (Fig. 2.4; *cf.* Observation).

The eight re-analysis datasets capture the major feature of precipitation spatial distribution in monsoon season (Fig. 2.4). However, these datasets tend to generate a significant wetter condition in southern EASM region (*i.e.* the South China Sea and the Philippine) and a prominent drier condition over the Korean peninsula and the Japan. The third generation of re-analysis datasets present a better performance (with small BIAS) in capturing the summer precipitation, especially in the mainland of China, the Korean Peninsula and the Japan than the first and the extended generation re-analysis datasets. It is worth mentioning that only the ERA-Interim and the ERA-20C produce more precipitation in the Indo-China Peninsula

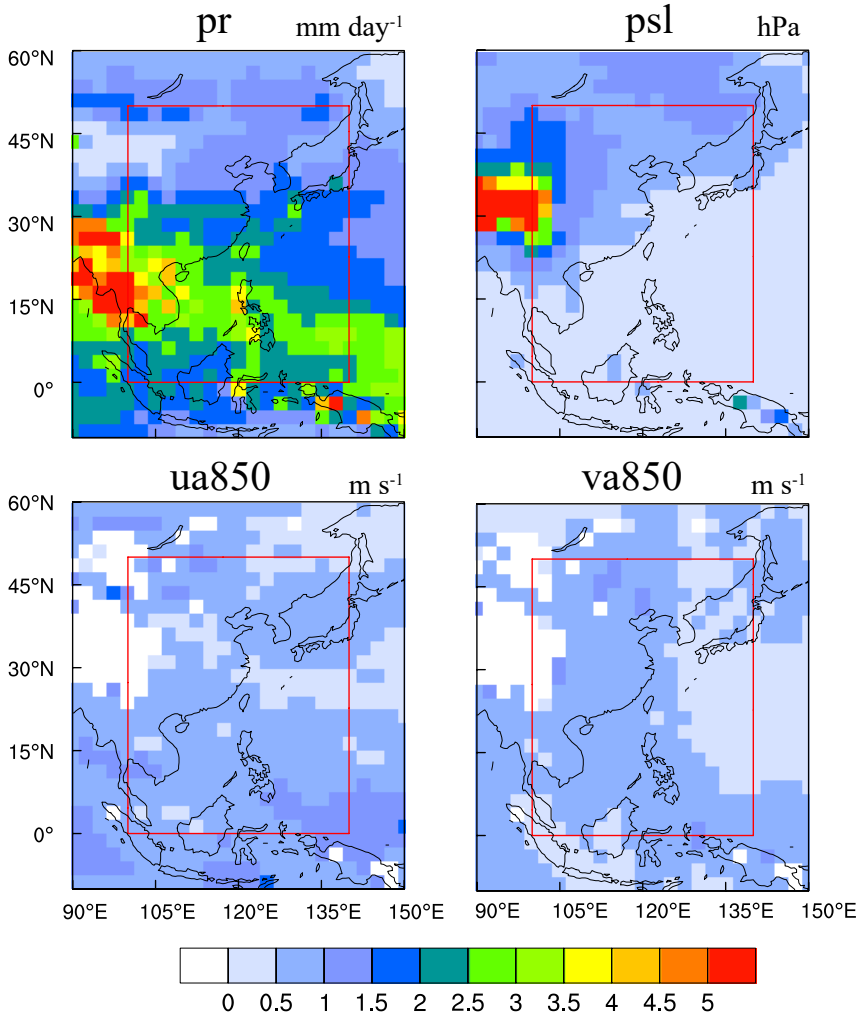

Figure 2.3 Spatial distribution of the multi-reanalysis ensemble deviation for June-July-August mean precipitation (pr), mean sea level pressure (psl), and winds at 850 hPa (ua850 and va850) from 1979 to 2010. The red box represents the East Asian summer monsoon region (0°-50°N, 100°-140°E).

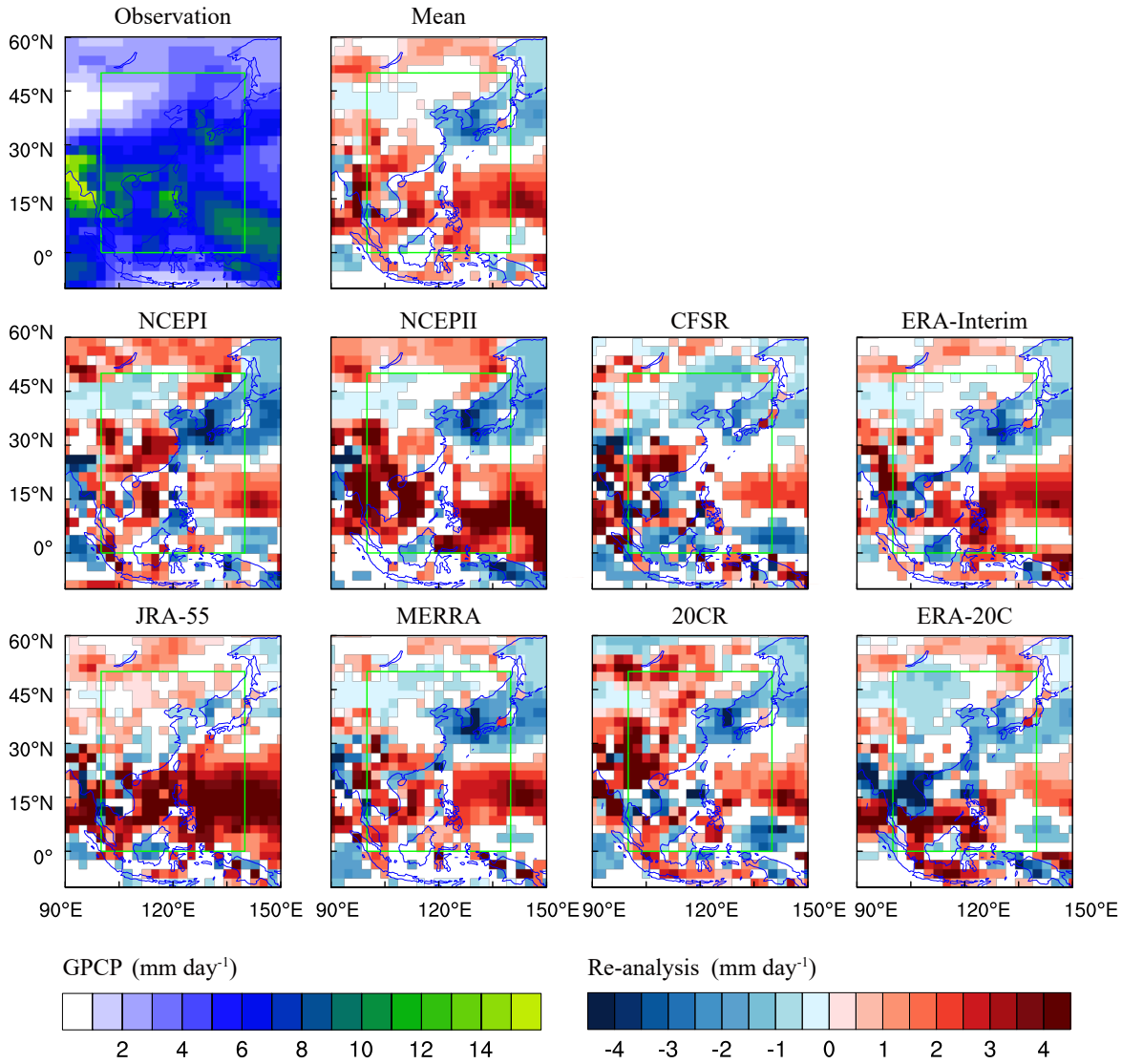

Figure 2.4 Summer (JJA) precipitation of the Global Precipitation Climatology Project (GPCP) and the precipitation anomalies 're-analysis minus GPCP' in 1979-2010. The presented anomalies of precipitation pass the Student's *t*-test at 0.05 level. The green box represents the East Asian summer monsoon region (0°-50°N, 100°-140°E).

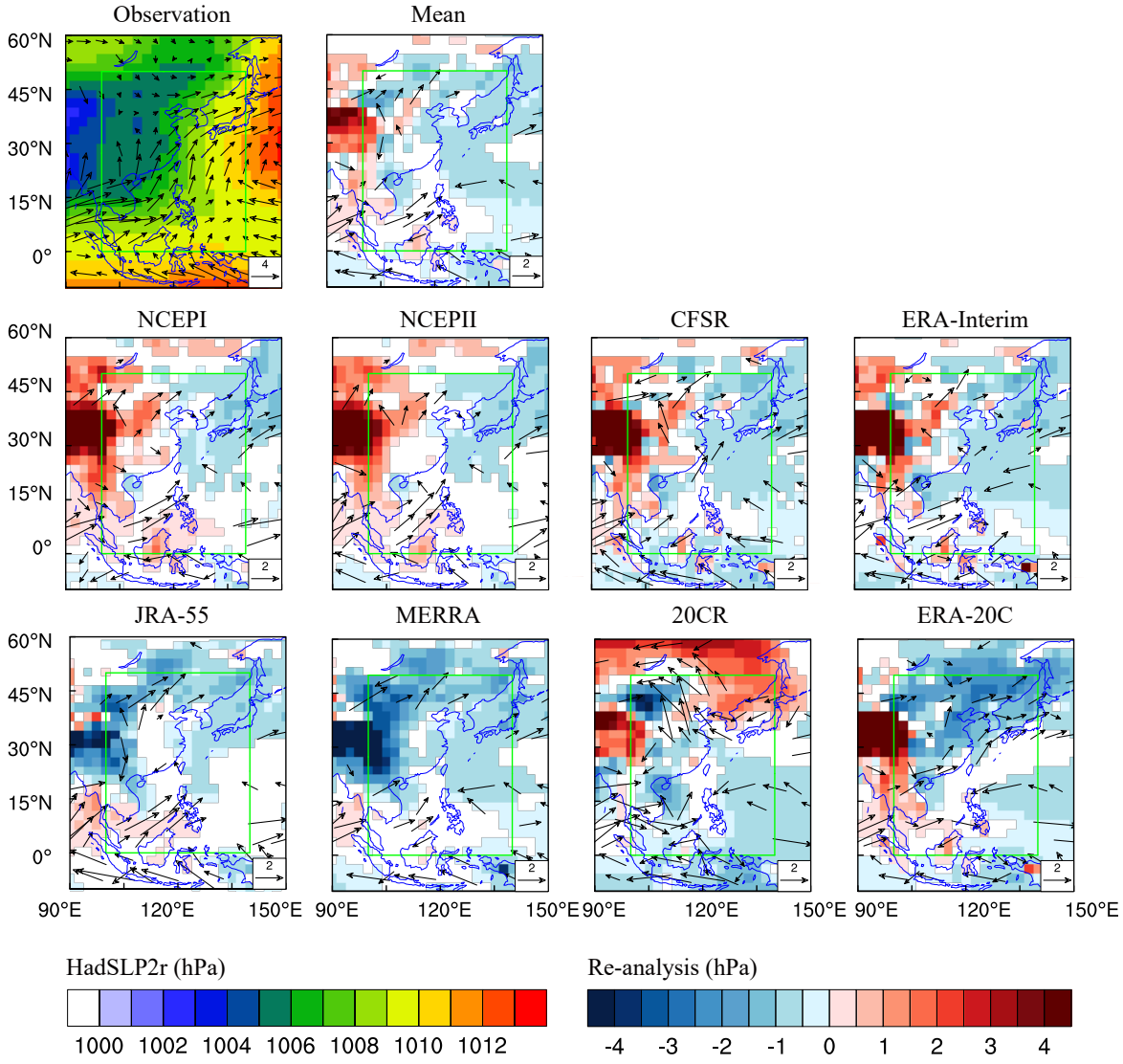

Figure 2.5 Summer (JJA) mean sea level pressure (observation shaded) of the extending Hadley Centre's monthly historical mean sea level pressure dataset (HadSLPr2) and wind fields at 850 hPa (Observation vector) of the Integrated Global Radiosonde Archive (IGRA) and the mean sea level pressure anomalies ‘re-analysis minus HadSLPr2; shaded’, and the winds anomalies ‘re-analysis minus IGRA; vector’ in 1979-2010. The presenting anomalies of precipitation pass the Student's *t*-test at 0.05 level. The green box represents the East Asian summer monsoon region (0°-50°N, 100°-140°E).

where the other six re-analysis datasets generate less precipitation. The large precipitation BIAS occurs along with the lower level general circulation (*i.e.* wind fields at 850 hPa) BIAS. There is a significant wind BIAS over the South China Sea and the Philippine Sea. In the northern China, the 20CR shows a large north-westward wind than the observation, but the other seven re-analysis datasets illustrate a good agreement with the observation (Fig. 2.4).

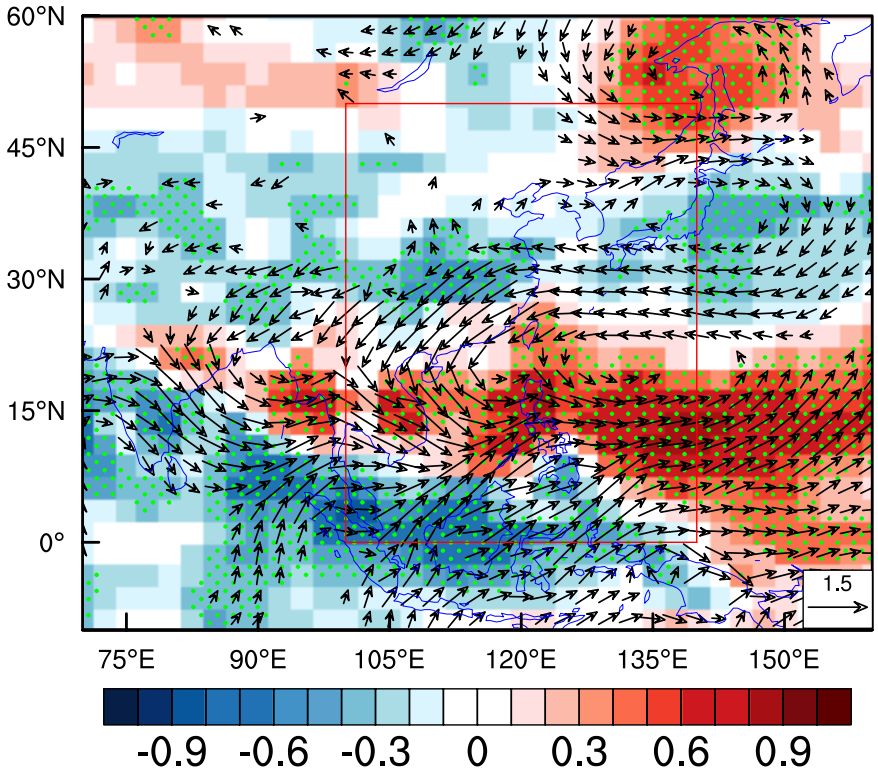

Figure 2.6 Correlation map between EASM index and June-July-August precipitation (shaded) and winds at 850 hPa (vector). Presenting correlation coefficient between EASM index and winds at 850 hPa pass the Student's *t*-test at 0.05 level. Green dotted areas are the correlation coefficient between EASM index and precipitation pass the significant test at 0.05 level. The color shows the correlation to the GPCP precipitation while the arrow represents the correlation of winds to the ERA-Interim dataset. The EASM index is calculated by the ERA-Interim. The red box represents the East Asian summer monsoon region (0°-50°N, 100°-140°E).

In summer season, the land (ocean) is a heat source (sink) with lower (higher) mean sea surface pressure (Fig. 2.5; Observation). The Tibetan Plateau presents a prominent low pressure centre due to the fact of its huge topography height. The first-generation re-analysis datasets produce higher psl in the Tibetan Plateau, the western of Indo-China Peninsula and the Indonesia; and lower psl in the Japan and the Sea of Japan (Fig. 2.5; NCEPI; NCEPII). The CFSR and the ERA-Interim have the same performance in presenting the psl over the

Tibetan Plateau and Japan, and illustrate no significant BIAS in the Indo-China Peninsula and the Indonesia. However, these two datasets generate lower psl over the East China Sea. Both the JRA-55 and the MERRA show the prominent negative BIAS of psl in the western (*e.g.* the Tibetan Plateau, south-west of China *etc.*) and the northern (*e.g.* Mongolia, northern China *etc.*) EASM region. The 20CR indicates a positive BIAS centre of psl in the south of Tibetan Plateau, the north-east of China, and the northern Sea of Japan; but produces lower psl in the western South China Sea and the Philippines Sea. Compared to the HadSLP2r, the ERA-20C generates higher psl over the Tibetan Plateau and in the western of Indo-China Peninsula, but lower psl in the northern EASM region.

2.3.3 Monsoon strength

The EASM is characterised by strong year-to-year variability. To measure the strength and study the long-term change of EASM, more than 25 monsoon indices have been produced in the last few decades. Wang *et al.* (2008*b*) classified these monsoon indices into five categories: 1) "east-west thermal contrast" index, 2) "north-south thermal contrast" index, 3) shear vorticity index, 4) "south-west monsoon" index, and 5) "South China Sea monsoon" index. Wang *et al.* (2008*b*) found that the Wang and Fan index (1999) outperforms the other 24 monsoon indices in capturing the three-dimensional circulation and total variance of the precipitation over East Asia. Figure 2.6 shows the correlation map between the Wang and Fan index and summer precipitation and winds at 850 hPa. The index can indicate the summer precipitation distribution and also the general circulation change over East Asia. Therefore, the Wang and Fan index was selected for the further study. The Wang and Fan index belongs to shear vorticity index. Its definition is standardised average zonal wind at 850 hPa in (5°-15°N, 90°-130°E) minus in (22.5°-32.5°N, 110°-140°E).

Figure 2.7a illustrates the observed (IGRA) and the multi-reanalysis ensemble mean produced EASM index (EASMI). The re-analysis ensemble mean shows good agreement with the observation in representing the EASMI. For the individual re-analysis, it can capture the phase of EASMI, only has a slight difference in capturing the EASMI magnitude (Fig. 2.7b). The range of correlation coefficient between the EASMI in observation and in re-analyses is from 0.97 to 0.99. The 20CR indicates an extremely strong monsoon year (EASMI >1) in 1997 and 2007, but the observation and the other re-analysis datasets show a normal monsoon year (EASMI $>$-1 and EASMI <1).

2.4 Summary and discussion of Chapter 2

In this chapter, eight current re-analysis datasets (20CR, CFSR, ERA-20C, ERA-Interim, JRA-55, MERRA, NCEPI, and NCEPII) have been inter-comparison to identify their difference in representing the EASM precipitation and general circulation. This chapter firstly analysed the inter-annual variability of four variables which are closely associated with the EASM behaviour (Fig. 2.2). The re-analyses show a high correlation coefficient and close normalised standard deviation to the observed regional mean zonal winds at 850 hPa and mean sea level pressure, but a large spread of this metrics for the precipitation and meridional winds at 850 hPa. The re-analyses generate a different precipitation due to its "forecast" intrinsic. MERRA is the only dataset which assimilates the rain rate from SSM/I and TRMM (section 2.2). However, it is not the best re-analysis in capturing the inter-annual variability of precipitation in the study region. The quality of precipitation strongly depends on the numerical weather models and data assimilation system (Bosilovich *et al.*, 2008; Lin *et al.*, 2014). CFSR shows a better estimation of observed precipitation due to the fact that it employs an advanced model and an updated convection parametrisation (modified Tiedtke shallow convection) than the NCEPI and NCEPII (Saha *et al.*, 2010).

The re-analyses exhibit a large spread in producing the precipitation and mean sea level pressure than the winds at 850 hPa (Fig. 2.3). The BIAS metric (Fig. 2.4-2.5) of each variable in different re-analysis datasets have been inter-compared. Due to the performance of forecast model, there is significant difference between each re-analysis dataset in representing precipitation (Fig. 2.4). The psl is directly assimilated from observation. However, we can find the prominent discrepancy among the re-analyses occurring in the west and north-east of China where the complex topography occupies. In these regions, the JRA-55 and the MERRA present negative biases to the observed psl, while the other six re-analyses illustrate positive biases (Fig. 2.5). The JRA-55 and the MERRA share the same data assimilation achieve with the ERA-Interim. The differences of psl between the re-analysis datasets might caused by the different land-surface model. A different land-surface-process might lead to a significant BIAS in the region where the surface pressure observation is sparse (Kobayashi *et al.*, 2015; Yi *et al.*, 2011). Another reason is the different horizontal resolution of re-analysis datasets which affected by the local topography. The local terrain height is an important factor to gain the psl.

The Wang and Fan monsoon index is calculated by zonal wind at 850 hPa, which can indicate the monsoon strength and precipitation distribution in East Asia. The EASM index in re-analyses show good agreements with observations, characterised by higher correlation coefficients (Fig. 2.7). Only the 20CR exhibits a slight difference in representing the magnitude of EASM index in specific years (*e.g.* 1997 and 2007). We, thus, can omit the

re-analysis difference in representing the EASM strength. The 20CR and ERA-20C are optional datasets to analyse the long-term variability of EASM in 20th century.

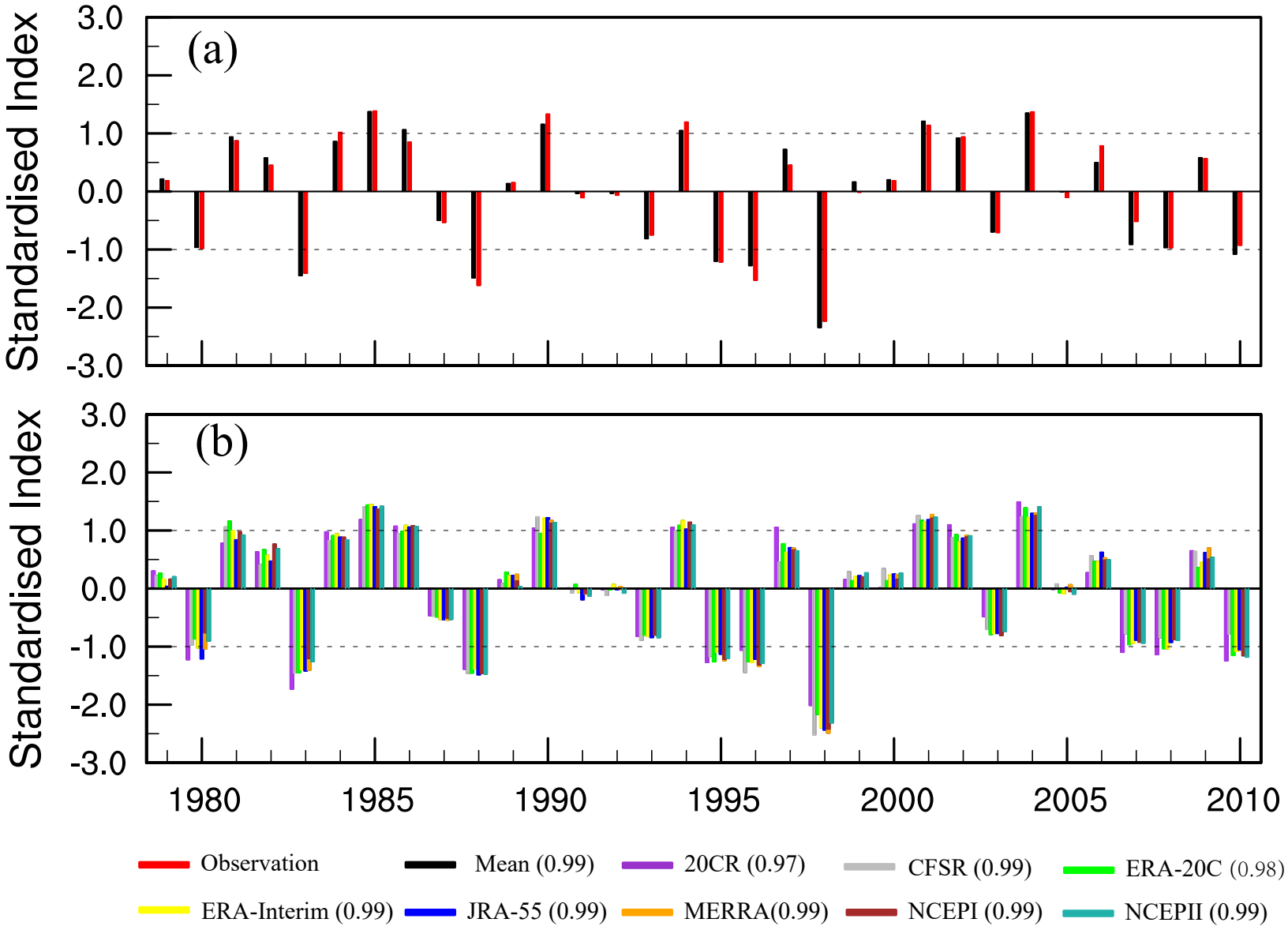

Figure 2.7 East Asian summer monsoon index of observation (IGRA) and multi-reanalysis ensemble mean (a), and individual re-analysis dataset (b). The number following the re-analysis presents the correlation coefficient between re-analysis produced and observed East Asian summer monsoon index.

Chapter 3

Multi-regional Climate Model Simulations of EASM: Validation

3.1 Introduction

RCMs are able to capture sub-grid scale processes (*e.g.* sea breeze, mountain precipitation *etc*.) over complex land surface, because they provide a high resolution forcing (Hong and Kanamitsu, 2014). RCMs simulations generate useful datasets to study the regional climate variability and climate change. To validate the RCM's performance, the re-analysis datasets are employed as boundary condition. Different boundary conditions lead to different performance of RCM (Laprise, 2008; Rummukainen, 2010; Staniforth, 1997). There are noticeable differences between each re-analysis datasets (Chapter 2). Thus, by using only one re-analysis to drive the RCMs is able to isolate the differences caused by individual boundary conditions.

RCM studies generally tend to over-estimate or under-estimate monsoon precipitation and temperature when compared with observations (Fu *et al.*, 2005; Gbobaniyi *et al.*, 2014; Nikulin *et al.*, 2012; Xue *et al.*, 2010). In this regard, it is important to evaluate the capability of RCMs in reproducing the present climate before using them for future scenarios (Flato *et al.*, 2013; Wang *et al.*, 2004*b*), especially in monsoon regions (Fu *et al.*, 2005; Nikulin *et al.*, 2012). In the last decade, numerous international RCM downscaling projects have been carried out focusing on monsoons, but over specific areas of interest (Giorgi *et al.*, 2009; Laprise, 2008). These projects include the Regional Model Inter-comparison Project for Asia (RMIP Asia; Fu *et al.* 2005) to evaluate and improve RCM simulations for the East Asian monsoonal region, the African Monsoon Multidisciplinary Analyses (AMMA; Redelsperger *et al.* 2006; Ruti *et al.* 2011) to address the main uncertainties in the atmospheric processes

controlling the monsoon system (Hourdin *et al.*, 2010), and the West African Monsoon Modelling and Evaluation (WAMME; Druyan *et al.* 2009; Xue *et al.* 2010) to study the role of land-atmosphere-aerosol interaction on West African monsoon processes. Each of these projects has made significant contributions to improve RCM simulations and to understand the evolution of monsoon mechanisms. However, the projects have been limited by international co-ordination and by the limited transfer of knowledge between the projects and the regions of interest. A world-wide inter-model comparison project with the common framework (*i.e.* CORDEX) was set up with the aim of obtaining comprehensive RCM data to study regional climate change (Giorgi *et al.*, 2009). East Asia is one of the focus areas within CORDEX, which is characterised by a complex monsoon system (Ding and Chan, 2005) and a heterogeneous land cover (Fu *et al.*, 2005; Gao *et al.*, 2006). Furthermore, the application of RCMs is in particular important over East Asia due to their better performances in reproducing the present monsoon climate. In addition, these models provide more reliable climate change signals over that region due to their high spatial resolutions (Gao *et al.*, 2006, 2013; Qian and Leung, 2007; Yu *et al.*, 2010).

Several studies have examined the performance of a single RCM in simulating precipitation over CORDEX-East Asia (CORDEX-EA). For example, COSMO-CLM (Rockel *et al.*, 2008) is able to capture precipitation patterns in a small river basin (Fischer *et al.*, 2013), but has a significant wet bias over steep orographic region (Wang *et al.*, 2013*b*). RegCM (Giorgi *et al.*, 1993) shows close agreement with the observed precipitation (Gao *et al.*, 2011, 2006), but a large positive bias over northern Asia during the cold season (Giorgi *et al.*, 2012), the performance of which is substantially dependent on model resolution (Gao *et al.*, 2008) and geographical regions (Gao *et al.*, 2012; Oh *et al.*, 2014). YSU-RSM (Hong and Kanamitsu, 2014) resembles the inter-annual variations of precipitation as well as extreme precipitation events (Lee *et al.*, 2014). These RCMs can represent the main climatological features of precipitation at different levels of accuracy (Giorgi *et al.*, 2012; Lee and Hong, 2014; Oh *et al.*, 2014; Wang *et al.*, 2013*b*). However, none of these studies have focused on an inter-comparison of the different models in simulating precipitation in this region.

This chapter presents the first evaluation results of the CORDEX-EA project using an ensemble of 5 RCM simulations driven by the ERA-Interim re-analysis data (Dee *et al.*, 2011). It examines the capacity of the individual RCMs and their multi-model ensemble means (MME) to reproduce the present climatology and to capture the Asian-Australian monsoon system.

3.2 RCMs, comparison data and methods

There are five RCMs participating in CORDEX-EA (Table 3.1). Following the modelling framework of the CORDEX project, the simulations are driven by ERA-Interim re-analysis data (1989-2008) at the lower and lateral boundaries, and are integrated over East Asia (Fig. 3.1) with a spatial horizontal resolution of 0.44 (50 km). The CORDEX-EA domain includes four sub-monsoon systems (*i.e.* the South Asian Summer Monsoon (SAS), the East Asian Summer Monsoon (EAS), the Western North Pacific Tropical Monsoon (WNP), and the Australian-Maritime Continent Monsoon (AUSMC); Fig. 3.1) (Christensen *et al.*, 2013).

COSMO-CLM (COSMO: the Consortium for Small-scale Modelling; CLM: Climate Limited-area Modelling or climate version of "Lokalmodell") is a non-hydrostatic regional climate model, which has a Arakawa-C horizontal grid (Arakawa and Lamb, 1981) and a terrain following height co-ordinate (Schär *et al.*, 2002) with rotated geographical co-ordinates in the vertical level. Wang *et al.* (2013*b*) adapted the COSMO-CLM in East Asia, but it is driven by the ERA-40 re-analysis (Uppala *et al.*, 2005). Following the CORDEX-EA framework, we re-run the simulation driven by the ERA-Interim. The model set-up has been adapted from Wang *et al.* (2013*b*), but using the Runge-Kutta split-explicit scheme for time integration and time step of 240s. The physical parametrisation schemes used in the simulation are the Tiedtke mass-flux convection scheme (Tiedtke 1989), the prognostic turbulent kinetic energy (TKE) turbulence scheme, the δ two-stream radiation scheme with full cloud-radiation feedback (Ritter and Geleyn, 1992), and the multi-layer soil scheme (Jacobsen and Heise, 1982).

HadGEM3-RA is a regional version of the atmospheric component of Hadley Centre Global Environment Model (HadGEM3-A). It is a non-hydrostatic regional climate model, which has a Arakawa-C horizontal grid and a terrain following, height-based vertical co-ordinate. The model includes semi-Lagrangian advection of all prognostic variables except density, permitting relatively long time steps to be used at high resolution (Davies *et al.*, 2005; Martin *et al.*, 2006). The simulation set-up with the general 2-stream radiation scheme (Cusack *et al.*, 1998; Edwards and Slingo, 1996), the non-local mixing scheme for unstable layers (Lock *et al.*, 2000), the local Richardson number scheme for stable layers (Smith *et al.*, 1990), the mixed phase micro-physics scheme (Wilson and Ballard, 1999), the revised mass flux scheme (Gregory and Rowntree, 1990) for deep and shallow convection (Grant and Brown, 1999), the MOSES-II with nine surface tile types plus coastal tiling (Essery *et al.*, 2003), and the (Smith *et al.*, 1990) scheme using parametrized RH*crit* (critical value of grid-box mean relative humidity) for cloud (Cusack *et al.*, 1998).

The new version of the RegCM regional climate modelling system version 4 (RegCM4) is a hydrostatic, compressible model with sigma-p vertical co-ordinates and a Arakawa-B

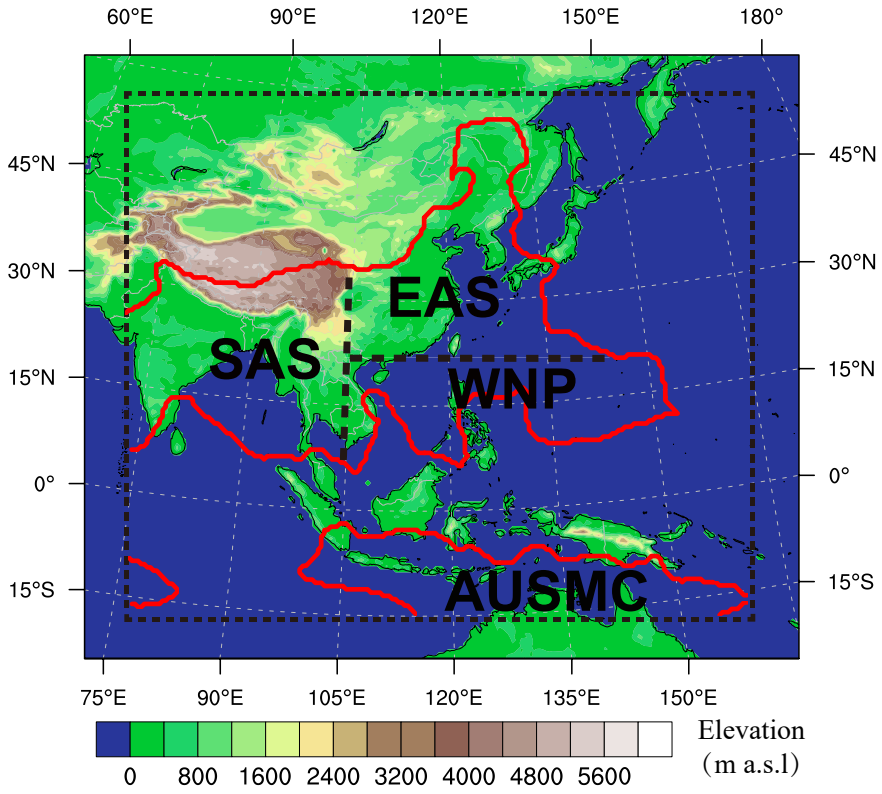

Figure 3.1 CORDEX-East Asia domain at 0.44° grid resolution with topography and the 4 sub-monsoon domains including the South Asian Summer monsoon (SAS), the East Asian Summer monsoon (EAS), the Western North Pacific Tropical monsoon (WNP) and the Australian-Maritime Continent monsoon (AUSMC).

horizontal grid (Giorgi *et al.*, 2012). The dynamical core of RegCM4 is the same as the Pennsylvania State University/National Centre for Atmospheric Research (PSU/NCAR) meso-scale model (MM5) (Grell *et al.*, 1994). The parametrization scheme of this study includes MIT-Emanuel cumulus scheme (Emanuel, 1991; Emanuel and Zivkovic-Rothman, 1999), modified Holtslag planetary boundary layer (PBL) scheme (Holtslag *et al.*, 1990), NCAR CCM3 (Community Climate Model version 3) radiation scheme (Kiehl *et al.*, 1996), and NCAR CLM3.5 (Community Land Model version 3.5) land surface scheme (Bonan *et al.*, 2002; Steiner *et al.*, 2009).

SNU-MM5 is an evolution version of MM5 (Lee *et al.*, 2004), which implemented the Von Strock *et al.* (2000) spectral nudging technique for lateral boundary handling. It uses a non-hydrostatic primitive equation system with a terrain-following sigma vertical co-ordinate. The Kain-Fritsch cumulus convective parametrization scheme (Kain and Fritsch, 1990), the Reisner II explicit moisture scheme (Reisner *et al.*, 1998), the CCM2 radiative transfer scheme (Briegleb, 1992), the CLM3 land surface model (Bonan *et al.*, 2002), and the Yonsei

University planetary boundary layer (YSUBL) scheme (Hong *et al.*, 2006) was configured in this study.

The perturbation model YSU-RSM is described by a two-dimensional sine series for the perturbation of vorticity, but by a two-dimensional cosine series for perturbations of pressure, divergence, temperature, and mixing ratio. Linear computations of horizontal diffusion and semi-implicit adjustment are only considered as perturbations, thus the error due to the re-evaluation of the linear forcing from the base fields is eliminated (Juang *et al.*, 1997; Juang and Kanamitsu, 1994). Lee *et al.* (2014) presents the detail of the parametrization scheme for the simulation.

For model evaluation of precipitation climatology and monsoon characteristics, the Asian Precipitation-Highly-Resolved Observational Data Integration Towards Evaluation of the Water Resources (APHRODITE; Yatagai *et al.*, 2009), the Climatic Research Unit (CRU; Harris *et al.*, 2014), the Global Precipitation Climatology Centre (GPCC; Schneider *et al.*, 2014), the GPCP (Adler *et al.*, 2003), the Tropical Rainfall Measuring Mission (TRMM; Huffman *et al.*, 2007) and the ERA-Interim re-analysis datasets have been used (Table 3.2). In addition, low level wind fields (850 hPa) from the ERA-Interim re-analysis dataset are compared against model results. To eliminate the small difference in the assimilation approach in order to derive the ERA-Interim precipitation, this study followed Nikulin *et al.* (2012) with base times 0000 UTC and 1200 UTC and forecast steps of 12h to obtain the daily precipitation. Then, the daily and monthly means was calculated. It is worthy to mention that the difference between APHRODITE, CRU and GPCC is not significant in terms of climatology. The pattern correlation co-efficient between APHRODITE and CRU (GPCC) climatology is 0.96 (0.97) for annual mean, 0.96 (0.96) for MAM, 0.95 (0.97) for JJA, 0.96 (0.97) for SON, and 0.97 (0.97) for DJF, respectively. Therefore, a merged APHRODITE, CRU and GPCC dataset is used to compare monsoon characteristics in CORDEX-EA. These precipitation datasets cover the time from 1989-2008, except APHRODITE (1989-2007) and TRMM (1998-2008). The validation data are remapped onto a common grid of 0.44° by bi-linear interpolation.

Three different skill measurements are applied to validate the performance of the RCMs on seasonal time scale for summer (JJA) and winter (DJF) from 1989-2008: the mean bias (BIAS), the pattern correlation co-efficient (PCC), and the root-mean-square error (RMSE). Detail information of the three skills are presented in Appendix B.

In addition, this study employed four monsoon metrics which are defined by Wang and Ding (2008). These metrics contribute to a new monsoon index which is based upon the physical processes of the coupled atmosphere-ocean-land system and its response to solar radiative forcing (Wang *et al.*, 2011). There are four parameters used for this index:

Table 3.1 Details of the regional climate models (RCMs) investigated in Chapter 3. Projection (Proj.)—RP: rotated polar, M: Mrcator, LC: Lamberg Conformal; Dynamics (Dyn.) —H: hydrostatic, NH: non-hydrostatic; PBL: planetary boundary layer

	Proj.	Horizontal resolution	Dyn.	Vertical coordinates/levels	Convection scheme	Radiation scheme	Cloud microphysics	Land surface scheme	PBL
COSMO-CLM[a]	RP	0.44°	NH	Terrain following/40	Tiedtke (1989)	Ritter and Geleyn (1992)	Baldauf and Schulz (2004)	Jacobsen and Heise (1982)	Davies and Turner (1977)
HadGEM3-RA[b]	RP	0.44°	NH	Terrain following/60	Grant and Brown (1999); Gregory and Rowntree (1990)	Cusack *et al.* (1999); Edwards and Slingo (1996)	Cusack *et al.* (1998)	MOSES-I (Essery *et al.*, 2003)	Lock *et al.* (2000); Smith *et al.* (1990)
RegCM4[c]	M	50 km	H	sigma 18	MIT (Emanuel and Zivkovic-Rothman, 1999)	NCAR CCM3 (Kiehl *et al.*, 1996)	Pal *et al.* (2000)	NCAR CLM3.5 (Bonan *et al.*, 2002; Steiner *et al.*, 2009)	Modified Holtslag (Holtslag *et al.*, 1990)
SNU-MM5[d]	M	50 km	NH	sigma 24	Kain-Fritsch (Kain and Fritsch, 1990)	CCM2 (Briegleb, 1992)	Lynn *et al.* (2005)	NCAR CLM3.5 (Bonan *et al.*, 2002)	YSU (Hong *et al.*, 2006)
YSU-RSM[e]	LC	50 km	H	sigma 28	Arakawa-Achubert (Hong and Pan, 1998)	Chou (1992); Chou *et al.* (1999)	Hong *et al.* (1998)	NOAH (Chen and Dudhia, 2001)	YSU (Hong *et al.*, 2006)

Institute running the models: [a]Freie Universität Berlin, Germany; [b]National Institute of Meteorological Research, South Korea; [c]National Institute of Meteorological Research, South Korea; [d]Seoul National University, South Korea; [e]Yonsei University, South Korea

Table 3.2 Main characteristics of the observational and re-analysis precipitation datasets.

Data set	Product	Full name	Temporal resolution	Reference
APHRODITE (www.chikyu.ac.jp/precip/)	APHRO_V1003R1 Monsoon Asia + Russia	Asian Precipitation-Highly-Resolved Observational Data Integration Towards Evaluation of the Water Resources	Daily	Yatagai *et al.* (2009)
CRU (www.cru.uea.ac.uk)	TS 3.21	Climatic Research Unit	Monthly	Harris *et al.* (2014)
ERA-Interim (www.ecmwf.int)	Re-analysis	Re-analysis data from European Centre for Medium-Range Weather Forecasts	Daily	Dee *et al.* (2011)
GPCC (http://gpcc.dwd.de)	v6	Global Precipitation Climatology Centre	Monthly	Schneider *et al.* (2014)
GPCP (http://precip.gsfc.nasa.gov/)	v2.2	Global Precipitation Climatology Project	Monthly	Adler *et al.* (2003)
TRMM (http://mirador.gsfc.nasa.gov/)	3B42	Tropical Rainfall Measuring Mission	3 hourly	Huffman *et al.* (2007)

(1) the annual mean precipitation (AM); (2+3) the first and second annual cycle modes of the annual variation of the precipitation (AC1 and AC2); and (4) monsoon precipitation intensity and monsoon domain (MPI and monsoon domain) (Lee and Wang, 2014; Wang *et al.*, 2011). Following Lee and Wang (2014), this chapter analysed the four parameters of each model simulation and MME to evaluate the capacities of the models in reproducing the Asian monsoon system. The PCC and the normalised RMSE (NRMSE) are used to evaluate the models' capacities. The NRMSE is defined as the RMSE normalised by the standard deviation of observation that is calculated with reference to regional mean of CORDEX-EA.

3.3 Results

3.3.1 Extreme rainfall events

We first checked the ability of each model to simulate an extreme rainfall event which caused severe flooding in the Yangtze River valley and north-east China in the summer of 1998 (Fu *et al.*, 2005). Figure 3.2 shows the total precipitation and mean wind vectors at 850hPa from 11-20 June 1998 of each RCM, the GPCP, the TRMM and the ERA-Interim, respectively. The GPCP, the TRMM and the ERA-Interim show much better consistency, although some significant differences can still be depicted on smaller spatial scales (*e.g.* in the Bay of Bengal and in the tropical eastern Pacific Ocean). The PCC between the GPCP and the TRMM, and the ERA-Interim is 0.90, and 0.85, respectively. All the three datasets capture the rainfall belts along 20°-35°N, 105°-150°E. The RCMs reveal high consistency in reproducing low-level winds compared to the ERA-Interim. Furthermore, the characteristic clockwise (anti-clockwise) circulation patterns over the Western Pacific Ocean-WPO (over north-east China and east Mongolia) which indicate anticyclone (cyclone) cells in corresponding regions are well captured by all the RCMs. The evaporated water vapour is transported within south-westerly monsoonal low-level winds. Over the western part of the WPO High, the moisture flux convergences resulting in rainfall belts along the Yangtze River valley, the East China Sea and the south of Japan, and in the Bay of Bengal. When compared to the observation, most of the models capture the rainfall distribution. More than 200 mm of precipitation accumulation is simulated along the rainfall bands and the calculated PCC ranges from 0.57 to 0.76. The RegCM4 (YSU-RSM) has the best (worst) performance to simulate the flooding, which is able (is not able) to simulate rainfall bands accurately. The MME improves both the precipitation (PCC: 0.84) and the low-level wind patterns when compared to all RCMs with a significant reduction of bias.

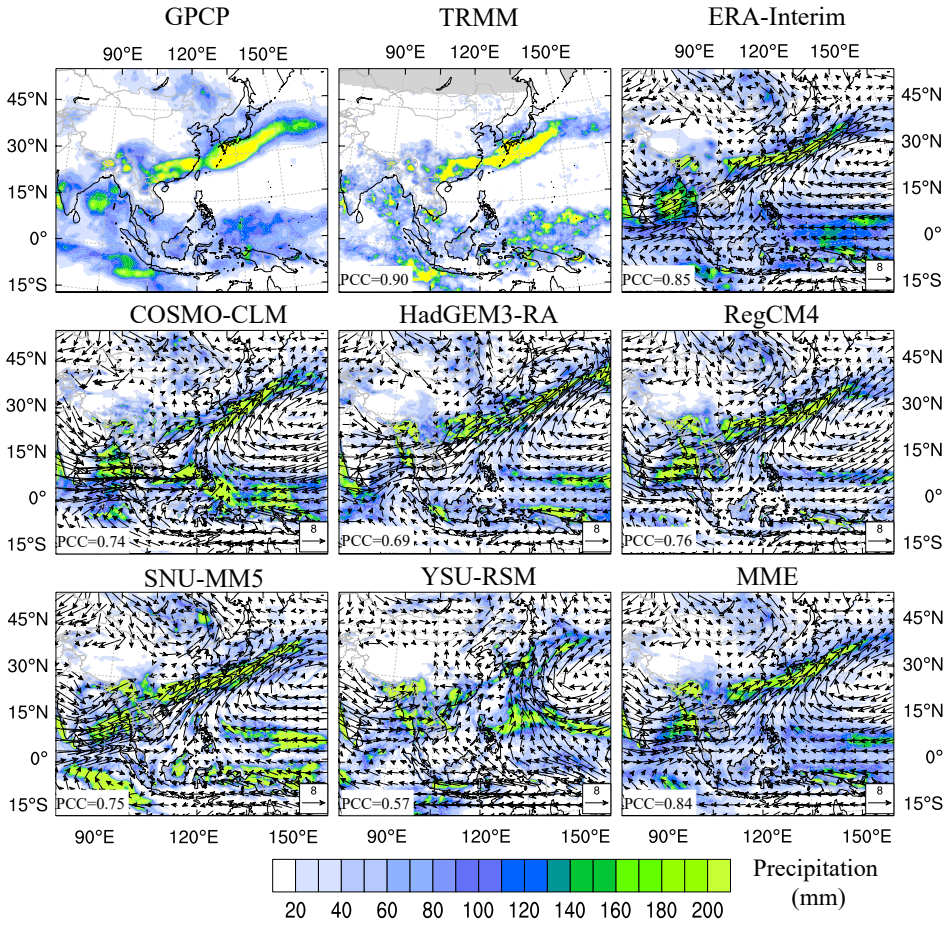

Figure 3.2 Total precipitation and wind vectors at 850 hPa (m s^{-1}) over the period 11-20 June 1998. The numbers in the lower/bottom left-hand corners show the pattern correlation coefficient (PCC) between the observed and simulated rainfall patterns (CORDEX-East Asia).

3.3.2 Seasonality

In summer months (June-July-August; JJA), the observed rain bands stretch from northern India, the Bay of Bengal, the northern Indo-China peninsula and the south of China (Fig. 3.3; GPCP). Meanwhile, the ITCZ reaches its northernmost location. The TRMM shows strong agreement with the GPCP in CORDEX-EA region, which slightly over-estimates (under-estimates) precipitation in the tropics (sub-tropics). The significant difference occurs at the western Tibetan Plateau and the western Indo-China peninsula (Fig. 3.3; TRMM). The ERA-Interim reveals similar summer rainfall patterns as the GPCP, but significantly over-estimates (under-estimates) precipitation in the equatorial Pacific Ocean and the western China (the south of Japan, the Korean peninsula, and the 35°-50°N, 155°-170°E Pacific

Ocean) (Fig. 3.3; ERA-Interim). Figure 3.3 illustrates the gauge-based precipitation datasets and the GPCP demonstrating much better consistency, although some significant differences are shown on smaller spatial scales (*e.g.* in southern India, western Indo-China peninsula, and western Tibetan Plateau).

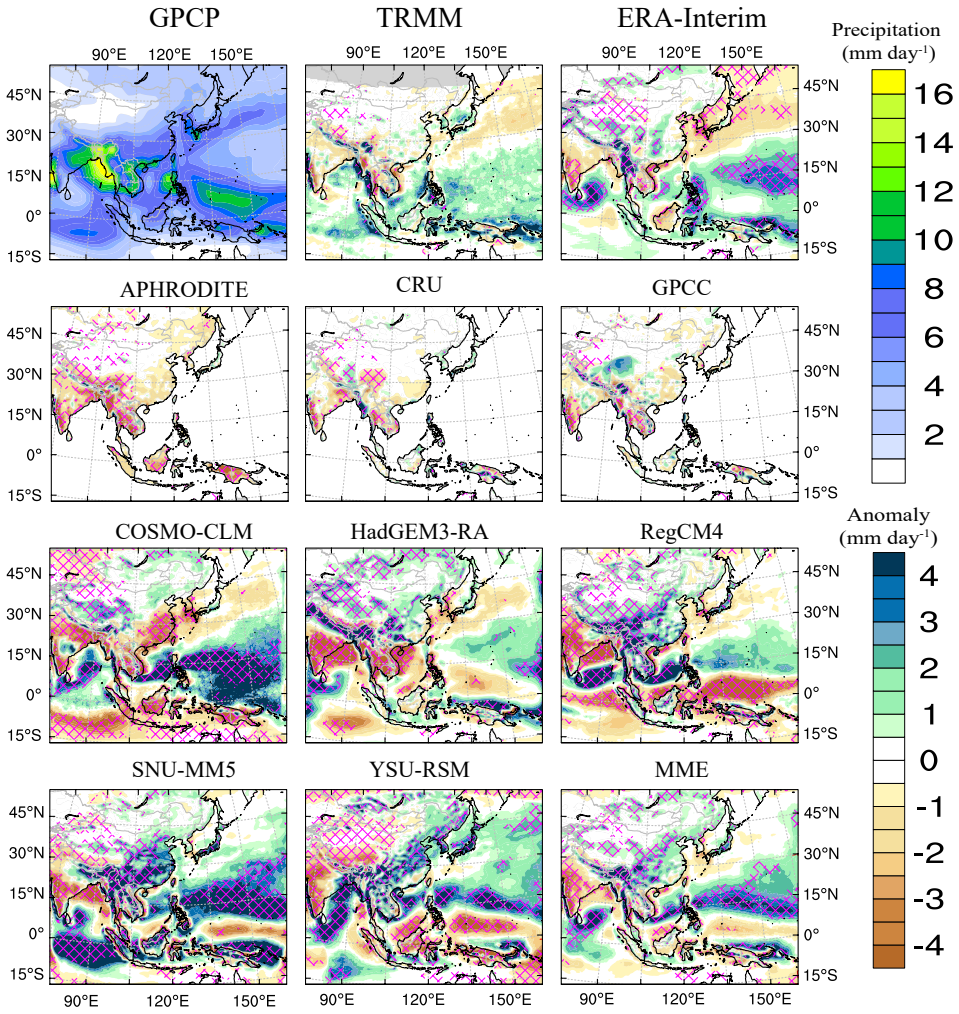

Figure 3.3 Summer (June-July-August; JJA) rainfall of the Global Precipitation Climatology Project (GPCP) and the rainfall anomalies 'observation minus GPCP', and 'model minus GPCP' from 1989-2008. The magenta grids illustrate the significance level at 0.001. MME: multi-model ensemble mean.

RCMs indicate good performance over north-east Asia (40°-50°N, 105°-120°E) and the north-west Pacific Ocean (140°-165°E, 30°-50°N), in which the absolute model bias is less than 1 mm day^{-1} while compared to the observations (Fig. 3.3). RCMs simulate a drier Indian sub-continent, except the COSMO-CLM reproduces a slight wetter central India. The COSMO-CLM, the HadGEM3-RA, the RegCM4 and the SNU-MM5 tend to

over-estimate the precipitation over the Tibetan Plateau, especially at the Himalayas (>4 mm day^{-1}), where the YSU-RSM simulates less precipitation (∼3 mm day^{-1}). COSMO-CLM and HadGEM3-RA (RegCM4, SNU-MM5 and YSU-RSM) exhibits negative (positive) bias over Indo-China peninsula. In Indonesia and Malaysia, the SNU-MM5 calculates wetter conditions (>4 mm day^{-1}) while other models simulate a drier conditions.

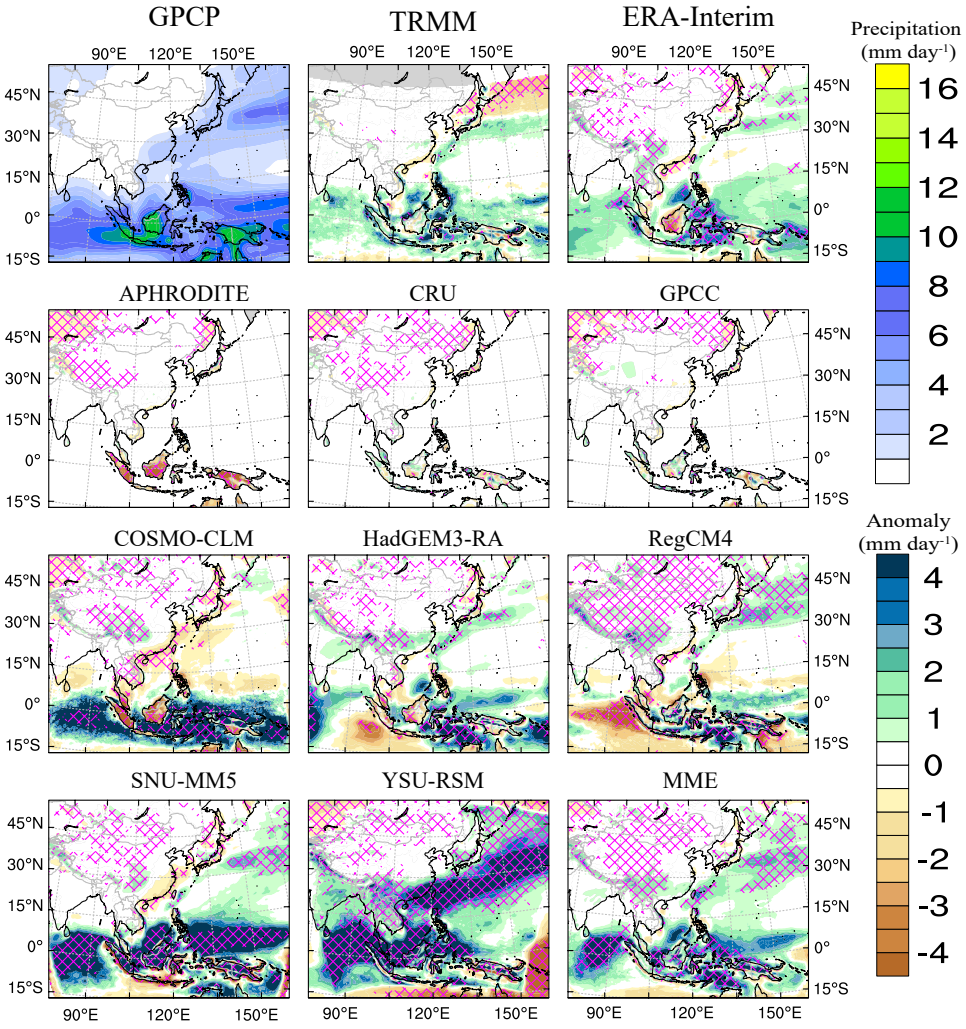

Figure 3.4 As in Fig.3.3, but for the winter season (DJF).

In the winter (DJF) season, the rain bands withdraw to the south with maximum of precipitation (>16 mm day^{-1}) in Indonesia and Malaysia (Fig. 3.4; GPCP). The TRMM shows a good agreement with the GPCP, which has a significant negative bias over the northern Pacific (Fig. 3.4; TRMM). The ERA-Interim and the gauge-based precipitation datasets have the same winter precipitation pattern as the GPCP. Significant negative biases (<1 mm day^{-1}) occur over the central Asia and the east of Siberia.

The RCMs have tendency to simulate wetter conditions in most part of the CORDEX-EA domain (Fig. 3.4). RCMs tend to over-estimate the winter precipitation ($\sim$1 mm day^{-1}) in the Tibetan Plateau and the equatorial ocean, while they have tendency to under-estimate it over central Asia. In south China and the South China Sea, the RCM biases show opposite signs among the individual simulations, where the YSU-RSM (COSMO-CLM) simulates a significant wetter (drier) bias while the other three models have non-significant bias. We found that the YSU-RSM demonstrates too much precipitation over 20°-40°N, 120°-165°E Pacific Ocean.

The statistical evaluation of the model performances in simulating the spatial precipitation patterns over four sub-monsoon domains during the present (1989-2008) climate period are presented in Table 3.3. For summer season, the TRMM is a good agreement with the GPCP over the four sub-monsoon domains, while the ERA-Interim significantly under-estimates (over-estimates) precipitation in the EAS (WNP). Compared to the GPCP, the APHRODITE has a significant dry bias, while the CRU and the GPCC are showing consistency.

The RCMs tend to simulate more precipitation in the SAS, the EAS and the WNP, but less precipitation in the AUSMC. In the SAS, the bias ranges from -0.07 to 1.51 mm day^{-1}, but only the YSU-RSM simulates a significant wetter condition (1.51 mm day^{-1}). The COSMO-CLM (BIAS: -1.00 mm day^{-1}) simulates a drier EAS, while the other four RCMs are wetter with the BIAS range from 0.38 to 1.93 mm day^{-1}. The same as in the EAS, the RCMs have a tendency to simulate more precipitation in the WNP, except the HadGEM3-RA (BIAS: -1.30 mm day^{-1}). RCMs slightly under-estimate the JJA rainfall in the AUSMC where the COSMO-CLM simulates the wettest condition (BIAS: 0.98 mm day^{-1}). Furthermore, the RCMs show higher RMSEs (1.28-5.50 mm day^{-1}) in the SAS and lower RMSEs (0.03-0.19 mm day^{-1}) in the AUSMC. The RCMs capture summer precipitation patterns better in the EAS (PCC: 0.95-0.97) than in the other three regions.

In winter season, the TRMM and the ERA-Interim show good agreement to the GPCP. The re-gridded gauge datasets slightly under-estimate the precipitation in the four sub-monsoon regions, especially in the EAS (BIAS: -0.52, -0.53, -0.56 mm day^{-1}, respectively). The APHRODITE has the significant negative bias for the DJF rainfall in the CORDEX-EA. When compared to summer season, the RCMs tend to over-estimate the winter precipitation in the four sub-monsoon regions, except in the AUSMC. It is worth mentioning that the COSMO-CLM simulates noticeable dry bias in the SAS and the WNP, where the other RCMs present significant wet bias. The RMSEs (0.68-1.43 mm day^{-1}) in the AUSMC are larger than in the SAS ($<$0.47 mm day^{-1}), in the EAS ($<$1.28 mm day^{-1}) and in the WNP ($<$0.64 mm day^{-1}).

In both seasons, the MME captures the precipitation patterns better than the individual models, leading to the highest PCC and the lowest BIAS and RMSE (Table 3.3). In JJA, the precipitation difference between the MME and the observations is from -1.0 to 1.0 mm day^{-1} in most parts of the CORDEX-EA (Fig. 3.3). The significant positive (negative) bias occurs at the 5°-15°N, 135°-165°E Pacific Ocean (the Indian sub-continent). For DJF, the MME shows wetter conditions than the GPCP (*e.g.* in central China, the Mongolia and the 28°-55°N, 140°-165°E Pacific Ocean), especially in the equatorial area (>3 mm day^{-1}) (Fig. 3.4). The bias between the MME and the GPCP is significant in the EAS and in the WNP for JJA, in the SAS, in the EAS, and in the WNP for DJF, respectively (Table 3.3).

3.3.3 Annual cycle

Figure 3.5 illustrates the mean annual cycle of precipitation averaged over four sub-monsoon regions as presented in Figure 3.1. The annual cycle depicts the prominent features of the precipitation in this region associated with the summer monsoon: dry conditions in the winter and a rainy season from May to September (November to March) in the northern (southern) hemisphere. The ERA-Interim and the TRMM show consistency to the GPCP in the EAS and the AUSMC, while slightly over-estimate the peak in the SAS and the WNP. In general, the two datasets exhibit good agreement to the GPCP in the monsoon process (*i.e.* onset and retreat).

In the SAS, most of the RCMs are in close agreement with the observations, only the YSU-RSM simulates a slightly wetter (<1 mm day^{-1}) summer and winter. In the EAS, the RCMs simulate two peaks in June and August. Furthermore, the RCMs demonstrate a large spread in simulating summer precipitation and a small amplitude in the pre-monsoon and post-monsoon seasons. The COSMO-CLM identifies a negative bias, while other models tend to a positive bias, especially in the summer. The YSU-RSM simulates a much wetter winter (2 mm day^{-1}) and summer. Over the WNP, most of the RCMs indicate an earlier onset of the rainy season (May) compared to observations (June) and indicates that it is much wetter throughout the year. As well as in the EAS, the YSU-RSM shows a much wetter winter (2 mm day^{-1}) and summer. The HadGEM3-RA calculates a consistent onset of the rainy season, but fails to simulate the maximum and the withdrawal of the monsoon. In the AUSMC, the models demonstrate the annual cycle well, only the YSU-RSM fails to exhibit the peak of the summer rainfall (January-March), while the HadGEM3-RA and the COSMO-CLM both over-estimate the rainy season rainfall.

The MME is closer to the observed annual cycle than the individual models. The RCMs have a better performance in simulating the annual cycle in the SAS and the AUSMC than in the EAS and the WNP.

Table 3.3 BIAS (mm day^{-1}), root-mean-square error (RMSE, mm day^{-1}) and pattern correlation coefficient (PCC) between the simulated precipitation and the observation (Global Precipitation Climatology Project, GPCP) for JJA and DJF over the 4 sub-monsoon domains (SAS: South Asian Summer monsoon, EAS: East Asian Summer monsoon, WNP: Western North Pacific tropical monsoon, AUSMC: Australian-Maritime Continent monsoon). MME: multi-model mean. $^{*}p < 0.01$; $^{**}p < 0.001$

		SAS			EAS			WNP			AUSMC		
		BIAS	RMSE	PCC	BIAS	RMSE	PCC	BIAS	RMSE	PCC	BIAS	RMSE	PCC
JJA	TRMM	0.96	1.15	0.96	0.07	0.11	0.99	0.82	0.39	0.97	-0.02	0.02	0.95
	ERA-Interim	0.28	0.64	0.96	-0.22**	0.28	0.97	1.13**	0.39	0.97	0.20	0.03	0.97
	APHRODITE	-1.71*	0.70	0.92	-0.95**	0.10	0.99	-2.39*	0.16	0.95	-0.44*	0.01	0.96
	CRU	-0.47*	0.41	0.96	-0.37	0.05	0.99	-0.79	0.09	0.96	0.04	0.00	0.95
	GPCC	0.62**	1.28	0.91	-0.35	0.08	0.98	-0.81	0.16	0.94	0.01	0.01	0.95
	COSMO-CLM	-0.07	1.27	0.93	-1.00	0.51	0.95	3.35**	2.43	0.92	-0.98**	0.11	0.88
	HadGEM3-RA	0.40	5.52	0.81	0.38**	0.54	0.95	-1.30*	0.70	0.92	-0.07	0.04	0.92
	RegCM4	-0.07	2.82	0.86	0.83**	0.72	0.95	2.16**	1.22	0.95	-0.19	0.07	0.85
	SNU-MM5	0.29	2.65	0.89	1.93**	1.02	0.96	3.12**	1.60	0.94	-0.03	0.14	0.83
	YSU-RSM	1.51**	3.45	0.90	1.83**	0.84	0.97	2.33**	0.98	0.96	0.11	0.19	0.80
	MME	0.41	1.56	0.93	0.80**	0.34	0.97	1.93**	0.75	0.96	-0.24	0.04	0.90
DJF	TRMM	0.01	0.01	0.95	0.10	0.03	0.96	0.15	0.05	0.95	0.80	0.20	0.99
	ERA-Interim	0.25*	0.04	0.86	0.09	0.04	0.95	0.63	0.10	0.95	0.57	0.18	0.98
	APHRODITE	-0.10*	0.00	0.94	-0.52*	0.00	0.98	-0.47*	0.01	0.90	-2.28**	0.08	0.98
	CRU	-0.10	0.00	0.94	-0.53**	0.00	0.98	-0.09	0.01	0.87	0.68*	0.03	0.99
	GPCC	0.06	0.00	0.91	-0.56**	0.01	0.97	-0.20	0.01	0.85	0.11	0.05	0.98
	COSMO-CLM	-0.14**	0.02	0.75	-0.22	0.06	0.90	-0.50*	0.04	0.95	2.48**	1.41	0.94
	HadGEM3-RA	0.49**	0.09	0.79	0.41**	0.08	0.95	0.12	0.07	0.93	1.24*	0.67	0.95
	RegCM4	0.35*	0.06	0.76	0.31*	0.06	0.93	-0.08	0.05	0.93	0.26	0.97	0.91
	SNU-MM5	0.00	0.02	0.89	-0.01	0.05	0.92	1.30**	0.39	0.93	0.35	0.82	0.93
	YSU-RSM	1.82**	0.47	0.93	2.24**	1.31	0.90	2.36**	0.65	0.90	-0.33	0.83	0.92
	MME	0.50*	0.05	0.93	0.55**	0.08	0.96	0.64**	0.09	0.96	0.74	0.35	0.97

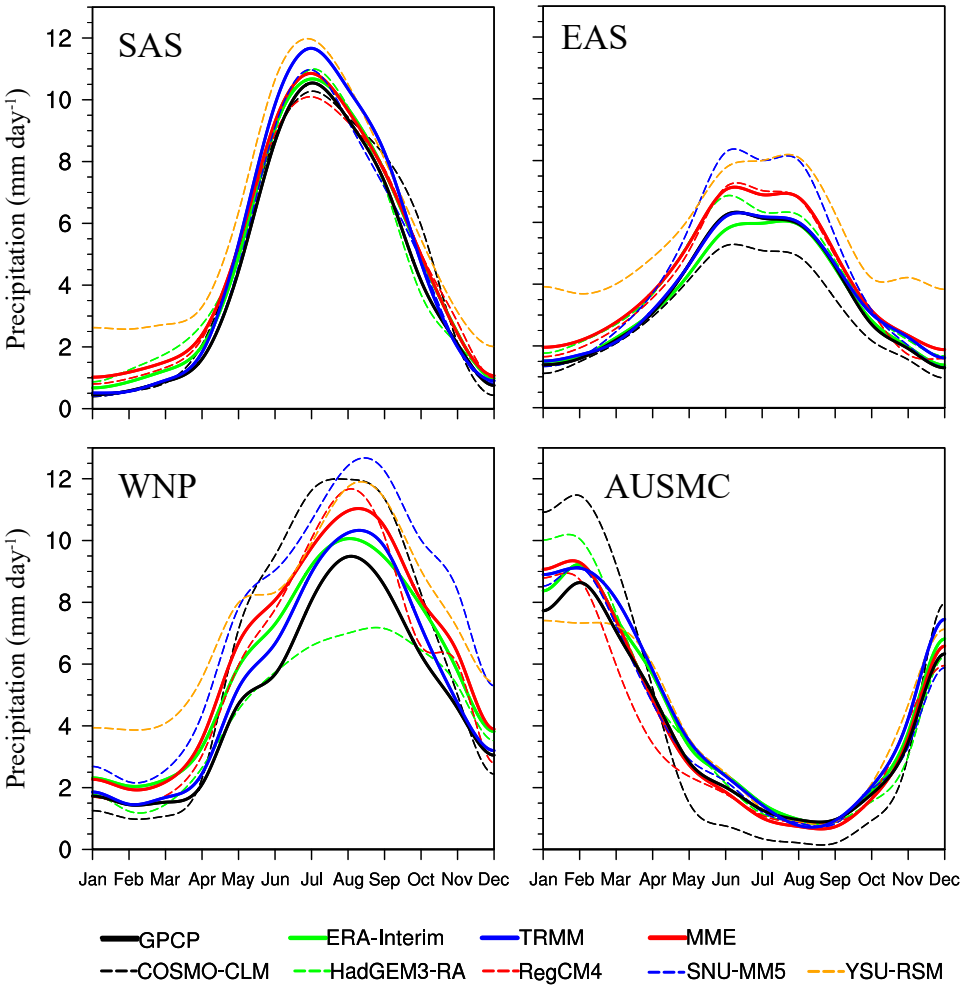

Figure 3.5 Annual cycle of monthly precipitation averaged over the 4 sub-monsoon domains for the period 1989-2008 for the Global Precipitation Climatology Project (GPCP, solid black line), the ERA-Interim (solid green line), the TRMM (solid blue line), each of the regional climate models (RCMs, coloured dashed lines) and their multi-model ensemble mean (MME, solid red line).

3.3.4 Inter-annual variability

The temporal statistics describing inter-annual variability of the JJA and the DJF mean precipitation averaged over the four sub-monsoon domains is shown in Figure 3.6 for the ERA-Interim, each of the RCM members and the MME compared to the GPCP. For the JJA, the inter-annual variability of the precipitation is less prominent over the SAS. The ERA-Interim calculates a low correlation co-efficient (0.33) with the GPCP. The majority of the RCMs fail to reproduce the year-to-year variations of the precipitation with a relatively low correlation co-efficient. We note that the RegCM4 shows a better performance in representing the inter-annual variations of rainfall with a higher correlation co-efficient of 0.60 and medium normalised standard deviations of 1.64. For the HadGEM3-RA, we calculated the lowest correlation co-efficient (0.11). The GPCP and the ERA-Interim represent a strong correspondence in the sign and magnitude of the inter-annual variability in the EAS with a high correlation co-efficient of 0.81. The RCMs exhibit a lesser discrepancy to the observations, with a generally higher correlation co-efficient in the EAS compared to the SAS. The HadGEM3-RA and the YSU-RSM have a worse performance to capture the inter-annual variability comparing to the other models. In the WNP, the RCMs exhibit a wide spread (ranging from 4 to 8 mm day^{-1}) in simulating the precipitation. The models fail to capture the inter-annual variability. The best performance is shown in the RegCM4 (correlation co-efficient: 0.72). Compared to GPCP, the RCMs capture the sign and magnitude of the inter-annual variability well. In the AUSMC, for the majority of the RCMs, the correlation co-efficient is above 0.76, while the correlation of the SNU-MM5 is much higher (0.91).

Similar as in summer season, RCMs illustrate an insufficient performance in representing the winter precipitation inter-annual variability over the SAS (Fig. 3.6; *cf.* DJF). The RCMs exhibit a good performance in capturing winter precipitation year-to-year variation over the EAS, the WNP and the AUSMC, with a closer agreement of inter-annual rainfall variability and a higher correlation co-efficient compared to the GPCP. The ERA-Interim shows a close correspondence in reproducing the sign and magnitude of winter precipitation to the GPCP over the four regions. The SNU-MM5 exhibits the best performance in capturing the winter precipitation inter-annual variability with a relative higher correlation co-efficient ($>$0.80) and closer year-to-year variation ($\sim$1.10) to the GPCP over the four sub-monsoon regions. We found that the YSU-RSM significantly over-estimates the winter precipitation ($>$2 mm day^{-1}) compared to the observation in the SAS, the EAS and the WNP. In addition, the YSU-RSM calculates the lowest correlation co-efficient compared to the other four models, especially in the SAS.

In summer and winter season, the MME shows a better overall variability than most RCMs in the four regions, with a relative smaller bias and higher correlation co-efficient. Note

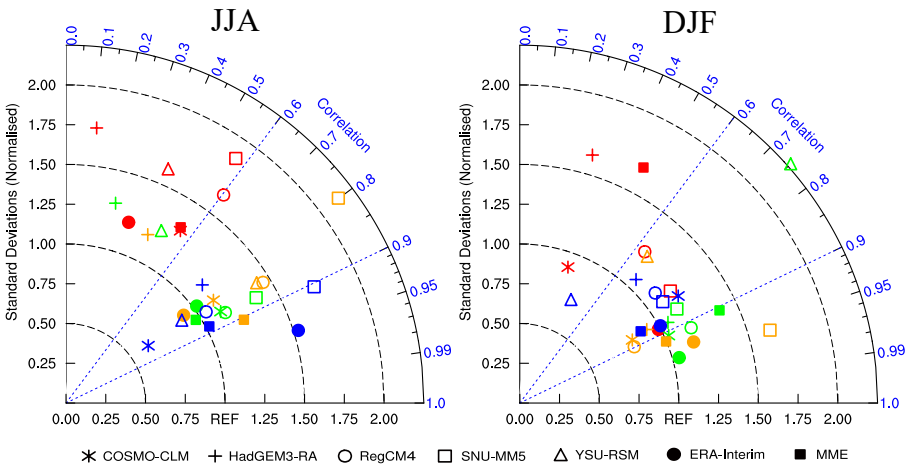

Figure 3.6 Temporal statistics describing inter-annual variability of the models in terms of the JJA and DJF mean precipitation, the multi-model ensemble mean (MME) and the ERA-Interim compared with the Global Precipitation Climatology Project (GPCP) over the South Asian Summer monsoon (red), the East Asian Summer monsoon (green), the Western North Pacific Tropical monsoon (orange) and the Australian-Maritime Continent monsoon (blue).

that the MME shows a relative larger difference of winter precipitation than the ERA-Interim, and several of the RCMs in the SAS.

3.3.5 Monsoon characteristics

Compared to the GPCP, the merged observation (APHRODITE, CRU and GPCC; PCC: 0. 98, NRMSE: 0.21) has small negative biases (-1 mm day^{-1}) of the annual mean precipitation over western India and the central China, whereas small positive biases occur over the Himalayas (Fig. 3.7a; *cf.* Observation). The MME is able to reproduce the observed spatial distribution features of the annual mean precipitation as well as the major tropical convergence zones over the ocean and the main rainfall belts in the extra-tropical Pacific. The differences between the observations and the individual model simulations show that the MME simulates wetter conditions over equatorial Indian Ocean, the Bay of Bengal, the equatorial western Pacific and southern Himalayas, but a drier central Asia and Indian sub-continent (Fig. 3.7a; *cf.* MME). Furthermore, over the tropics, the HadGEM3-RA simulates more accurate precipitation patterns, while the COSMO-CLM, the SNU-MM5 and the YSU-RSM show wetter and the RegCM4 drier conditions. The PCC of the individual models vary from 0.91 to 0.95, and the NRMSEs vary from 0.66 to 1.19. Compared to other RCMs, the HadGEM3-RA (SNU-MM5) has a relative better (worse) performance (NRSME: 0.66 (1.19)) in reproducing

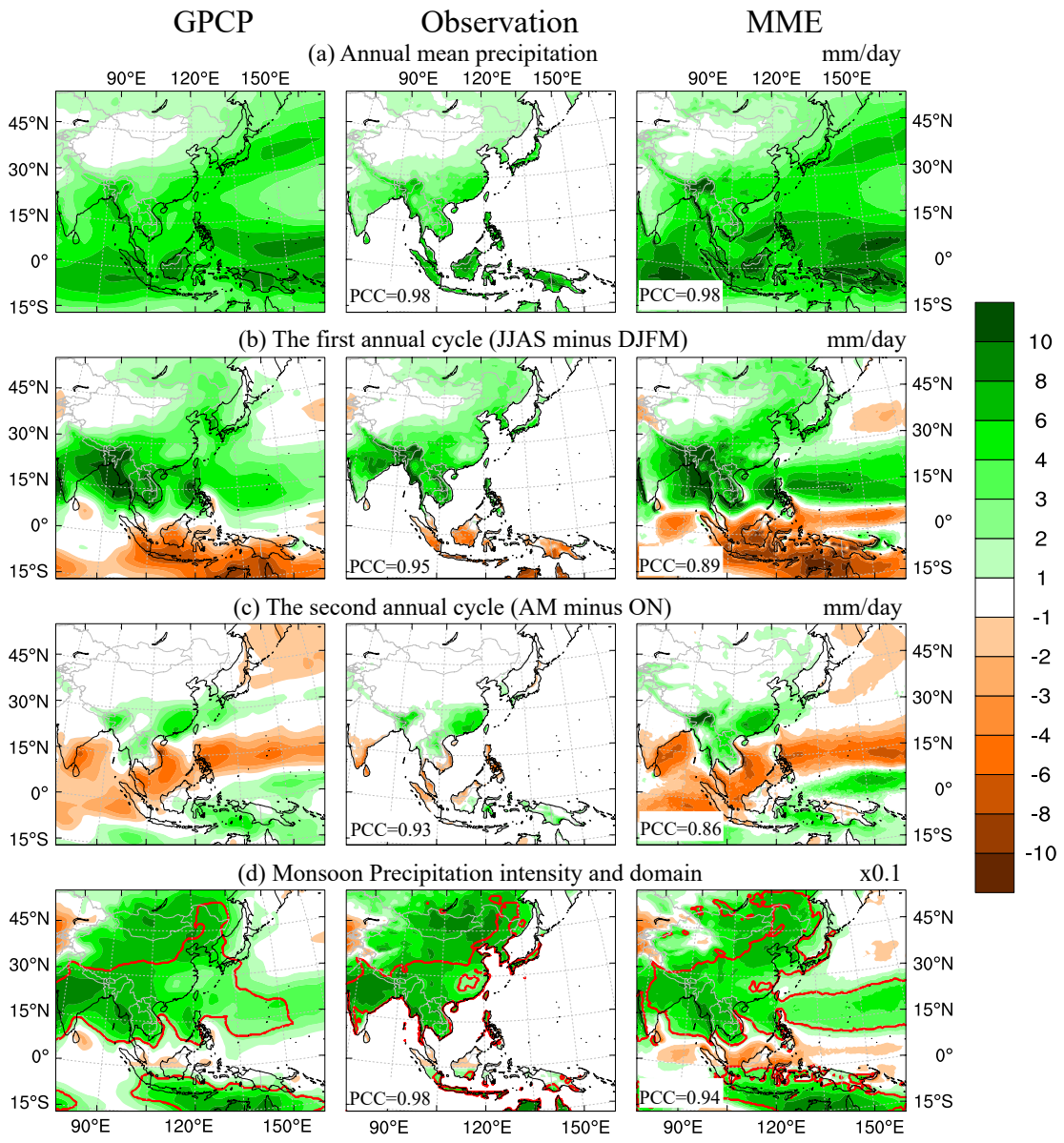

Figure 3.7 Comparison of the precipitation climatology (1989-2008) between the Global Precipitation Climatology Project (GPCP), the merged observation (APHRODITE, CRU, GPCC; datasets are described in Table 3.2) and the multi-model ensemble mean (MME): (a) annual precipitation rate (mm d^{-1}); (b) the first annual cycle mode (AC1, June-September minus December-March); (c) the second annual cycle model (AC2, April-May minus October-November); and (d) monsoon precipitation intensity (non-dimensional) and domain. The numbers in the bottom left-hand corners show the pattern correlation coefficient (PCC) between the observed and the simulated patterns (CORDEX-East Asia).

spatio-temporal patterns of annual mean precipitation. The MME is significantly better than the individual models in simulating the annual mean precipitation with a PCC of 0.98 and a NRMSE of 0.61 (Fig. 3.8).

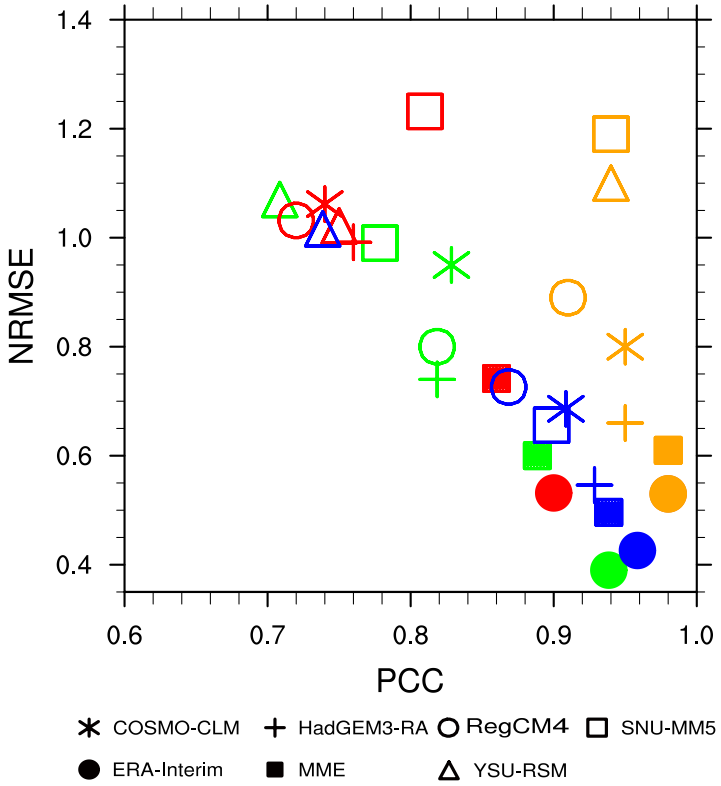

Figure 3.8 Performance of the regional climate models and their multi-model ensemble mean (MME) on precipitation climatology (1989-2008): the annual mean precipitation (orange), the first annual cycle mode (June-September minus December-March; green), the second annual cycle mode (April-May) minus October-November; red, and the monsoon precipitation intensity (the ratio of 'summer minus winter' to annual total precipitation; blue). The abscissa and ordinates are pattern correlation coefficient (PCC) and domain-averaged root-mean-square error normalised by the observed spatial standard deviation (NRMSE), respectively.

The first annual cycle mode (AC1, summer-winter asymmetric mode) is the difference in the precipitation between June-September (JJAS) and December-March (DJFM), while the second annual cycle mode (AC2, spring-fall asymmetric mode) is the difference between April-May (AM) and October-November (ON) (Lee and Wang, 2014; Wang and Ding, 2008). Compared to the GPCP, the Observation represents the first and the second annual cycle mode with a high degree of accuracy. The MME tends to over-estimate the magnitude of the AC1 over the extra-tropical Pacific Ocean and to under-estimate it over the East China Sea

(Fig. 3.7b; *cf.* MME). The model simulations can reproduce the observed AC1 realistically with PCCs ranging from 0.71 to 0.83 and NRMSEs ranging from 0.74 to 1.07, respectively (Fig. 3.8). However, the SNU-MM5 simulates a stronger AC1 over both the NWP and the EAS. At the same time, the SNU-MM5 has almost the worst performance (PCC: 0.71, NRMSE: 0.99) in representing the AC1. Furthermore, the model simulations have difficulties in capturing the AC2, as the model spread for this mode is much larger. The PCCs vary from 0.72 to 0.81 and the NRMSEs vary from 0.73 to 1.22, respectively (Fig. 3.8). The MME out-performs to show the AC1 and AC2 better than the individual models, and is more effective for the AC1 than the AC2. The MMEs PCC is 0.89 (0.86) and its NRMSE is 0.60 (0.73) for the AC1 (AC2), respectively, averaged over the CORDEX East Asia region.

Wang *et al.* (2011) defined the monsoon precipitation intensity (MPI) as the ratio of "summer minus winter" compared to annual total precipitation, and the monsoon domain as the regions where the "summer minus winter" precipitation exceeds 2.5 mm day^{-1} and the summer precipitation exceeds 55 percent of the annual total. Compared to the GPCP, the Observation captures the MPI and monsoon domain over land well with a PCC of 0.98 and an NRMSE of 0.43. The individual models show a good performance in representing the MPI pattern with PCCs ranging from 0.74 to 0.93 and NRMSEs ranging from 0.55 to 1.02 (Fig. 3.8). The YSM-RSM has the worst performance in simulating the MPI with the lowest PCC (0.74) and NRMSE (1.02), and the MPI is significantly under-estimated. The HadGEM3-RA shows the best agreement in the MPI (PCC: 0.93, NRMSE: 0.55) and the monsoon domain compared to the GPCP. The MME exhibits an eastern extension of the WNP domain towards the middle Pacific and a northern extension of the EAS domain towards eastern Siberia, while it fails to show the monsoon domain over the East China Sea. Similar to other three metrics, the MME improves the performance to reproduce the MPI when compared to the individual models with a higher PCC (0.94) and a lower NRMSE (0.50).

3.4 Summary and discussion of Chapter 3

This is the first evaluation of the precipitation climatology based upon an ensemble of regional climate model simulations performed within the CORDEX-EA project. In this regard, five different RCMs, driven by the ERA-Interim, have been run at ∼50 km horizontal resolution over the period from 1989-2008. We examined the performance of the individual models and the ensemble mean in reproducing present-day inter-annual variability, annual cycle, and seasonal mean precipitation as well as monsoon characteristics. Gridded monthly precipitation datasets (*i.e.* the GPCP and the ERA-Interim) have been used as comparison data to evaluate the model performances.

(1) The RCMs from the CORDEX-EA are able to capture the pronounced extreme rainfall event as observed from 11-20 June 1998 (Fig. 3.2), which could not be reproduced well by former RCM studies (*e.g.* RMIP Asia; Fu *et al.* 2005). Models from the RMIP Asia tend to over-estimate the precipitation at high latitudes (Fu *et al.*, 2005) and fail to reproduce the heavy rainfall belts along the Yangtze River valley, the East China Sea and the south of Japan. This might be due to a new RCM generation (*e.g.* RegCM4) used for the CORDEX-EA with better physical parametrisation compared to the RCMs (*e.g.* RegCM2) from RMIP Asia (Giorgi *et al.*, 2012). Furthermore, the SNU-MM5 also joined in the RMIP (named as SNU RCM). The SNU-MM5 and the SNU RCM have the same physical package, but a different convection scheme, Kain-Fritsch and Grell, respectively (Fu *et al.*, 2005; Hong *et al.*, 2006). The SNU-MM5 shows a better performance in capturing the extreme rainfall event than the SNU RCM from RMIP. Kain-Fritsch convection scheme is able to better capture the extreme rainfall than the Grell in SNU-MM5/SNU RCM.

(2) In general, most of the CORDEX-EA RCMs capture the main features of the seasonal mean rainfall patterns (Fig. 3.3 and Fig. 3.4), the annual cycles (Fig. 3.5), and the inter-annual variability (Fig. 3.6). However, we found significant biases in the individual models depending on both the region and the season. In summer, the RCMs tend to over-estimate the precipitation over the Tibetan Plateau, except the YSU-RSM, which simulates a drier Tibetan Plateau. All the RCMs simulate a significant drier Indian sub-continent (>3 mm day^{-1}) (Fig. 3.3). In winter, the RCMs have tendency to reproduce a wetter continent. The HadGEM3-RA and the RegCM4 capture the precipitation well, while the COSMO-CLM, SNU-MM5 and YSU-RSM are too wet (>4 mm day^{-1}) in the tropics (Fig. 3.4). The RCMs simulate the annual cycle better in the SAS and the AUSMC than in the EAS or the WNP (with less difference from the observation), especially in summer (Fig. 3.5). Furthermore, the models show the precipitation inter-annual variability better in the EAS and the AUSMC than in the SAS and the WNP (Fig. 3.6). The MME generally out-performs many of the individual models with biases of similar magnitude compared to observational datasets. Similar as earlier findings in multi-model studies (Gbobaniyi *et al.*, 2014; Nikulin *et al.*, 2012; Paeth *et al.*, 2011), the good performance is mostly influenced by the elimination of the opposite-signed biases among the models, *e.g.* in south China and the Tibetan Plateau.

Compared to the GPCP, the significant bias over the south Himalayas and the Kunlun Mountains owning to the low density of meteorological station (Wu *et al.*, 2011; Yatagai *et al.*, 2009). Therefore, the bias of the RCMs in small-scale region is not accurate due to the uncertainty of observations (Stephens *et al.*, 2012). In addition, the models substantially differ in simulating monsoon precipitation indicating that the internal dynamics and physics playing an essential role on the RCMs performance. The RegCM4 and the SNU-MM5

show the same pattern in the precipitation bias over the continent due to using the same land surface scheme and a similar radiation scheme. However, the RegCM4 and the SNU-MM5 present a different bias pattern over ocean (Fig. 3.3, *c.f.* RegCM4 and SNU-MM5). We can conclude that the convection scheme plays an important role on simulating monsoon precipitation, especially over the ocean, which coincides to the finding from Sylla *et al.* (2011). Furthermore, the RegCM4 and the SNU-MM5 has the same dynamic core, but the RegCM4 (SNU-MM5) adapts hydrostatic (non-hydrostatic) primitive equations (Giorgi *et al.*, 2012; Lee *et al.*, 2004). Additionally, the RegCM4 shows better performance in capturing short-to-long term temporal scale of precipitation than the SNU-MM5. Non-hydrostatic model do not outperform hydrostatic model. It is worth mentioning that only the HadGEM3-RA does not implement the spectral nudging technique. The HadGEM3-RA exhibits an acceptable performance in capturing the pattern and the annual cycle of precipitation, but a relative worse performance in representing the inter-annual variability of precipitation.

The COSMO-CLM and the SNU-MM5 have significant positive bias over the extra-tropical Pacific (10°-20°N, 120°-165°E), but the COSMO-CLM under-estimates the summer precipitation over south China while the SNU-MM5 over-estimates it. Hence, the COSMO-CLM and the SNU-MM5 illustrate a compelling discrepancy of annual cycle over the EAS and the WNP. Moreover, The HadGEM3-RA fails to capture the annual cycle in the WNP (Fig. 3.5) because the significant under-estimating precipitation over the South China Sea (Fig. 3.3, *c.f.* HadGEM3-RA). In SAS, the RCMs show a large discrepancy among each other in simulating seasonal rainfall on inter-annual time scale due to the un-coupled RCMs do not capture the large-scale Ocean oscillation (Jiang *et al.*, 2013*a*). In addition, ENSO provides the most systematic forcing of inter-annual variability for Asian monsoon system (Annamalai *et al.*, 2007; Wang, 2006; Wang *et al.*, 2000). RCMs exhibit the different performance in describing the year-to-year variation in the four sub-monsoon regions. In East Asia, the RCMs might be having the ability to capture the Pacific-East Asian teleconnection which is a mechanism that links central Pacific SST anomalies with East Asian climate variations (Wang *et al.*, 2000). However, the RCMs show the worst performance in capturing the inter-annual variability in South Asia due to most of the climate models could not represent the correlation between observed precipitation and ENSO (Annamalai *et al.*, 2007). After fixing this problem, the coupled RCM will be a helpful approach in the future regional dynamic downscaling.

(3) For the monsoon characteristics, the RCMs show close correspondence to the observations (Fig. 3.7 and Fig. 3.8). The monsoon is characterised by an annual reversal of the low-level winds and well-defined dry and wet seasons (Wang and Ding, 2008), the variability of which is of great importance for simulating future climate impacts (Colman *et al.*, 2011;

Turner and Annamalai, 2012; Wang, 2006). The metric of annual mean precipitation, the AC1 and the AC2 is the basis for MPI and monsoon domain. The accuracy of MPI and monsoon domain indicates the model performance in capturing the intra-seasonal rainfall variations. The MPI strongly depends on the difference of precipitation between rainy and dry season. YSU-RSM shows an insufficient performance in capturing the annual cycle, especially in winter season over the SAS, the EAS and the WNP (Fig. 3.5). Hence, YSU-RSM has fewer skills (higher NRMSE and lower PCC) to represent the AC1 and MPI (Fig. 3.8). Furthermore, the IPCC AR5 indicates that multi-model ensemble means from CMIP5 fails to capture the MPI and the monsoon domain over the Western North Pacific-East Asia monsoon region, while its performance is improved when compared to CMIP3 (Flato *et al.*, 2013), because the high resolution RCMs are able to resolve the topography and coastlines. The RCMs better capture the monsoon characteristics over the Korean Peninsula, the Korea Strait and southern Japan than the CMIP5 models.

This chapter discussed the CORDEX-East Asia models in representing the precipitation climatology and monsoon characteristics under validation framework. Current set up of the RCMs can be used for further dynamical downscaling. A downscaling application will be launched (in Chapter 4) to address if the set up improve the model performance (from AOGCM to RCM) in producing the EASM. It employs a prediction system (MPI-ESM-LR) from Chapter 5 to drive the COSMO-CLM.

Chapter 4

Dynamical Downscaling with COSMO-CLM in East Asia

4.1 Introduction

Chapter 3 has validated the set up of CORDEX models in representing the precipitation climatology and monsoon characteristics in East Asia. Current set up of the five RCMs can be used to provide useful information on a fine resolution. Toward the major target of this thesis, this chapter uses a particular downscaling simulation to test the improvement by a high resolution RCM. COSMO-CLM (CCLM) was selected for the simulation. The model parametrization scheme is the same as the one used in chapter 3. The driving data is generated by MPI-ESM-LR which contributes to the chapter 5 for studying the seasonal prediction of EASM. This chapter compares the performance of CCLM and MPI-ESM-LR, in simulating the seasonal precipitation and the EASM index.

4.2 Experiment design and comparison data

In this chapter, two experiments (1979-2005) are analysed, which participate in the CORDEX-East Asia project. The boundary condition of the two simulations are the ERA-Interim and the MPI-ESM-LR. The MPI-ESM-LR is a low resolution (atmosphere: T63L47; ocean: GR15L40) of Max Planck Institute for Meteorology (MPI-M) earth system model (MPI-ESM). The first run (r1i1p1) of MPI-ESM-LR is used as the boundary condition in this study. Monthly precipitation, mean sea level pressure, zonal and meridional winds from ERAI-CCLM (boundary condition: ERA-Interim) and MPI-CCLM (boundary condition:

MPI-ESM-LR) are used in this study. Section 3.2 shows the details of CCLM and its parameter schemes.

The GPCP was selected as comparison data for precipitation. The reference data for general circulation is ERA-Interim re-analysis dataset. The MPI-ESM-LR was also applied into comparison. All the datasets are remapped to CORDEX-East Asia grids by bi-linear interpolation.

4.3 Result

4.3.1 Seasonality

The main rainfall band migrates with ITCZ shifting. In winter months (Fig. 4.1; DJF), the rainfall band occurs in the tropics of south Hemisphere. In summer (Fig. 4.1; JJA), the ITCZ reaches its northernmost location. There are two rainfall branches in the East Asia. The south branch is from the Bay of Bengal to the Philippine Sea, while the north branch occurs from the eastern China to the north-west of Pacific Ocean. The GCM (Fig. 4.1; *i.e.* MPI-ESM-LR) can capture the shifting of rainfall band. However, it simulates a wetter-drier-wetter condition from the south to the north in the CORDEX-East Asia region. In all the fourth seasons, the MPI-ESM-LR shows a significant negative BIAS of rainfall in the India, the Indo-China peninsula, the south-east of China and the north-west of Pacific Ocean.The MPI-ESM-LR does not simulate the accurate location of the rainfall bands in summer months. It simulates less precipitation in both of the north and south precipitation branches.

Compared to the GPCP, the CCLM produces a significant BIAS of precipitation in specific region and season (Fig. 4.1; ERAI-CCLM). The BIAS centre is shifting with the season change. In the winter, a prominent positive BIAS (>4 mm day^{-1}) centre occurs in the tropics of southern Hemisphere. Then it northward transforms to the north hemisphere in the spring. In the summer months, the positive BIAS centre reaches its northernmost location. It moves southward to the equator in the autumn.

The BIAS of the MPI-CCLM simulated precipitation has the same distribution as the MPI-ESM-LR. However, the CCLM enlarges the BIAS of precipitation. In the summer months, the MPI-CCLM shows a significant negative BIAS (<-4 mm day^{-1}) in the east and south of China where the MPI-CCLM illustrates a slight negative BIAS ($\sim$-1 mm day^{-1}).

The large difference of precipitation is associated to the prominent BIAS of general circulation. In the northern Hemisphere, a northward wind BIAS brings a wetter condition (*e.g.* the western Pacific Ocean) while a southward wind BIAS leads to a dryer condition in the east and south of China.

The statistical evaluation of model performance in simulating the spatial precipitation, zonal and meridional winds at 850 hPa over the CORDEX-East Asia domain during the present (1979-2005) climate period are presented in Table 4.1. The MPI-CCLM exhibits a worse performance in representing the precipitation and wind fields than the ERAI-CCLM and the MPI-ESM-LR. It simulates a larger BIAS and RMSE, but a smaller PCC than its driven data (MPI-ESM-LR).

4.3.2 Monsoon characteristics

Figure 4.2 shows the CCLM and its driven data in capturing the EASM index (EASMI). The EASMI is widely used in studying the variability of EASM (Wang *et al.*, 2008*b*). Its definition has been presented in the Section 2.3.3. There is no doubt that the EASMI simulated by RCM strongly depends upon its driven GCM. The cross correlation coefficient between the ERA-Interim, the MPI-ESM-LR, the ERAI-CCLM, and the MPI-CCLM is presented in Table 4.2. The EASMI produced by ERAI-CCLM exhibits a good agreement with the observation. Compared to the observation, the ERAI-CCLM can capture the phase of EASMI (*i.e.* strong, weak and normal monsoon) in most years. Its EASMI shows a high correlation coefficient (0.92) to the observed.

The MPI-ESM-LR does not capture the inter-annual variation of observed EASMI with a low correlation coefficient (0.24). In specific monsoon year (*e.g.* 1985, 1998 *etc.*), the MPI-ESM-LR does not accurately represent the EASMI. The MPI-CCLM exhibits the consistent as the MPI-ESM-LR in producing the EASMI. It shows a worse EASMI than its driven GCM (*i.e.* MPI-ESM-LR).

The EASMI can indicate the summer rainfall distribution in the East Asia (Fig. 4.3). The Asian summer monsoon rainfall shows a “Sandwich” pattern. In strong monsoon years, the maximum rainfall bands occur from the Indo-China peninsula to the Philippine Sea, and the north-east of Asia; while the maximum rainfall bands occur in the Indonesia and Malaysia, and from the Yangtze River to the north-west of Pacific. The ERAI-CCLM exhibits the similar correlation pattern as the observation. But it cannot represent the significant negative centre in the Yangtze River and Japan.

The correlation between the MPI-ESM-LR simulated EASMI and precipitation shows the negative-positive-negative-positive distribution from south to north. The main precipitation band is shifted southwards. Furthermore, the correlation map does not capture the prominent negative band from the Yangtze River to the Japan. The MPI-CCLM shows a similar correlation map as the MPI-ESM-LR.

Table 4.1 BIAS (mm day^{-1}), root-mean-square error (RMSE, mm day^{-1}) and pattern correlation coefficient (PCC) between the simulated precipitation and the observation (Global Precipitation Climatology Project, GPCP) for DJF-to-SON over the CORDEX-East Asia domain. $^{*}p < 0.01$; $^{**}p < 0.001$

		pr			ua850			va850		
		BIAS	RMSE	PCC	BIAS	RMSE	PCC	BIAS	RMSE	PCC
DJF	MPI-ESM-LR	1.02**	1.24	0.91	-0.01	0.19	0.94	0.06	0.06	0.86
	ERAI-CCLM	0.68**	0.54	0.92	-0.43**	0.22	0.97	0.00	0.00	0.91
	MPI-CCLM	1.34**	2.02	0.89	-0.08	0.24	0.92	-0.27*	0.13	0.81
MAM	MPI-ESM-LR	0.64**	0.52	0.91	0.50**	0.39	0.94	0.16**	0.05	0.86
	ERAI-CCLM	0.77**	0.64	0.89	-0.36**	0.15	0.95	0.17**	0.03	0.82
	MPI-CCLM	1.56**	2.61	0.87	0.22*	0.19	0.80	0.28**	0.11	0.69
JJA	MPI-ESM-LR	0.66**	0.51	0.90	0.09	0.17	0.91	0.04	0.02	0.90
	ERAI-CCLM	0.33**	0.14	0.89	0.01	0.01	0.94	0.13**	0.01	0.85
	MPI-CCLM	1.15**	1.45	0.85	0.46**	0.49	0.82	0.43**	0.20	0.72
SON	MPI-ESM-LR	0.74**	0.77	0.93	0.06	0.11	0.94	0.13**	0.03	0.86
	ERAI-CCLM	0.51**	0.29	0.90	-0.26**	0.08	0.94	0.14**	0.02	0.85
	MPI-CCLM	1.34**	2.14	0.89	0.04	0.14	0.86	0.21**	0.07	0.76

Table 4.2 Cross correlation coefficient between the observed and the model simulated East Asian summer monsoon index. $^{**}p < 0.001$

	ERA-Interim	MPI-ESM-LR	ERAI-CCLM	MPI-CCLM
ERA-Interim	1.00	0.25	0.92**	0.11
MPI-ESM-LR		1.00	0.25	0.77**
ERAI-CCLM			1.00	0.15
MPI-CCLM				1.00

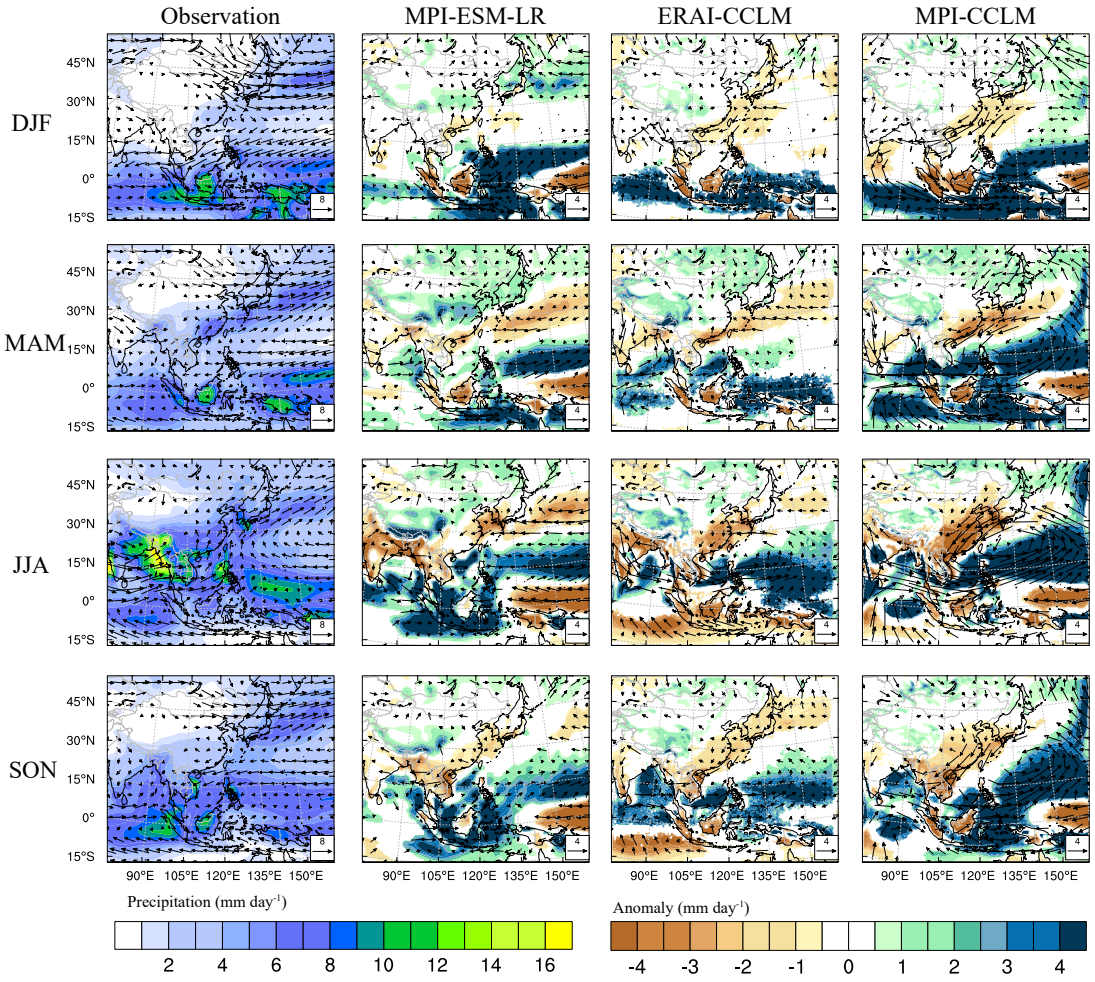

Figure 4.1 Seasonal mean precipitation and wind vectors at 850 hPa (m s^{-1}), and seasonal anomalies of precipitation 'model minus GPCP', and seasonal anomalies of winds 'model minus ERA-Interim'. The presented anomalies of precipitation and winds pass the Student's *t*-test at 0.05 level.

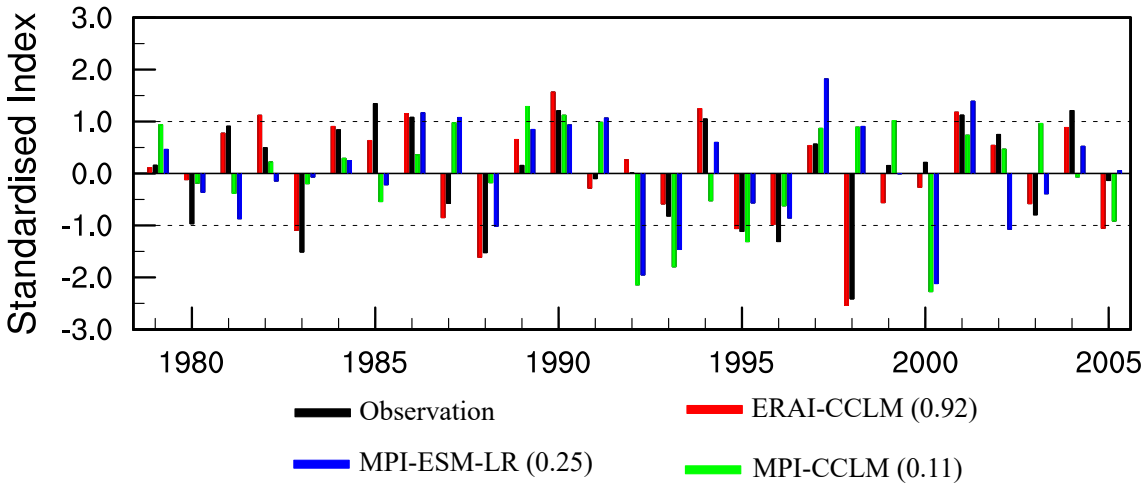

Figure 4.2 Observed and model simulated East Asian summer monsoon index (EASMI). The number following the model presents the correlation coefficient between the model produced and observed EASMI. The two black dotted lines indicate the category of monsoon year. The strong monsoon year is defined as EASMI >1, while the weak monsoon is EASMI <-1.

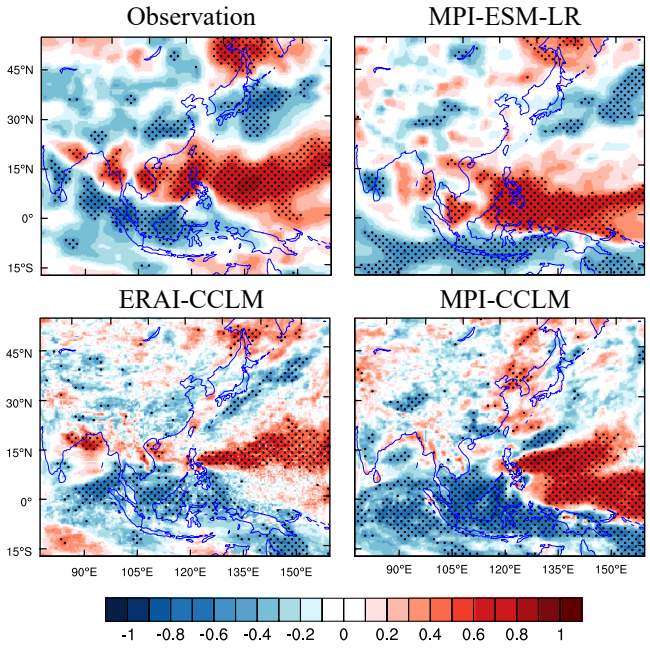

Figure 4.3 Observed and model simulated correlation map between the East Asian summer monsoon index (EASMI) and the summer (June-July-August) precipitation. The black dots indicate 0.05 significant level based upon the Student's *t*-test.

4.4 Summary and discussion of Chapter 4

Following the CORDEX-East Asia projection framework, this chapter has introduced an application of dynamical downscaling in East Asia. The model employs the same set up as Chapter 3. The performance of RCM (CCLM) in presenting the seasonality of general circulation and precipitation (Fig. 4.1), the monsoon characteristics (Fig. 4.2 and 4.3) have been discussed. Compared to the observed condition, the CCLM shows significant BIAS in specific regions. The BIAS centre is shifting with the season/ITCZ change. The possible reason is the CCLM overestimating precipitation in ITCZ region. This might be resolved by the improvement of model parametrisation. Furthermore, the CCLM's performance strongly depends upon its boundary condition. The RCM tends to amplify the error when it is given an unrealistic boundary condition. For example, the MPI-ESM-LR underestimates (-2 to -1 mm day^{-1}) the summer rainfall band from the Yangtze River to the south of Japan where the MPI-CCLM produces a larger negative BIAS (-4 to -2 mm day^{-1}).

There is a smaller correlation coefficient between the RCM simulated EASM index and observation than that in the GCM (Fig. 4.2). The RCM does not add value to the GCM in producing the year-to-year variation of the EASM index. In general, the RCMs have potential to add value to the GCMs on specific processes and forcing acting at sub-GCM grid scales (Giorgi and Gutowski, 2015). Actually, the EASM is a large scale rather than a sub-GCM grid scale phenomena (Ding and Chan, 2005; Tao and Chen, 1987). This might be the reason for the poor performance of RCM than GCM in capturing the inter-annual variability of EASM index. Both of the RCM and GCM do not depict the relationship between the EASMI and the monsoon precipitation (Fig. 4.3). There is a potential to improve the model ability in capturing the EASM index and the monsoon precipitation.

This chapter is a preparation work for downscaling the prediction results to a finer resolution. A reliable prediction results is required for further downscaling. Next chapter will discuss the MPI-ESM-LR and the other five prediction systems in predicting the EASM on seasonal time-scale.

Chapter 5

Seasonal Predictability of East Asian Summer Monsoon in CMIP5 models

5.1 Introduction

As the evolution and variability of EASM critically impacts on both the economy and society, accurate EASM prediction is an important and long-standing issue in climate community. The internal processes of the atmosphere comprise various short time-scales and associated stochastic non-linear processes. The predictability of such internal processes are only possible for a few days (Lorenz, 1960). Thus, the source of predictability on a longer time-scale must come from the lower boundary conditions (Charney and Shukla, 1981; Shukla, 1998). The ocean gives the climate system a memory that can result in monthly to yearly atmospheric deviations due to its large heat storage capacity. Therefore, the teleconnection between the SST and the EASM can provide us with the capability to predict the variation of the EASM (Chang *et al.*, 2000*a*; Kang *et al.*, 2004; Wang *et al.*, 2005). ENSO is the most useful factor to indicate SST anomalies. In general, a weak (strong) EASM is associated with the warm (cold) phase of the ENSO (Wang *et al.*, 2000). A strong relationship between the EASM and the ENSO has been found since the 1970s (Yun *et al.*, 2010). It provides a reliable predictor for the empirical/statistical model of EASM prediction (Sohn *et al.*, 2012; Wang *et al.*, 2015; Wu *et al.*, 2009). Nevertheless, it cannot fully depict the variability on a multi-time scale.

In the last two decades, numerous articles have presented the performance of GCMs to simulate and predict the EASM (Kang *et al.*, 2004; Sohn *et al.*, 2012; Wang *et al.*, 2005, 2007; and many others). The AGCMs studies, however, show the limitations of dynamical monsoon prediction due to the non-linear characteristics of the atmosphere and the inaccurate performance of the AGCMs (Kang *et al.*, 2004; Wang *et al.*, 2005; Zhou *et al.*, 2009). A new

generation of GCMs, coupled atmosphere-ocean-land GCMs (AOGCMs) or earth system models (ESMs) are widely used to evaluate the predictability of the EASM (Wang *et al.*, 2007, 2009). These simulations with prescribed SST simulations improve the model performance in representing the seasonal to inter-annual lead modes of the EASM (Wang *et al.*, 2007, 2009), but still behave poorly in reproducing the EASM rainfall over land due to the prescribed SST which leads to an incorrect rainfall-SST teleconnection (Wang *et al.*, 2004*a*). Sperber *et al.* (2013) assessed the progress of the model from coupled model inter-comparison project phase 3 (CMIP3) (Meehl *et al.*, 2007) to phase 5 CMIP5 (Taylor *et al.*, 2012) in simulating the Asian summer monsoon. They found that there is no single model that performs superior to the other models in all aspects of the predictive skill metric (*i.e.* the time mean, the climatological annual cycle, the inter-annual variability, and the intra-seasonal variability of the ASM). The models simulate not only a too weak ENSO-monsoon teleconnection, but also a too weak East Asian zonal wind-rainfall teleconnection (Sperber *et al.*, 2013).

Initial conditions as well as physical processes and the resolution of the model play a vital role in predicting climate (Smith *et al.*, 2007). Initialised simulations (*i.e.* decadal hindcast) add skills to simulate the ENSO, compared to non-initialised simulations (*i.e.* historical) on seasonal-to-decadal time-scale in CMIP5 (Meehl *et al.*, 2014; Meehl and Teng, 2012). After initialised with the observed initial conditions and boundary forcing, the models in CMIP5 can predict the ENSO up to 15 months in advance (Choi *et al.*, 2016). This extended prediction skill of the ENSO suggests that the EASM can be predicted on a seasonal time-scale if the dynamic link between the ENSO and monsoon circulations is well represented in these models. Following scientific issues will be addressed: What is the CMIP5 models performance in predicting the EASM and do the models improve with the initialisation?

5.2 Models, data and methods

In this chapter, six prediction systems are assessed, which contribute to CMIP5 in historical (*i.e.* non-initialised) and decadal hindcast (*i.e.* initialised) simulations (Table 5.1). This study only employs the six prediction systems because only these systems have performed a yearly initialisation. The BCC-CSM1-1 has three ensemble members which are initialised on 1st September, 1st November and 1st January, respectively. The initialisation of HadCM3 takes place on each pre-year 1st November while the other four systems are initialised on 1st January. The full-field initialisation is named HadCM3-ff to distinguish it from the anomaly initialisation in HadCM3. Because of the better spatial coverage of the observation precipitation. The satellite era (1979-2005) is selected for this study. The first lead year

results from initialised simulations are used to assess the seasonal predicting skills of the CMIP5 models. Table 5.2 shows the brief configurations of the six prediction systems.

The main datasets which are used for the comparison in this study include: (1) monthly precipitation data from the Global Precipitation Climatology Project (GPCP; Adler *et al.*, 2003); (2) monthly general circulation data from ECMWF Interim re-analysis (ERA-Interim; Dee *et al.*, 2011); and (3) monthly mean SST from National Oceanic and Atmospheric Administration (NOAA) improved Extended Reconstructed SST version 4 (ERSST v4; Huang *et al.*, 2015*a*). All the model data and the comparison data are remapped onto a common grid of 2.5°x2.5° by bi-linear interpolation to reduce the uncertainty associated with different data resolutions.

The pattern correlation coefficient (PCC) is applied to analyse the model performance in capturing the spatial pattern with reference to the observational data. There are two types of pattern correlation statistics: centred and un-centred. The centred (un-centred) statistic measures the similarity of two patterns after (without) the removal of the global mean. The un-centred PCC is used due to the fact that centred correlations alone are not sufficient for the attribution of seasonal prediction. This chapter also employs the anomaly correlation coefficient (ACC) to analyse the model performance in reproducing observational variations on a different time-scale, which is calculated by the anomaly of each variable. The root-mean-square error (RMSE) is employed to test the model deviation from the observation. Appendix B presents the detail of definition for PCC, ACC and RMSE.

Table 5.1 Detail of the prediction system investigated in Chapter 3

System	Institute	Resolution		Non-Initialisation	Initialisation		Reference
		Atmospheric	Oceanic	Members	Members	Type	
BCC-CSM1-1	Beijing Climate Center, China	T42L26	1lonx1.33lat L40	3	3	Full-field	Wu *et al.* (2014)
CanCM4	Canadian Centre for Climate Modelling and Analysis, Canada	T63L35	256x192 L40	10	10	Full-field	Arora *et al.* (2011)
GFDL-CM2p1	Geophysical Fludi Dynamics Laboratory, USA	N45L24	1lonx0.33-1lat L50	10	10	Full-field	Delworth *et al.* (2006)
HadCM3	Met Office Hadley Centre, UK	N48L19	1.25x1.25 L20	10	10+10	Full-field and Anomaly	Smith *et al.* (2013)
MIROC5	Atmosphere and Ocean Research Institute, Japan	T85L40	246x192 L40	5	6	Anomaly	Tatebe *et al.* (2012)
MPI-ESM-LR	Max Planck Institute for Meteorology, Germany	T63L47	GR15 L20	3	3	Anomaly	Matei *et al.* (2012)

Table 5.2 Brief summaries of initialisation strategies used by modelling groups in Chapter 3. ECMWF: European Centre for Medium-Range Weather Forecasts; GODAS: Global Ocean Data Assimilation System; NCEP: National Centers for Environmental Prediction; S: Salinity; SODA: Simple Ocean Data Assimilation; T: Temperature.

Model	Atmosphere	Ocean	Internet
BCC-CSM1-1	-	integration with ocean T nudged to SODA product above 1500 m	http://forecast.bcccsm.ncc-cma.net/
CanCM4	ECMWF re-analysis	off-line assimilation of SODA and GODAS subsurface ocean T and S adjuusted to reserve model T-S	http://www.cccma.ec.gc.ca/
GFDL-CM2p1	GFDL re-analysis	assimilates observations of T, S from World Ocean Database	https://www.gfdl.noaa.gov/multi-decadal-prediction-stream/
HadCM3	ECMWF re-analysis	off-line ocean re-analysis product	http://cera-www.dkrz.de/WDCC/CMIP5/
MIROC5	-	integration using observational gridded ocean T and S	http://amaterasu.ees.hokudai.ac.jp/
MPI-ESM-LR	NCEP re-analysis	off-line ocean hindcast forced with NCEP	http://cera-www.dkrz.de/WDCC/CMIP5/

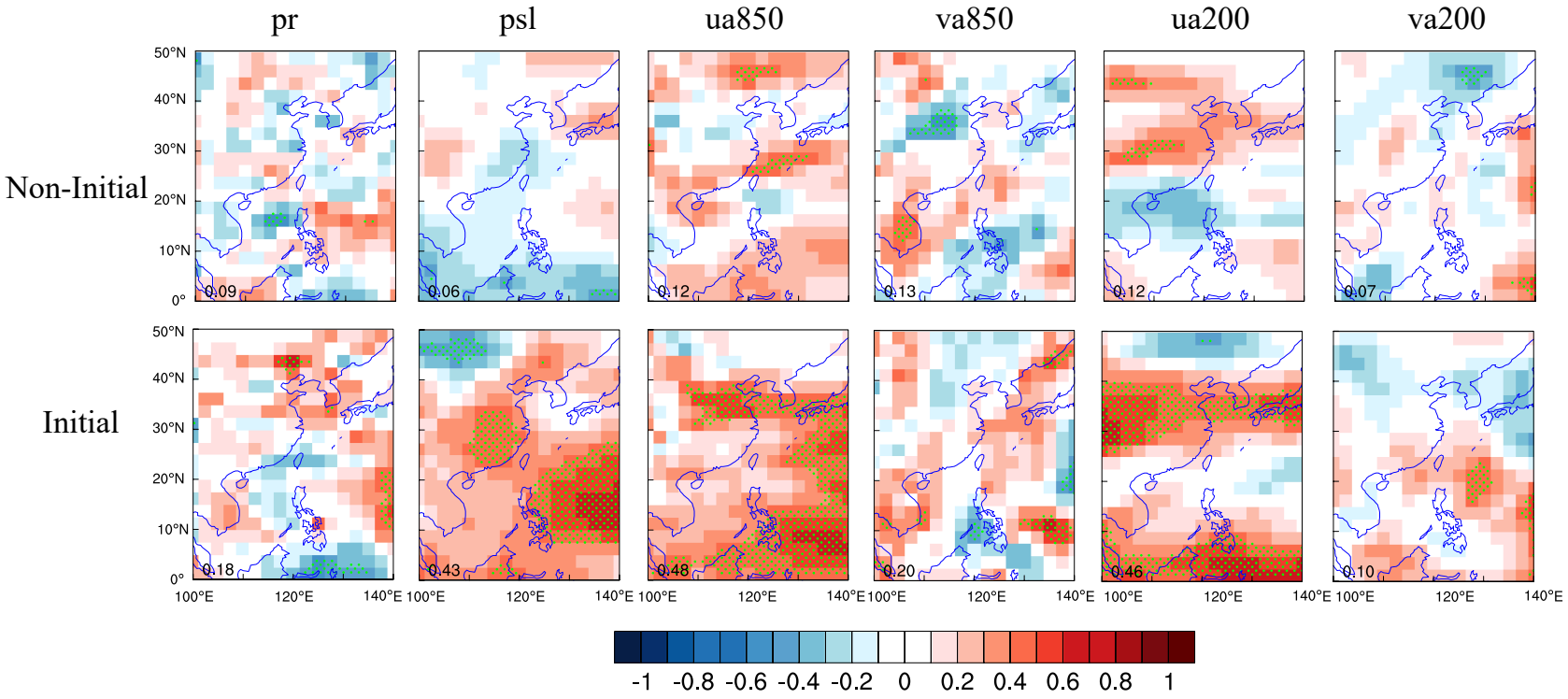

Figure 5.1 Anomaly correlation coefficient of six variables (*i.e.* precipitation, mean sea level pressure, and winds over 850 hPa and 200 hPa) between multi-model ensemble mean and observations in non-initialisation and initialisation. The green dotted grids illustrate the significant level at 0.05. The number at lower left corner indicates the ratio of significant grid points to entire grids. The GPCP was employed as the reference data for precipitation (pr) while winds (*i.e.* ua850, va850, ua200 and va200) and mean sea level pressure (psl) were compared with ERA-Interim re-analysis.

5.3 Seasonal prediction skill of the EASM

The EASM has complicated spatial and temporal structures that encompass the tropics, subtropics, and mid-latitudes (Ding, 1994; Tao and Chen, 1987). In late spring, an enhanced rainfall pattern is observed in the Indochina Peninsula and in South China Sea. Then, the rainfall belt advances northwards to the south of China. In early summer, the rainfall concentration occurs in the Yangtze River Basin and in southern Japan, namely, the Meiyu and Baiu season, respectively. The rainfall belt can arrive as far as northern China, the Korean Peninsula (called the Changma rainy season) and central Japan in July (Ding, 2004; Ding and Chan, 2005).

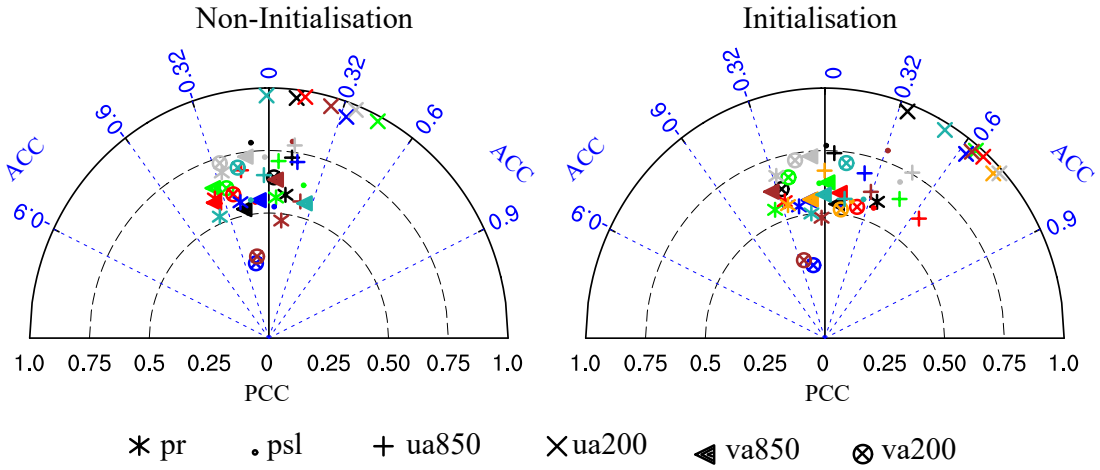

Figure 5.2 Taylor diagram display of pattern (PCC) and temporal (ACC) correlation metrics of six variables between observation and model simulation in the EASM region (0°-50°N, 100°-140°E). Each coloured marker represents a model, *i.e.* the BCC-CSM1-1 (black), the CanCM4 (green), the GFDL-CM2p1 (red), the HadCM3 (blue), the MIROC5 (brown), the MPI-ESM-LR (light-sea-blue), the HadCM3-ff (orange) and the multi-model ensemble mean (grey). The reference datasets are same as that in Fig. 5.1.

The EASM is characterised by both seasonal heterogeneous rainfall distribution and associated large-scale circulation systems (Wang *et al.*, 2008*a*). In summer, water moisture is transported from the Pacific Ocean to central and eastern Asia by the south-west surface winds. Generally, a strong summer monsoon year is followed by precipitation in northern China, while a weak summer monsoon year is usually accompanied by heavier rainfall along the Yangtze River basin (Ding, 1994; Zhou and Yu, 2005).

For multi-model ensemble mean (MME), the prediction skill of the EASM precipitation and the associated general circulation variables (*i.e.* zonal and meridional wind, and mean sea level pressure) is presented in Figure 5.1. Compared to the non-initialised experiment, a

larger predictability area can be found in the initialised experiment. The individual model shows an acceptable performance (high PCC) in capturing the observational spatial variation of the six variables, which are related to EASM, but a poor performance in calculating the observational temporal variation (low ACC) (Fig. 5.2). There is no improvement in estimating the spatial variation of the six variables with initialisation. We can see that the models show a higher ACC in the initialised simulations than in the non-initialised ones. The improvement of simulating the temporal variation of zonal winds (*i.e.* ua850 and ua200) is larger than the rainfall and meridional winds. Therefore, the monsoon index based on general circulation parameters is a potential tool to predict the EASM.

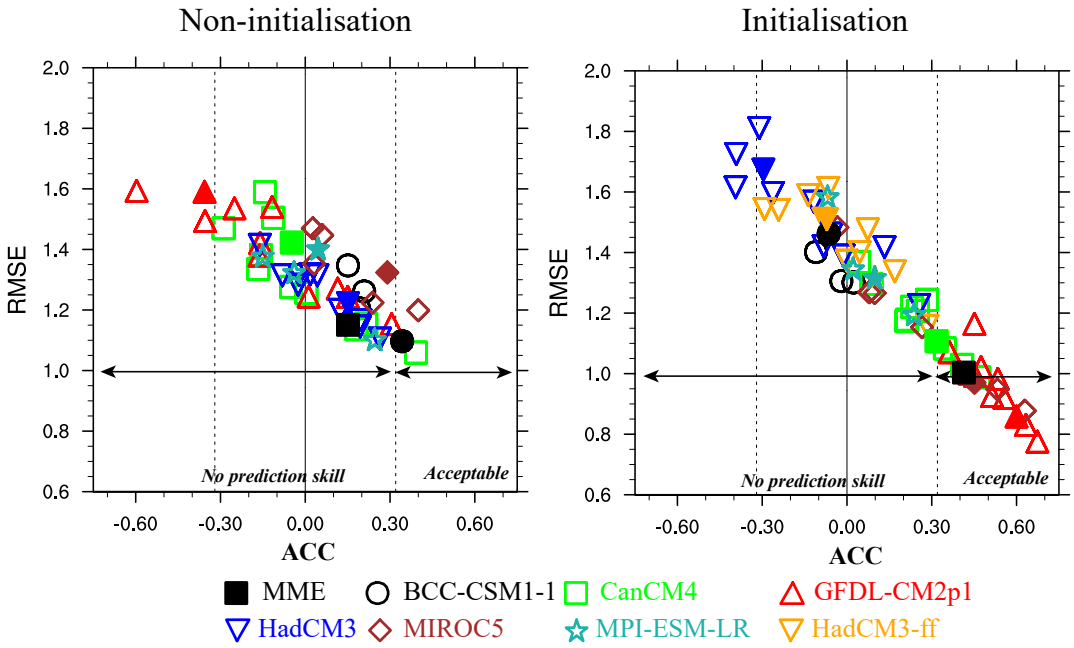

Figure 5.3 Performance of the model ensemble member (hollow marker), its ensemble mean (solid marker) and multi-model ensemble mean (black solid square) on the EASM index. The abscissa and ordinates are the temporal correlation coefficient (ACC) and the root-mean-square error (RMSE), respectively. The observed EASM index is calculated by zonal wind at 850 hPa from the ERA-Interim re-analysis data. Vertical black dot lines indicate the significant level at 0.1. The vertical black line indicates the correlation between the simulating and the observational EASM index is 0.

In the last few decades, more than 25 general circulation indices have been produced to research the variability and long-term change of the EASM. Wang *et al.* (2008*a*) classified them into five categories and discussed their ability to capture the main features of the EASM. It found that the Wang and Fan index (1999) shows the best performance in capturing the

total variance of the precipitation and three-dimensional circulation over East Asia. I, thus, select the Wang and Fan index for the further analysis. Its definition is standardised average zonal wind at 850hPa in (5°-15°N, 90°-130°E) minus in (22.5°-32.5°N, 110°-140°E).

In the non-initialised simulations, the CanCM4 and the GFDL-CM2p1 simulate the EASM index at a negative phase, while the BCC-CSM1-1, the HadCM3, the MIROC5 and the MPI-ESM-LR all represent a positive phase. Without initialisation, all the models do not capture the observed EASM as indicated by a low ACC (Fig. 5.3). Compared to the non-initialised simulations, the CanCM4, the GFDL-CM2p1 and the MIROC5 improve the skill simulating the EASM, while the BCC-CSM1-1 and the HadCM3 show a worse performance with initialisation. Particularly, the HadCM3 significantly loses its predictive skill in capturing the EASM in the anomaly initialised simulation. There is only small change in the MPI-ESM-LR from non-initialised simulation to initialised simulation.

5.4 EASM-ENSO coupled mode in CMIP5

Two methods are usually applied to identify the leading modes of geophysical fields: singular value decomposition (SVD), and empirical orthogonal function (EOF). The SVD is used to analyse the co-variability modes between two geophysical fields (Bretherton *et al.*, 1992). However, the SVD modes are not orthogonal and cannot be used to re-construct the full variability; in addition, the SVD modes of precipitation and SST are strongly dominated by the SST variability in the tropics, not by the rainfall variability (Lau and Wu, 2001). This study employs the EOF method to analyse the leading EOF modes of six meteorological variables anomaly in the EASM region (0°-50°N, 100°-140°E). The first EOF mode of precipitation is characterised by a "sandwich" pattern which shows sharp contrast between the prominent rainfall centre over Malaysia, the Yangtze River valley and the south of Japan, and the enhanced rainfall over the Indo-China Peninsula and the Philippine Sea (Fig. 5.4). The increased precipitation is associated with cyclones in the low-level (850 hPa) and anti-cyclones in the upper level (200 hPa).

The correlation coefficient of the first eigenvector and the associated principal component (PC) between the model simulation and the observation in the non-initialised and the initialised simulation is presented in Figure 5.5. The models capture the eigenvector of the first EOF for the six meteorological fields in non-initialised simulation. However, they fail to reproduce the associated PC of the first leading EOF mode. Compared to the non-initialised simulation, the initialised models show no improvement simulating the first leading EOF mode of rainfall. However, they exhibit a better performance in representing the first leading EOF mode of zonal wind. The CanCM4 and the GFDL-CM2p1 capture the first PC of ua850,

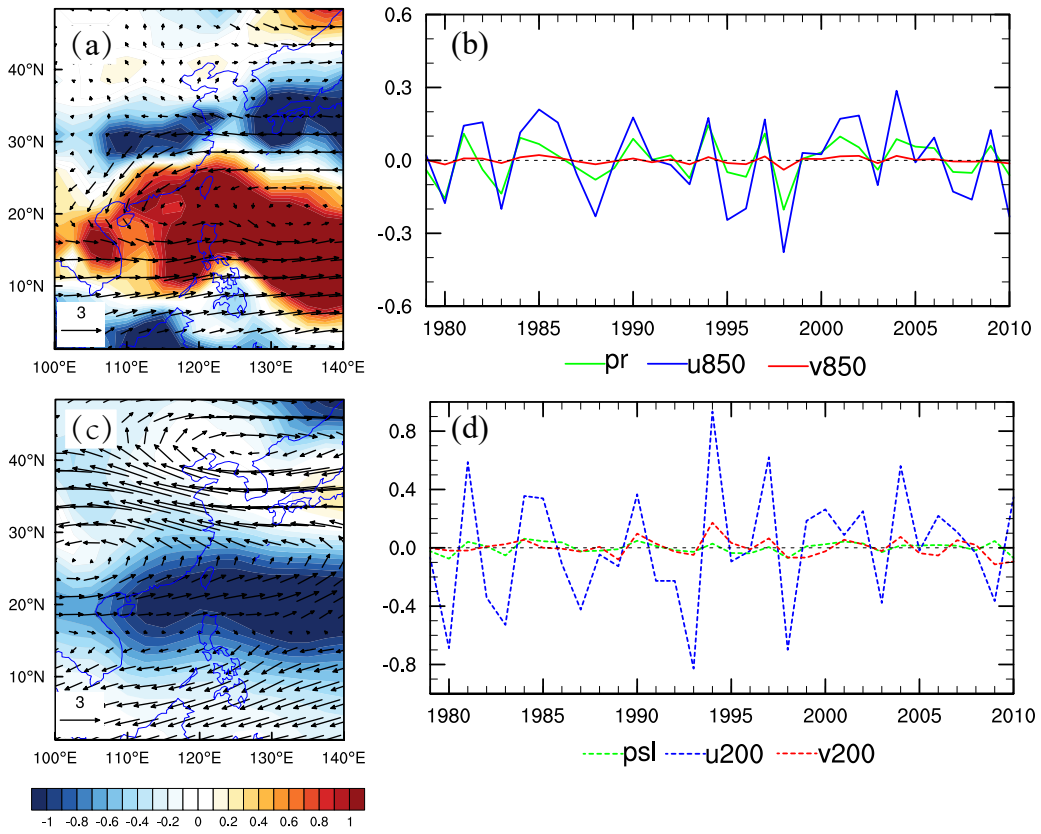

Figure 5.4 Spatial distribution of observational of the first leading EOF mode of June-July-August precipitation and winds over 850 hPa (a), mean sea level pressure and winds over 200 hPa (c) and the associated principal component (PC; b, d). The GPCP and ERA-Interim data from 1979-2005 were used for the EOF analysis in the EASM domain.

contrary to the other five models. For the zonal wind at 200 hPa, the BCC-CSM1-1 fails to simulate its first EOF mode while the other six models can. Then, only the GFDL-CM2p1 accurately simulates the first EOF eigenvectors and the associated PC of va850, which is not reproduced in the other models. All models do not capture the spatial-temporal variation of the first EOF mode of meridional wind at 200 hPa. The GFDL-CM2p1 and the MIROC5 simulates a reasonable leading EOF mode and associated PC of psl, while the other models cannot capture it.

Figure 5.7 shows the fractional (percentage) variances of the six variables of the first EOF mode with the total variances from the observation, and the model simulation in non-initialisation and in initialisation. The observational total variances for the pr, the ua850, the ua200, the va850, the va200 and the psl, are depicted by the first lead EOF mode in 21.2, 59.0, 36.5, 20.6, 28.5 and 50.0 (percent), respectively. The models simulate the comparable

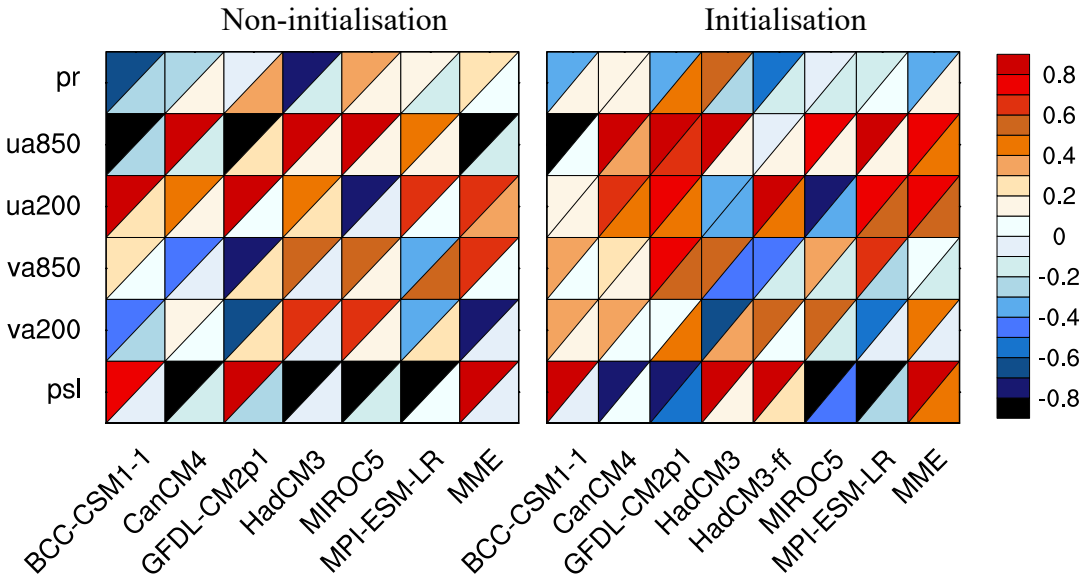

Figure 5.5 Portrait diagram display of correlation metrics between the observation and the model simulation of the first lead EOF mode for the six fields in the non-initialisation (left) and the initialisation (right). Each grid square is split by a diagonal in order to show the correlation with respect to both the eigenvector (upper left triangle) and its associated principal components (lower right triangle) reference data sets.

explained variances, which show a slight discrepancy for the first leading mode in the non-initialisation. From non-initialised simulation to initialised simulation, the CGCMs tend to enhance the first EOF lead mode due to the fact that they show larger fractional variances of the total variances of the six variables. We note that the CanCM4 and the GFDL-CM2p1 significantly increase the fractional variances from non-initialisation to initialisation.

The ENSO is a dominant mode of the inter-annual variability of the coupled ocean and atmosphere climate system, which has strong effects on the inter-annual variation of the EASM (Wang *et al.*, 2000; Wu *et al.*, 2003). Wang *et al.* (2015) summarised the first EOF lead mode of the ASM is the ENSO developing mode. As previously mentioned, the first EOF mode is improved in the initialised simulations, compared to the non-initialised simulation. This also can be found in the ENSO indices (Fig. 5.9). Niño3.4 and southern oscillation index (SOI) represent the oscillation of two components in the earth system (ocean and atmosphere). Niño3.4 is calculated by the SST anomaly in the central Pacific (5°S-5°N, 190°-240°E), while SOI is based upon the anomaly of the sea level pressure differences between Tahiti (17.6°S, 210.75°E) and Darwin (12.5°S, 130.83°E). To calculate the SOI, the grid data have been interpolated to the Tahiti and the Darwin point by bilinear interpolation.

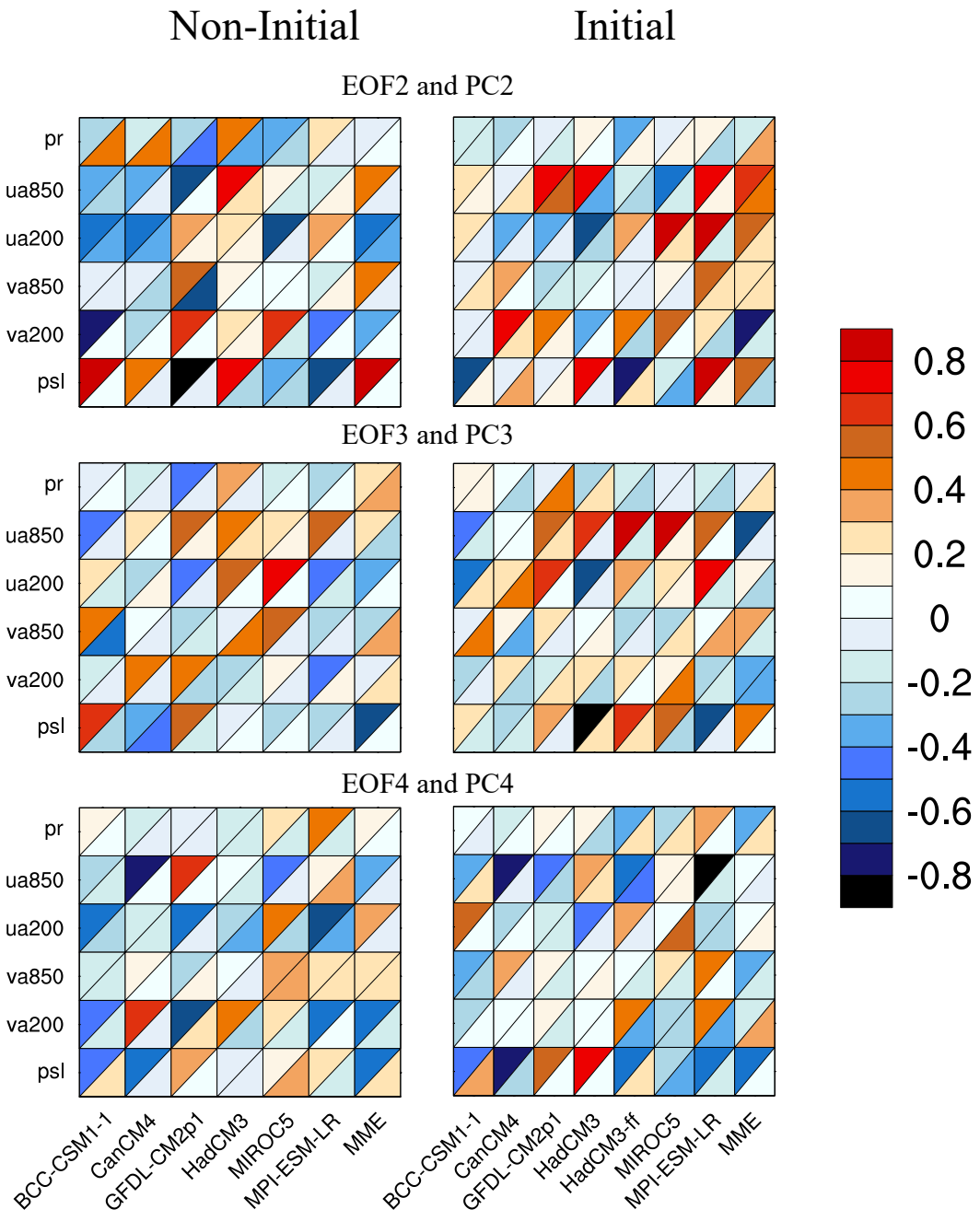

Figure 5.6 Same as Fig. 5.5, but for the second, third and fourth lead EOF modes.

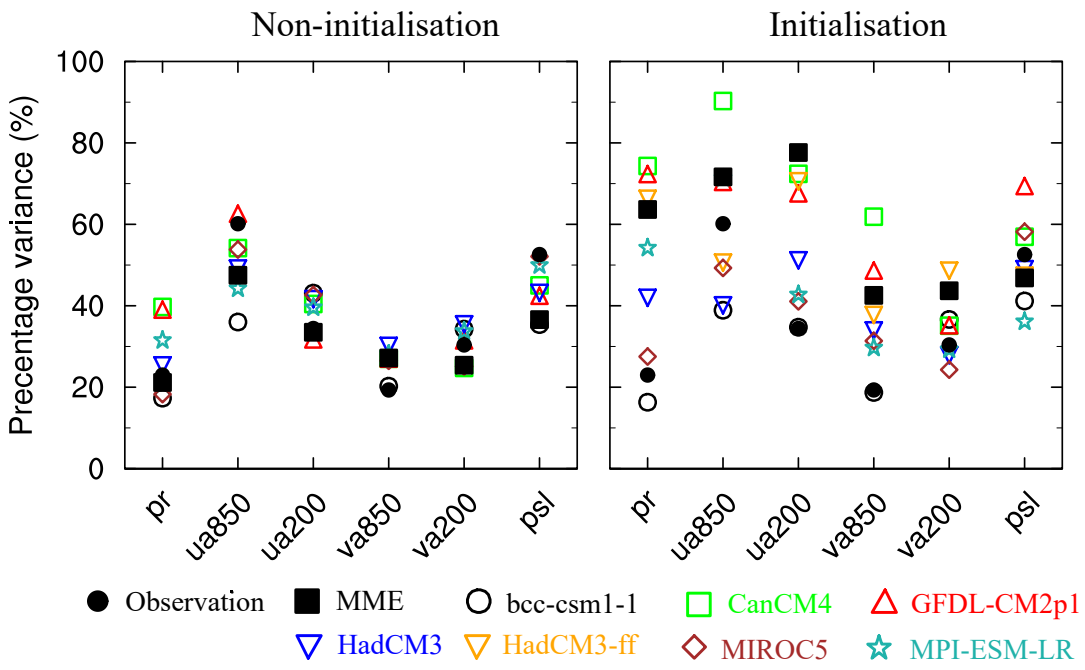

Figure 5.7 Fraction variance (per cent) explained by the first EOF mode for six fields in the non-initialisation (left) and the initialisation (right).

The individual members and their ensemble mean of the six models show a low correlation coefficient to the observational Niño3.4 and the SOI in the non-initialised simulations. These two indices show strong anti-phase in the observation, with correlation range is -0.94 to -0.92 for four seasons. The models can describe the anti-correlation between Niño3.4 and the SOI, but with a weaker correlation. Compared to the non-initialisation, there is a significant improvement in capturing the observational Niño and the SOI in initialised experiments. The initialisation lowers the spread of Niño3.4 and the SOI simulations in all the six models. There is a noticeable change between the model in producing the relationship between the Niño3.4 and the SOI. We can find that the GFDL-CM2p1 (HadCM3) shows a lower (higher) Niño3.4 -SOI correlation in initialisation than that in non-initialisation. With initialisation, the ensemble mean of each model outperforms its individual members in capturing Niño3.4 and the SOI, while without initialisation it shows a worse performance than individual members in simulating Niño3.4 and the SOI.

The EASM strongly relies on the pre-season ENSO due to the lag response of the atmosphere to the SST anomaly (Wu *et al.*, 2003). The lead-lag correlation coefficients between the EASM index and Niño3.4, and the SOI from JJA(-1) to JJA(+1) are illustrated in Figure 5.10. The pre-season Niño3.4 (SOI) presents a significant negative (positive)

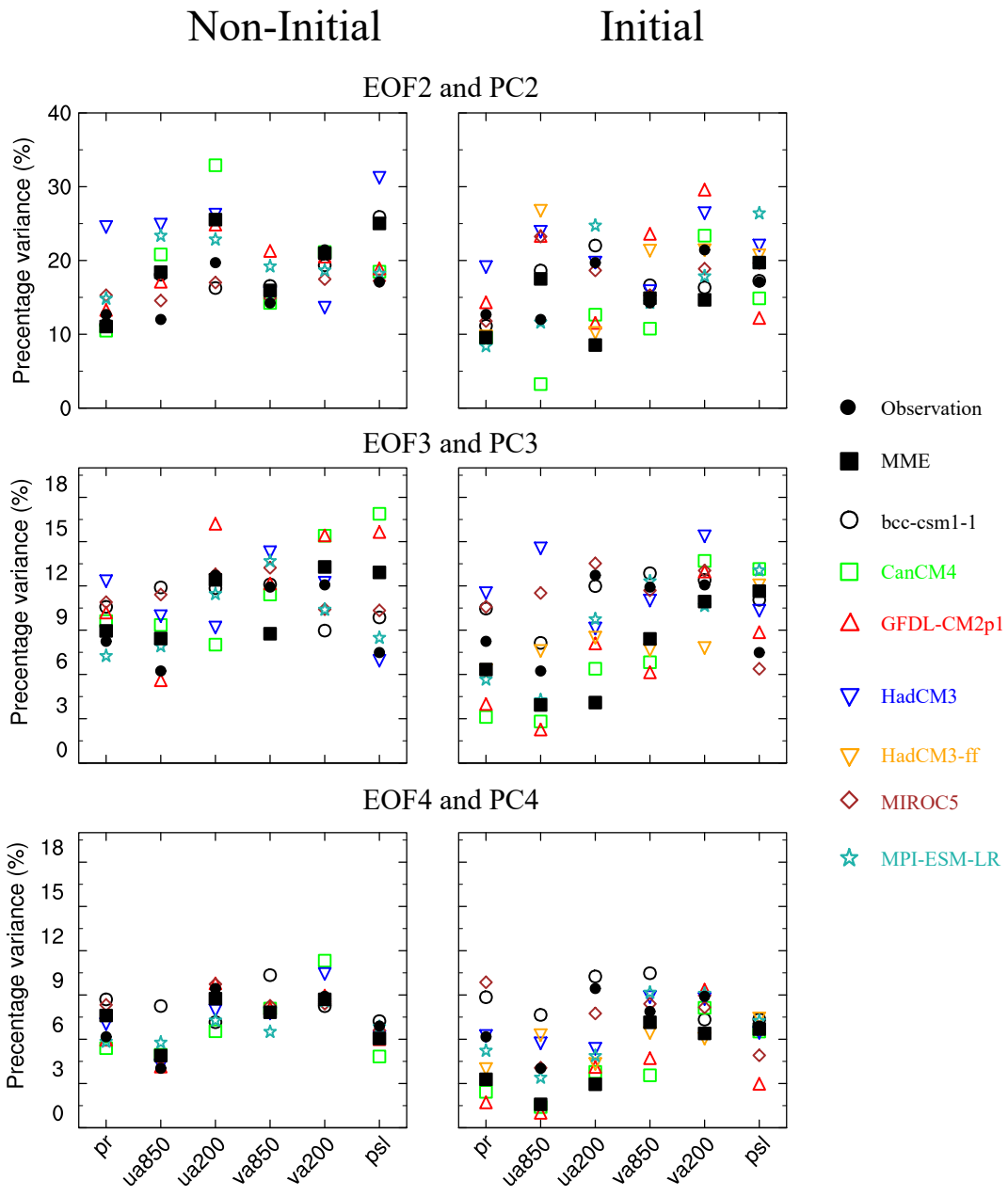

Figure 5.8 Same as Fig. 5.7, but for the second-to-fourth lead EOF modes.

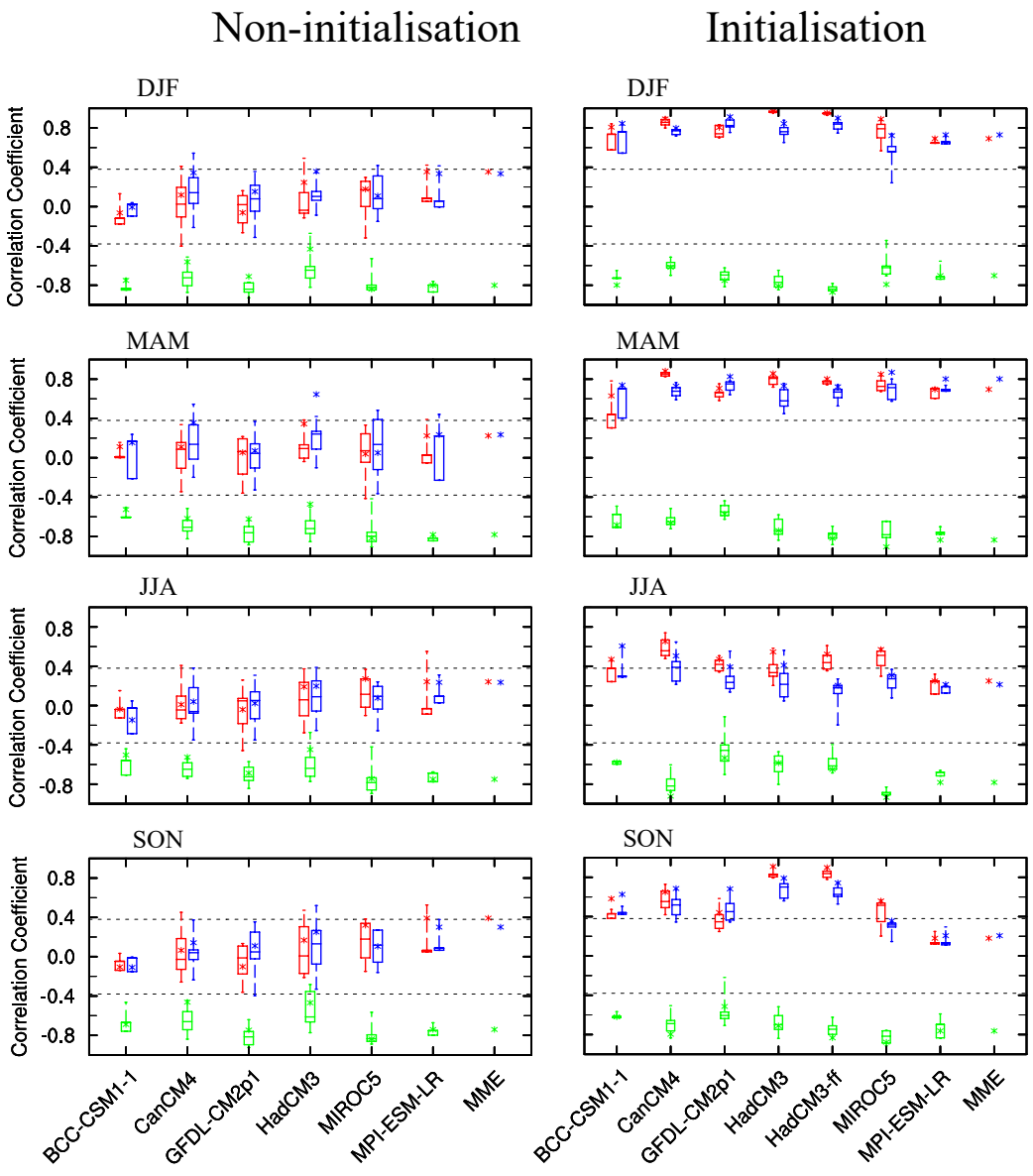

Figure 5.9 Model prediction skill in representing the observed Niño3.4 index (red), the SOI (blue) from the DJF to SON in non-initialisation (left) and initialisation (right). The correlation coefficient between the model simulated Niño3.4 and the SOI (green). Box and whisker diagram shows ensemble mean of each model (asterisk), median (horizontal line), 25th and 75th percentiles (box), minimum and maximum (whisker). The two black dotted lines indicate 0.05 significant level based on Student's *t*-test.

correlation to the EASM, while the post-season Niño3.4 (SOI) shows a notable positive (negative) correlation.

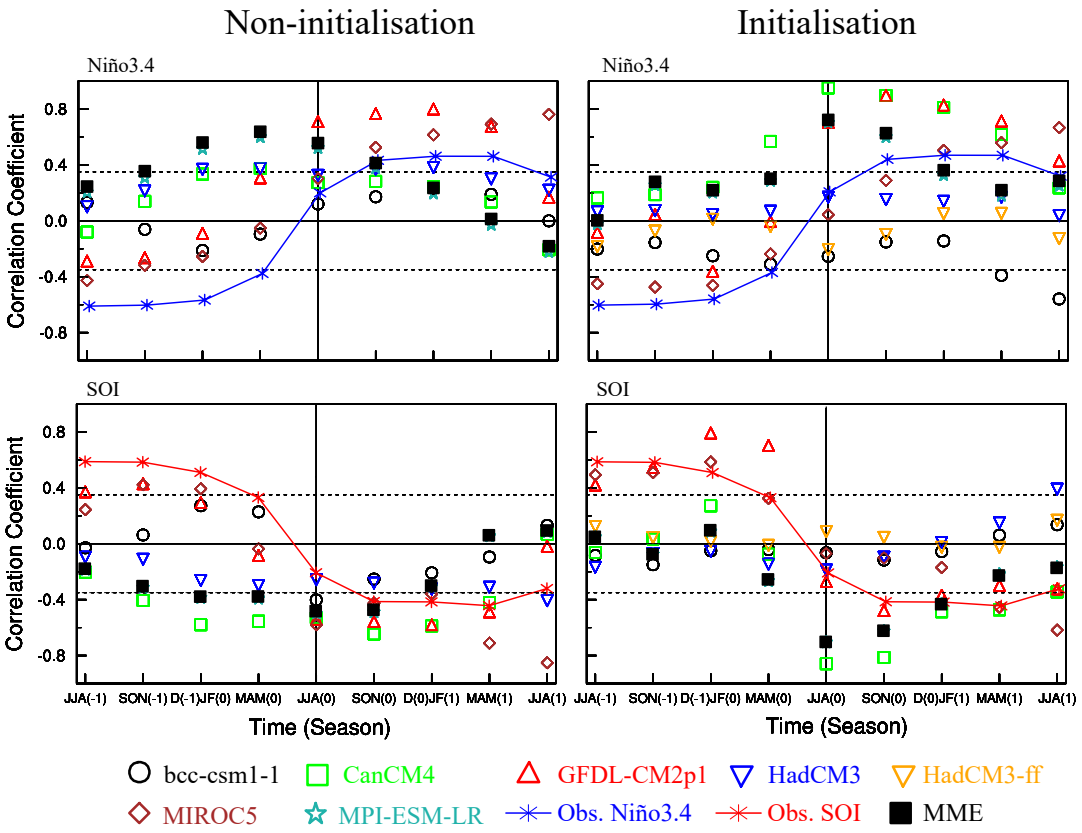

Figure 5.10 Lead-lag correlation coefficients between the EASM index and Niño3.4 (upper), and SOI (lower) in non-initialised simulations (left) and initialised ones (right) for observation (marker line) and models (marker) from JJA(-1) to JJA(+1). The two black dotted lines are 0.05 significant level based upon Student's *t*-test. The vertical line represents JJA(0), where the simultaneous correlations between the EASM index and Niño3.4, and SOI are shown.

This lead-lag correlation coefficient phase is called the Niño3.4-/SOI-EASM coupled mode (Wang *et al.*, 2008*a*). In the non-initialised cases, the models do not produce the teleconnection between the ENSO and the EASM. The CanCM4, the HadCM3 and the MPI-ESM-LR fail to represent the lead-lag correlation coefficient difference between pre-/post-season ENSO and EASM. The BCC-CSM1-1, the GFDL-CM2p1 and the MIROC5 capture the coupled mode of the ENSO and the EASM. However, the pre-season ENSO has a weak effect on the EASM. Compared to the non-initialised cases, the MIROC5 and the GFDL-CM2p1 both demonstrate a significant improvement in simulating Niño3.4 (SOI)-EASM coupled mode with initialisation. The BCC-CSM1-1, the HadCM3, and the

HadCM3-ff show no improvement, with insignificant correlation between Niño3.4 (SOI) and the EASM. The CanCM4 and the MPI-ESM-LR illustrate a high correlation between the EASM and the simultaneous-to-post-season ENSO, rather than the pre-season ENSO. Therefore, the depiction of Niño3.4-/SOI-EASM coupled mode is a dominating factor for models in response to the initialisation.

5.5 Summary and discussion of Chapter 5

Six earth system models from CMIP5 have been selected in this study. The improvement of the rainfall, the mean sea level pressure, the zonal wind and the meridional wind in the EASM region from non-initialised experiments to initialised experiments have been discussed. The models show a better performance in capturing the inter-annual variability of zonal wind than precipitation in initialised experiments (Fig. 5.2). Thus, the zonal wind index is an additional factor which can be used to improve the prediction skill of the model. Additionally, the prediction skill of the Wang and Fan monsoon index in both the two experiments have been calculated. The GFDL-CM2p1, the CanCM4 and the MIROC5 show a significant advancement in simulating the EASM from non-initialised to initialised simulation with a lower RMSE and a higher ACC (Fig. 5.3). There is a slight change of the MPI-ESM-LR in initialisation. Compared to the non-initialised simulation, the BCC-CSM1-1 and the HadCM3 loses prediction skill.

To test the possible mechanisms of the models' negative performance in the non-initialisation and the initialisation, the leading mode of the six fields have been calculated, which are associated to the EASM. The models demonstrate a better agreement with the observational first EOF mode in the initialised simulations (Fig. 5.5). The first lead mode of zonal wind at 200 hPa shows a significant improvement in the models except the BCC-CSM1-1 in initialisation. Therefore, a potential predictor could be an index based upon the zonal wind at 200 hPa.

Compared to the non-initialised simulations, the models enhance the first EOF mode with a higher fraction of variance to the total variance in initialisation (Fig. 5.7). The first EOF mode of the EASM is the ENSO developing mode (Wang *et al.*, 2015). I have, thus, analysed the seasonal simulating skill of Niño3.4 and the SOI in each model (Fig. 5.9). The models show a poor performance in representing Niño3.4 and the SOI in the non-initialised simulation. Initialisation improves the model simulating skill of Niño3.4 and the SOI. We can find a noticeable change of simulated Niño3.4-SOI correlation coefficient while the models were initialised (Fig. 5.9). This shows the change of ocean-atmosphere

interaction between the non-initialised and initialised simulations. Additionally, the initialised simulations decrease the spread of simulated Niño3.4 index and SOI in ensemble members.

In general, the pre-season warm phase of the ENSO (*i.e.* El Niño) leads to a weak EASM producing more rainfall over the South China Sea and north-west China, and less rainfall over the Yangtze River Valley and the south of Japan; the cold phase of the ENSO (La Niña) illustrates a reverse rainfall pattern to El Niño in East Asia. The pre-season Niño3.4 (SOI) exhibits a strong negative (positive) correlation to the EASM, while the correlation between the post-season Niño3.4 (SOI) and the EASM illustrates an anti-phase as the pre-season (Fig. 5.10). In the non-initialised experiments, the models do not capture Niño3.4-/SOI-EASM coupled mode. Only the MIROC5 has the ability to represent the Niño3.4-EASM coupled mode in the initialised simulations. For the SOI-EASM coupled mode, the GFDL-CM2p1 and the MIROC5 capture it with initialisation, while the BCC-CSM1-1, the HadCM3, the HadCM2-ff, the CanCM4 and the MPI-ESM-LR do not.

On seasonal time-scale, the initialised models exhibit a better performance in representing the general circulation of the EASM than that without initialisation. There are two initialisation methods in this study, full-field and anomaly initialisation (Table 5.1). The full-field initialisation produces more skillful predictions on the seasonal time-scale in predicting regional temperature and precipitation (Magnusson *et al.*, 2013; Smith *et al.*, 2013). In this study, the GFDL-CM2p1 and the MIROC5 show positive response to the initialisation, with full-field and anomaly initialisation, respectively. Only the HadCM3 was initialised by the two initialisation techniques. However, there is no major difference between the two initialised cases in simulating the EASM. We argue that the model parametrisation plays a more important role than the initialisation method to predict the EASM.

In the study, the models are initialised by observed atmospheric component (*i.e.* zonal and meridional wind, geopotential height, *etc.*) and the oceanic component (*i.e.* SST; Meehl *et al.* 2014, 2009; Taylor *et al.* 2012). Because of the large heat content of ocean, the ocean oscillation index (*i.e.* Niño3.4) shows seasonal-to-decadal prediction skills in initialised experiments (Choi *et al.*, 2016; Jin *et al.*, 2008; Luo *et al.*, 2008). The models demonstrate a comparable prediction skill in simulating Niño3.4 and the SOI. The Southern Oscillation is the atmospheric response to the ocean oscillation. The changing correlation between the simulated Niño3.4 and the SOI is detectable while the models were initialised with observations. We can conclude that the ocean-atmosphere interaction is also effected by the initialisation.

Wang *et al.* (2015) found that the second EOF mode of ASM is the Indo-western Pacific monsoon-ocean coupled mode, the third is the Indian Ocean dipole (IOD) mode, and the fourth is the trend mode. The Indo-western Pacific monsoon-ocean coupled mode is the

atmosphere-ocean interaction mode (Wang *et al.*, 2013*a*; Xiang *et al.*, 2013), which is supported by positive thermodynamic feedback between the western North Pacific (WNP) anticyclone and the underlying Indo-Pacific sea surface temperature anomaly dipole over the warm pool (Wang *et al.*, 2015). The IOD leads to a noticeable increased precipitation from the South Asian subcontinent to south-eastern China and conspicuously suppressed the precipitation over the WNP (Wang *et al.*, 2015). It affects the Asian monsoon by the meridional asymmetry of the monsoonal easterly shear during the boreal summer, which can particularly strengthen the northern branch of the Rossby wave response to the south-eastern Indian Ocean SST cooling, leading to an intensified monsoon flow as well as an intensified convection (Wang *et al.*, 2015, 2003; Wang and Xie, 1996; Xiang *et al.*, 2011). We noted that the models simulate a reasonable first EOF mode (Fig. 5.5), but show no skill in capturing the other EOF leading modes (Fig. 5.6). We argue that the models cannot well represent the monsoon-ocean interaction, even initialised by observed conditions. The models cannot simulate the third EOF leading mode of the EASM due to the fact that the predictability of the IOD is only on a three-month time-scale (Choudhury *et al.*, 2015). Current initialisation strategy enhances the ENSO signal in the model simulation, but depresses the other climate signals (Fig. 5.8). It might be caused by the difference resolution between atmosphere and ocean (Marotzke *et al.*, 2016). Therefore, reducing the resolution jump between the components of earth system might improve the model prediction skill.

It is worth mentioning that it is an extremely weak monsoon and strong El Niño year in 1998. The CanCM4, the GFDL-CM2p1, the MIROC5 and the MPI-ESM-LR have the ability to simulate the extreme monsoon event, while the BCC-CSM1-1, and the HadCM3 do not capture it even with initialisation. There is potential for the BCC-CSM and the HadCM models to improve the teleconnection between the ENSO and the EASM.

This chapter presents a research level study for seasonal prediction of EASM. There is an application level for global climate prediction system which is the International Research Institute for Climate and Society (IRI) real-time seasonal climate forecast system (http://iri.columbia.edu/our-expertise/climate/forecasts/#Seasonal_Climate_Forecasts). It provides a real-time prediction information. This prediction system employs 4 AGCMs (ECHAM4.5, CCM3.6, COLA and GFDL-AM2p14) which are forced by prescribed SST. The system shows a low skill in predicting climate over East Asia (Barnston *et al.*, 2010). This is a "tier 2" prediction strategy. It is not suitable to predict the EASM due to the incorrect SST-rainfall relationship (Jiang *et al.*, 2013*b*; Wang *et al.*, 2005, 2009). Therefore, monsoon community employs a "tier 1" method to study the prediction of EASM (Jiang *et al.*, 2013*b*; Kim *et al.*, 2012; Wang *et al.*, 2009; Zhou *et al.*, 2009). The method uses AOGCMs which are initialised by observations.

For the "tier 1" prediction system, it is an initial value problem to predict monsoon variability (Palmer *et al.*, 2004). Furthermore, to predict the climate on seasonal time-scale, the prediction performance strongly depends upon the initial conditions (Smith *et al.*, 2007). Therefore, initialisation certainly important for seasonal prediction of EASM. Previous studies are partly initialisation, only initialisation with ocean (Wang *et al.*, 2009; Zhou *et al.*, 2009). This initialisation method shows the improvement in predicting the EASM on seasonal time-scale (Wang *et al.*, 2009; Zhou *et al.*, 2009). A new initialisation strategy (initialisation in both ocean and atmosphere) has been implemented in CMIP5 models (Meehl *et al.*, 2014). The new initialisation method exhibits significant advantage in predicting the ENSO signal (Choi *et al.*, 2016; Meehl *et al.*, 2014; Meehl and Teng, 2012). This study has tested the prediction skill of EASM in CMIP5 models under the new initialisation strategy. There is prominent diversity of CMIP5 models in response the initialisation. The future research will focus on optimise the models to improve their response to the initialisation.

Chapter 6

Summary, Conclusions and Outlook

6.1 Summary and conclusions

This study presents a comprehensive investigation of the dynamical downscaling and seasonal prediction for the EASM. Its final objective is predicting the EASM at fine resolution. The path is set up a one way nest downscaling method to predict the EASM. The prediction systems' output will be selected as the boundary condition for dynamical downscaling over East Asia. This work evaluates the parametrisations of models for dynamical downscaling over East Asia and initial strategies for the seasonal prediction of the EASM. Multi-datasets (*i.e.* re-analyses, RCM simulations, and GCM simulations) have been used in this study. Firstly, the study assesses the spread of eight re-analysis datasets (*i.e.* 20CR, CFSR, ERA-20C, ERA-Interim, JRA-55, MERRA, NCEPI and NCEPII) in representing the EASM due to the re-analysis datasets are employed as the boundary condition for dynamical downscaling and the initial condition for climate prediction (Chapter 2). The re-analysis datasets have been compared to observations, *i.e.* GPCP, IGRA and HadSLP2r. Then, the study investigates five RCMs (*i.e.* COSMO-CLM, HadGEM3-RA, RegCM4, SNU-MM5 and YSU-RSM) to capture the precipitation climatology and monsoon characteristics over East Asia (Chapter 3). The RCMs follow a common evaluation framework (CORDEX-East Asia) to validate their current climate simulation driven by the ERA-Interim re-analysis. In addition, the COSMO-CLM is also used for dynamic downscaling over East Asia, which is driven by MPI-ESM-LR (Chapter 4). Its set up has been tested in Chapter 3. Finally, six prediction systems (*i.e.* BCC-CSM1-1, CanCM4, GFDL-CM2p1, HadCM3, MIROC5 and MPI-ESM-LR) have been applied for investigating the seasonal predictability of the EASM (Chapter 5).

To conclude this study, I return to the original research questions and summarise the main findings:

a.) How large is the spread of the re-analysis datasets in representing the EASM?

Over East Asia, the eight re-analysis datasets show a small spread in representing the year-to-year variation of mean sea level pressure and zonal winds. However, there is significant difference between the eight re-analysis datasets in capturing the year-to-year variation in precipitation and meridional wind, especially over the ocean. One can also find a spatial disparity between the various datasets in representing the precipitation, the low level winds and the mean sea level pressure. For the EASM index, the eight re-analysis datasets show good consistency. In general, all the re-analysis datasets can be selected as the boundary condition for regional climate downscaling and as the initial condition for EASM prediction.

b.) What is the difference between CORDEX-East Asia models in capturing the precipitation climatology?

The CORDEX-East Asia models are able to capture the principal features of the seasonal mean precipitation patterns, the annual cycles and the inter-annual variability in precipitation. However, significant biases in the individual models can be found in specific regions during some seasons. For example, in summer, the RCMs tend to over-estimate the precipitation over the Tibetan Plateau, except the YSU-RSM, which simulates a drier Tibetan Plateau. In dry season, the RCMs have tendency to produce a wetter continent. In the EASM region, the RCMs also show noticeable biases in representing the regional mean precipitation. The SNU-MM5 and the YSU-RSM simulate more summer precipitation, whereas the COSMO-CLM produces less summer precipitation. Regarding the inter-annual variability of summer precipitation in EASM region, the COSMO-CLM, the RegCM4, and the SNU-MM5 exhibit a high correlation coefficient ($>$0.8) and a normalised standard deviation ($\sim$1.0) comparable to the observations. The HadGEM3-RA and the YSU-RSM show a lower simulation skill (low correlation coefficient).

c.) How good are the CORDEX-East Asia models in producing the monsoon characteristics?

Under the current set up, the models generally performs well characterised by their ability in capturing a reasonable monsoon metrics, *i.e.* annual mean precipitation, first and second annual cycle mode, and monsoon precipitation intensity. The HadGEM3-RA shows a better performance than the other four models in producing the monsoon metrics. However, no individual model represents all the monsoon features (*e.g.* mean state, inter-annual variability, metrics *etc.*) significantly better than the other models. The multi-model ensemble mean outperforms an individual model in simulating the monsoon characteristics as it averages out the variability in the individual model realisations (Tebaldi and Knutti, 2007). In general,

the current set up of the CORDEX-East Asia models can be used for further dynamical downscaling of the EASM.

d.) Is the downscaling method improving the model performance in representing the EASM?

Both the global climate model (MPI-ESM-LR) and the regional climate model (COSMO-CLM) generally capture the mean state of climate. In the complex terrain areas (*e.g.* Tibetan Plateau, Indonesia and Malaysia *etc.*), the COSMO-CLM presents a more reliable (smaller BIAS) climate than the MPI-ESM-LR. However, in the core region of the EASM (*i.e.* the Indo-China Peninsula, China, Korea and Japan), the COSMO-CLM produces an inferior precipitation pattern than the MPI-ESM-LR. The large bias in precipitation is always associated with a significant difference of low level general circulation. Regarding the EASM index, both the MPI-ESM-LR and the COSMO-CLM do not simulate its year-to-year variation. The RCM produced EASM-index strongly depends upon the GCM-data which is MPI-ESM-LR. In the case analysed here (Chapter 4), there is no improvement of RCM in simulating the EASM precipitation and also the corresponding general circulation. Because the verification data are smooth, the benefit of the enhanced horizontal resolution might not be seen due to technical reasons.

e.) How are the six prediction systems capturing the EASM under forcing by observations?

Given observed initial conditions, the AOGCMs show the ability to predict the climate on seasonal time-scale. In East Asia, it is difficult to predict the precipitation even with the model initialised by observations. Compared to the precipitation, there is a significant improvement in the prediction of general circulation (*e.g.* zonal winds) when models were initialised with observation data. A general circulation based index has the potential to better predict the EASM.

f.) What is the difference between the six systems in predicting the EASM on seasonal time-scale?

The six prediction systems exhibit different response to the initialisation. Initialisation adds skill in predicting the EASM index in the GFDL-CM2p1 and the MIROC5 model, no significant change can be seen in the CanCM4 and the MPI-ESM-R simulations, while the HadCM3 and the BCC-CSM1-1 lose the prediction skill. The current system that initialises both the atmosphere and the ocean amplifies the ENSO signal. The simulation of the ENSO-EASM linkage determines the model's performance in predicting the EASM. The different performance of the models are caused by the different reproduction of this ENSO-EASM

coupled mode in the model. The GFDL-CM2p1 and the MIROC5 capture this mode, while the other models fail to simulate it. The MPI-ESM-LR fails to predict an accurate EASM which limits its usefulness for dynamical downscaling application.

6.2 Outlook

This study has introduced a framework to predict the EASM on seasonal time-scale at high resolution. It can be developed as an application level of prediction system. To optimise the prediction framework, there are some topics for further study.

Improvement of models: The CORDEX-East Asia RCMs produce acceptable precipitation climatology in East Asia. However, noticeable bias in precipitation occurs in the regions dominated by the EASM. The COSMO-CLM underestimates (overestimates) the summer precipitation in the south-east of China (South China Sea and west Pacific Ocean). An advanced convection scheme might be able to address this issue. The large bias in precipitation is always associated to the large bias in low level general circulation. Furthermore, both the GCM (MPI-ESM-LR) and the RCM (COSMO-CLM) fail to produce the relationship between the EASM index and the monsoon precipitation resulting in a low prediction skill in monsoon precipitation. There is strong need to improve the simulation of low level winds over East Asia.

Improving the skill of individual prediction systems: This study has analysed the predictability of EASM in six prediction systems. Several systems (*i.e.* HadCM3 and BCC-CSM1-1) show a negative response to the current initialised method. Testing a new initialisation strategy has the potential to resolve the negative response problem in the two prediction systems. Additionally, the MPI-ESM-LR shows a higher skill in predicting the climate under a new initialisation (Marotzke *et al.*, 2016). This might improve the prediction skill of EASM in the MPI-ESM-LR system. We can introduce the MPI-ESM-LR with the new initialisation into our prediction framework to replace the previous one. It will be helpful to improve the prediction skill of the framework.

Developing a new monsoon index: The zonal winds over 200 hPa show a higher predictability than the lower level winds (over 850 hPa) and the surface precipitation. However, current monsoon index is based upon the zonal wind over 200 hPa and cannot accurately represent the monsoon precipitation distribution and monsoon structure (Wang *et al.*, 2008*b*). A new monsoon index which can be used to monitor and predict the EASM needs be developed.

References

Adler RF, Huffman GJ, Chang A, Ferraro R, Xie PP, Janowiak J, Rudolf B, Schneider U, Curtis S, Bolvin D, Gruber A, Susskind J, Arkin P, and Nelkin E (2003) The version-2 global precipitation climatology project (GPCP) monthly precipitation analysis (1979-present). *J Hydrometeorol* 4: 1147–1167. doi:10.1175/1525-7541(2003)004⟨1147:tvgpcp⟩2.0.co;2.

Allan R and Ansell T (2006) A new globally complete monthly historical gridded mean sea level pressure dataset (HadSLP2): 1850–2004. *J Climate* 19: 5816–5842. doi:10.1175/jcli3937.1.

Annamalai H, Hamilton K, and Sperber KR (2007) The south asian summer monsoon and its relationship with ENSO in the IPCC AR4 simulations. *J Climate* 20: 1071–1092. doi:10.1175/jcli4035.1.

Arakawa A and Lamb VR (1981) A potential enstrophy and energy conserving scheme for the shallow water equations. *Mon Weather Rev* 109: 18–36. doi:10.1175/1520-0493(1981)109⟨0018:apeaec⟩2.0.co;2.

Arora VK, Scinocca JF, Boer GJ, Christian JR, Denman KL, Flato GM, Kharin VV, Lee WG, and Merryfield WJ (2011) Carbon emission limits required to satisfy future representative concentration pathways of greenhouse gases. *Geophys Res Lett* 38: L05805. doi:10.1029/2010gl046270.

Baldauf M and Schulz J (2004) Prognostic precipitation in the lokal modell (LM) of DWD. *COSMO Newsletter* No. 4: 177–180.

Barnett TP and Schlesinger ME (1987) Detecting changes in global climate induced by greenhouse gases. *J Geophys Res - Atmos* 92: 14772–14780. doi:10.1029/JD092iD12p14772.

Barnston AG, Li SH, Mason SJ, DeWitt DG, Goddard L, and Gong XF (2010) Verification of the first 11 years of IRI's seasonal climate forecasts. *Journal of Applied Meteorology and Climatology* 49: 493–520. doi:10.1175/2009jamc2325.1.

Betts AK, Zhao M, Dirmeyer PA, and Beljaars ACM (2006) Comparison of ERA40 and NCEP/DOE near-surface data sets with other ISLSCP-II data sets. *J Geophys Res* 111: D22S04. doi:10.1029/2006jd007174.

Bonan GB, Oleson KW, Vertenstein M, Levis S, Zeng X, Dai Y, Dickinson RE, and Yang ZL (2002) The land surface climatology of the community land model coupled to the NCAR community climate model. *J Climate* 15: 3123–3149. doi:10.1175/1520-0442(2002)015⟨3123:tlscot⟩2.0.co;2.

Bosilovich MG, Chen J, Robertson FR, and Adler RF (2008) Evaluation of global precipitation in reanalyses. *J Appl Meteor Climatol* 47: 2279–2299. doi:10.1175/2008jamc1921.1.

Bosilovich MG, Robertson FR, and Chen J (2011) Global energy and water budgets in MERRA. *J Climate* 24: 5721–5739. doi:10.1175/2011jcli4175.1.

Bretherton CS, Smith C, and Wallace JM (1992) An intercomparison of methods for finding coupled patterns in climate data. *J Climate* 5: 541–560. doi:10.1175/1520-0442(1992)005⟨0541:aiomff⟩2.0.co;2.

Briegleb BP (1992) Longwave band model for thermal-radiation in climate studies. *J Geophys Res D: Atmos* 97: 11475–11485.

Bromwich DH and Fogt RL (2004) Strong trends in the skill of the ERA-40 and NCEPNCAR reanalyses in the high and midlatitudes of the Southern Hemisphere, 1958-2001. *J Climate* 17: 4603–4619. doi:10.1175/3241.1.

Chang CP (2004) *East Asian monsoon*. World Scientific series on meteorology of East Asia. World Scientific, Hackensack, NJ.

Chang CP, Zhang Y, and Li T (2000*a*) Interannual and interdecadal variations of the East Asian summer monsoon and tropical pacific SSTs. Part I: Roles of the subtropical ridge. *J Climate* 13: 4310–4325. doi:10.1175/1520-0442(2000)013⟨4310:iaivot⟩2.0.co;2.

Chang CP, Zhang Y, and Li T (2000*b*) Interannual and interdecadal variations of the East Asian summer monsoon and tropical pacific SSTs. Part II: Meridional structure of the monsoon. *J Climate* 13: 4326–4340. doi:10.1175/1520-0442(2000)013⟨4326:iaivot⟩2.0.co;2.

Charney JG and Shukla J (1981) *Predictability of monsoons*, In *Monsoon Dynamics*, (edited by Lighthill J and Pearce RP), pp. 99–109. Cambridge Univ. Press, New York.

Chen F and Dudhia J (2001) Coupling an advanced land surfacehydrology model with the Penn StateNCAR MM5 modeling system. Part I: Model implementation and sensitivity. *Mon Weather Rev* 129: 569–585. doi:10.1175/1520-0493(2001)129⟨0569:caalsh⟩2.0.co;2.

Chen G, Iwasaki T, Qin H, and Sha W (2014) Evaluation of the warm-season diurnal variability over East Asia in recent reanalyses JRA-55, ERA-Interim, NCEP CFSR, and NASA MERRA. *J Climate* 27: 5517–5537. doi:10.1175/jcli-d-14-00005.1.

Chen TJG and Chang CP (1980) The structure and vorticity budget of an early summer monsoon trough (Mei-Yu) over southeastern China and Japan. *Mon Weather Rev* 108: 942–953. doi:10.1175/1520-0493(1980)108⟨0942:tsavbo⟩2.0.co;2.

Choi J, Son SW, Ham YG, Lee JY, and Kim HM (2016) Seasonal-to-interannual prediction skills of near-surface air temperature in the CMIP5 decadal hindcast experiments. *J Climate* 29: 1511–1527. doi:10.1175/jcli-d-15-0182.1.

Chou MD (1992) A solar radiation model for use in climate studies. *J Atmos Sci* 49: 762–772. doi:10.1175/1520-0469(1992)049⟨0762:asrmfu⟩2.0.co;2.

Chou MD, Lee KT, Tsay SC, and Fu Q (1999) Parameterization for cloud longwave scattering for use in atmospheric models. *J Climate* 12: 159–169. doi:10.1175/1520-0442-12.1.159.

Choudhury D, Sharma A, Sivakumar B, Sen Gupta A, and Mehrotra R (2015) On the predictability of SSTA indices from CMIP5 decadal experiments. *Environ Res Lett* 10: 074013. doi:10.1088/1748-9326/10/7/074013.

Christensen JH, Krishna Kumar K, Aldrian E, An SI, Cavalcanti IFA, de Castro M, Dong W, Goswami P, Hall A, Kanyanga JK, Kitoh A, Kossin J, Lau NC, Renwick J, Stephenson D, Xie SP, and Zhou T (2013) *Climate Phenomena and their Relevance for Future Regional Climate Change*, In *Climate Change 2013: The Physical Science Basis. Contribution of Working Group I to the Fifth Assessment Report of the Intergovernmental Panel on Climate Change*, (edited by Stocker TF, Qin DH, Plattner GK, Tignor M, Allen SK, Boschung J, Nauels A, Xia Y, Bex V, and Midgley PM), pp. 1229–1231. Cambridge University Press, Cambridge, United Kingdom and New York, NY, USA.

Colman RA, Moise AF, and Hanson LI (2011) Tropical Australian climate and the Australian monsoon as simulated by 23 CMIP3 models. *J Geophys Res* 116: D10116. doi:10.1029/2010jd015149.

Compo GP, Whitaker JS, Sardeshmukh PD, Matsui N, Allan RJ, Yin X, Gleason BE, Vose RS, Rutledge G, Bessemoulin P, Brnnimann S, Brunet M, Crouthamel RI, Grant AN,

Groisman PY, Jones PD, Kruk MC, Kruger AC, Marshall GJ, Maugeri M, Mok HY, Nordli , Ross TF, Trigo RM, Wang XL, Woodruff SD, and Worley SJ (2011) The twentieth century reanalysis project. *Quart J Roy Meteor Soc* 137: 1–28. doi:10.1002/qj.776.

Cusack S, Edwards JM, and Crowther JM (1999) Investigating k distribution methods for parameterizing gaseous absorption in the Hadley Centre climate model. *J Geophys Res D: Atmos* 104: 2051–2057. doi:10.1029/1998jd200063.

Cusack S, Slingo A, Edwards JM, and Wild M (1998) The radiative impact of a simple aerosol climatology on the Hadley Centre atmospheric. *Quart J Roy Meteor Soc* 124: 2517–2526. doi:10.1256/smsqj.55116.

Davies HC and Turner RE (1977) Updating prediction models by dynamical relaxation: an examination of the technique. *Quart J Roy Meteor Soc* 103: 225–245. doi:10.1002/qj.49710343602.

Davies T, Cullen MJP, Malcolm AJ, Mawson MH, Staniforth A, White AA, and Wood N (2005) A new dynamical core for the Met Office's global and regional modelling of the atmosphere. *Quart J Roy Meteor Soc* 131: 1759–1782. doi:10.1256/qj.04.101.

Dee DP, Uppala SM, Simmons AJ, Berrisford P, Poli P, Kobayashi S, Andrae U, Balmaseda MA, Balsamo G, Bauer P, Bechtold P, Beljaars ACM, van de Berg L, Bidlot J, Bormann N, Delsol C, Dragani R, Fuentes M, Geer AJ, Haimberger L, Healy SB, Hersbach H, Hlm EV, Isaksen L, Kllberg P, Köhler M, Matricardi M, McNally AP, Monge-Sanz BM, Morcrette JJ, Park BK, Peubey C, de Rosnay P, Tavolato C, Thpaut JN, and Vitart F (2011) The ERA-Interim reanalysis: configuration and performance of the data assimilation system. *Quart J Roy Meteor Soc* 137: 553–597. doi:10.1002/qj.828.

Delworth TL, Broccoli AJ, Rosati A, Stouffer RJ, Balaji V, Beesley JA, Cooke WF, Dixon KW, Dunne J, Dunne KA, Durachta JW, Findell KL, Ginoux P, Gnanadesikan A, Gordon CT, Griffies SM, Gudgel R, Harrison MJ, Held IM, Hemler RS, Horowitz LW, Klein SA, Knutson TR, Kushner PJ, Langenhorst AR, Lee HC, Lin SJ, Lu J, Malyshev SL, Milly PCD, Ramaswamy V, Russell J, Schwarzkopf MD, Shevliakova E, Sirutis JJ, Spelman MJ, Stern WF, Winton M, Wittenberg AT, Wyman B, Zeng F, and Zhang R (2006) GFDL's CM2 global coupled climate models. Part I: Formulation and simulation characteristics. *J Climate* 19: 643–674. doi:10.1175/jcli3629.1.

Ding R, Ha KJ, and Li J (2009) Interdecadal shift in the relationship between the East Asian summer monsoon and the tropical Indian Ocean. *Climate Dyn* 34: 1059–1071. doi:10.1007/s00382-009-0555-2.

Ding Y (2004) *Seasonal march of the East-Asian summer monsoon.*, In *East Asian Monsoon*, (edited by Chang CP), book section 3-53, p. 560. World Scientific, Singapore. doi: 10.1142/9789812701411_0001.

Ding Y and Chan JCL (2005) The East Asian summer monsoon: an overview. *Meteorol Atmos Phys* 89: 117–142. doi:10.1007/s00703-005-0125-z.

Ding YH (1992) Summer monsoon rainfalls in China. *J Meteorolog Soc Jpn* 70: 373–396.

Ding YH (1994) *Monsoons over China*. Kluwer Academic Publisher, Dordrecht Boston, London.

Drosdowsky W and Zhang H (2003) *Verification of Spatial Fields*, In *Forecast Verification: A Practitioner's Guide in Atmospheric Science*, (edited by Jolliffe LT and Stephenson DB), pp. 128–129. John Wiley & Sons Ltd, England.

Druyan LM, Feng J, Cook KH, Xue Y, Fulakeza M, Hagos SM, Konar A, Moufouma-Okia W, Rowell DP, Vizy EK, and Ibrah SS (2009) The WAMME regional model intercomparison study. *Climate Dyn* 35: 175–192. doi:10.1007/s00382-009-0676-7.

Durre I, Vose RS, and Wuertz DB (2006) Overview of the integrated global radiosonde archive. *J Climate* 19: 53–68. doi:10.1175/jcli3594.1.

Edwards JM and Slingo A (1996) Studies with a flexible new radiation code. I: Choosing a configuration for a large-scale model. *Quart J Roy Meteor Soc* 122: 689–719. doi: 10.1002/qj.49712253107.

Emanuel KA (1991) A scheme for representing cumulus convection in large-scale models. *J Atmos Sci* 48: 2313–2329. doi:10.1175/1520-0469(1991)048⟨2313:asfrcc⟩2.0.co;2.

Emanuel KA and Zivkovic-Rothman M (1999) Development and evaluation of a convection scheme for use in climate models. *J Atmos Sci* 56: 1766–1782. doi: 10.1175/1520-0469(1999)056⟨1766:daeoac⟩2.0.co;2.

Essery R, Pomeroy J, Parviainen J, and Storck P (2003) Sublimation of snow from coniferous forests in a climate model. *J Climate* 16: 1855–1864. doi:10.1175/1520-0442(2003)016⟨1855:sosfcf⟩2.0.co;2.

Feser F, Rockel B, von Storch H, Winterfeldt J, and Zahn M (2011) Regional climate model add value to global model data: A review and selected examples. *Bull Amer Meteor Soc* 92: 1181–1192. doi:10.1175/2011bams3061.1.

Fischer T, Menz C, Su B, and Scholten T (2013) Simulated and projected climate extremes in the Zhujiang river basin, south China, using the regional climate model COSMO-CLM. *Int J Climatol* 33: 2988–3001. doi:10.1002/joc.3643.

Flato G, Marotzke J, Abiodun B, Braconnot P, Chou SC, Collins W, Cox P, Driouech F, Emori S, Eyring V, Forest C, Gleckler P, Guilyardi E, Jakob C, Kattsov V, Reason C, and Rummukainen M (2013) *Ealuation of Climate Models*, In *Climate Change 2013: The Physical Science Basis. Contribution of Working Group I to the Fifth Assessment Report of the Intergovernmental Panel on Climate Change*, (edited by Stocker TF, Qin DH, Plattner GK, Tignor M, Allen SK, Boschung J, Nauels A, Xia Y, Bex V, and Midgley PM), pp. 810–815. Cambridge University Press, Cambridge, United Kingdom and New York, NY, USA.

Fu C, Wang S, Xiong Z, Gutowski WJ, Lee DK, McGregor JL, Sato Y, Kato H, Kim JW, and Suh MS (2005) Regional climate model intercomparison project for Asia. *Bull Amer Meteor Soc* 86: 257–266. doi:10.1175/bams-86-2-257.

Gao X, Shi Y, and Giorgi F (2011) A high resolution simulation of climate change over China. *Science China Earth Sciences* 54: 462–472. doi:10.1007/s11430-010-4035-7.

Gao X, Shi Y, Song R, Giorgi F, Wang Y, and Zhang D (2008) Reduction of future monsoon precipitation over China: comparison between a high resolution RCM simulation and the driving GCM. *Meteorol Atmos Phys* 100: 73–86. doi:10.1007/s00703-008-0296-5.

Gao X, Shi Y, Zhang D, Wu J, Giorgi F, Ji Z, and Wang Y (2012) Uncertainties in monsoon precipitation projections over China: results from two high-resolution RCM simulations. *Clim Res* 52: 213–226. doi:10.3354/cr01084.

Gao X, Xu Y, Zhao Z, Pal JS, and Giorgi F (2006) On the role of resolution and topography in the simulation of East Asia precipitation. *Theor Appl Climatol* 86: 173–185. doi: 10.1007/s00704-005-0214-4.

Gao XJ, Wang ML, and Filippo G (2013) Climate change over China in the 21st century as simulated by BCC_CSM1.1-RegCM4.0. *Atmoshperic and Oceanic Science Letter* 6: 381–386. doi:10.3878/j.issn.1674-2834.13.0029.

Gates WL (1992) AMIP - the atmospheric model intercomparison project. *Bull Amer Meteor Soc* 73: 1962–1970. doi:10.1175/1520-0477(1992)073⟨1962:Atamip⟩2.0.Co;2.

Gbobaniyi E, Sarr A, Sylla MB, Diallo I, Lennard C, Dosio A, Dhidiou A, Kamga A, Klutse NAB, Hewitson B, Nikulin G, and Lamptey B (2014) Climatology, annual cycle and

interannual variability of precipitation and temperature in CORDEX simulations over West Africa. *Int J Climatol* 34: 2241–2257. doi:10.1002/joc.3834.

Giorgi F, Christensen J, Hulme M, von Storch H, Whetton P, Jones R, Mearns L, Fu C, Arritt R, Bates B, Benestad R, Boer G, Buishand A, Castro M, Chen D, Cramer W, Crane R, Crossly J, Dehn M, Dethloff K, Dippner J, Emori S, Francisco R, Fyfe J, Gerstengarbe F, Gutowski W, Gyalistras D, Hanssen-Bauer I, Hantel M, Hassell D, Heimann D, Jack C, Jacobeit J, Kato H, Katz R, Kauker F, Knutson T, Lal M, Landsea C, Laprise R, Leung L, Lynch A, May W, McGregor J, Miller N, Murphy J, Ribalaygua J, Rinke A, Rummukainen M, Semazzi F, Walsh K, Werner P, Widmann M, Wilby R, Wild M, and Xue Y (2001) *Regional Climate Information- Evaluation and Projections*, In *Climate Change 2001: The Scientific bases*, (edited by Houghton J), pp. 583–638. Cambridge University Press.

Giorgi F, Coppola E, Solmon F, Mariotti L, Sylla MB, Bi X, Elguindi N, Diro GT, Nair V, Giuliani G, Turuncoglu UU, Cozzini S, Gttler I, OBrien TA, Tawfik AB, Shalaby A, Zakey AS, Steiner AL, Stordal F, Sloan LC, and Brankovic C (2012) RegCM4: model description and preliminary tests over multiple CORDEX domains. *Clim Res* 52: 7–29. doi:10.3354/cr01018.

Giorgi F and Gutowski WJ (2015) Regional dynamical downscaling and the CORDEX initiative. *Annu Rev Environ Resour* 40: 467–490. doi:10.1146/annurev-environ-102014-021217.

Giorgi F, Jones C, and Asrar GR (2009) Addressing climate information needs at the regional level: the CORDEX framework. *WMO Bulletin* 58: 175–183.

Giorgi F, Marinucci MR, and Bates GT (1993) Development of a second-generation regional climate model (RegCM2). Part I: Boundary-layer and radiative transfer processes. *Mon Weather Rev* 121: 2794–2813. doi:10.1175/1520-0493(1993)121⟨2794:doasgr⟩2.0.co;2.

Giorgi F and Mearns LO (1991) Approaches to the simulation of regional climate change - a review. *Rev Geophys* 29: 191–216. doi:10.1029/90rg02636.

Goddard L, Mason SJ, Zebiak SE, Ropelewski CF, Basher R, and Cane MA (2001) Current approaches to seasonal-to-interannual climate predictions. *International Journal of Climatology* 21: 1111–1152. doi:10.1002/joc.636.

Grant ALM and Brown AR (1999) A similarity hypothesis for shallow-cumulus transports. *Quart J Roy Meteor Soc* 125: 1913–1936. doi:10.1002/qj.49712555802.

Gregory D and Rowntree PR (1990) A mass flux convection scheme with representation of cloud ensemble characteristics and stability-dependent closure. *Mon Weather Rev* 118: 1483–1506. doi:10.1175/1520-0493(1990)118⟨1483:amfcsw⟩2.0.co;2.

Grell G, Dudhia J, and Stauffer D (1994) A description of the fifth-generation Penn State/NCAR mesoscale model (MM5). *NCAR Technical Note NCAR/TN-398+STR* doi: 10.5065/d60z716b.

Guan Z and Yamagata T (2003) The unusual summer of 1994 in East Asia: IOD teleconnections. *Geophys Res Lett* 30: 1544. doi:10.1029/2002gl016831.

Hadley G (1735) Concerning the cause of the general trade-winds: By Geo. Hadley, Esq; F. R. S. *Philos Trans Roy Soc London* 39: 58–62. doi:10.1098/rstl.1735.0014.

Halley E (1686) An historical account of the trade winds, and monsoons, observable in the seas between and near the tropicks, with an attempt to assign the phisical cause of the said winds, by E. Halley. *Philos Trans Roy Soc London* 16: 153–168. doi: 10.1098/rstl.1686.0026.

Hann J (1908) *Handbuch der Klimatologie*, vol. 1. Engelhorn, Stuttgart.

Harris I, Jones PD, Osborn TJ, and Lister DH (2014) Updated high-resolution grids of monthly climatic observations - the CRU TS3.10 dataset. *Int J Climatol* 34: 623–642. doi:10.1002/joc.3711.

Hines KM, Bromwich DH, and Marshall GJ (2000) Artificial surface pressure trends in the NCEPNCAR reanalysis over the Southern Ocean and Antarctica. *J Climate* 13: 3940–3952. doi:10.1175/1520-0442(2000)013⟨3940:asptit⟩2.0.co;2.

Holtslag AAM, De Bruijn EIF, and Pan HL (1990) A high resolution air mass transformation model for short-range weather forecasting. *Mon Weather Rev* 118: 1561–1575. doi: 10.1175/1520-0493(1990)118⟨1561:ahramt⟩2.0.co;2.

Hong SY, Juang HMH, and Zhao Q (1998) Implementation of prognostic cloud scheme for a regional spectral model. *Mon Weather Rev* 126: 2621–2639. doi:10.1175/1520-0493(1998) 126⟨2621:iopcsf⟩2.0.co;2.

Hong SY and Kanamitsu M (2014) Dynamical downscaling: Fundamental issues from an NWP point of view and recommendations. *Asia-Pac J Atmos Sci* 50: 83–104. doi: 10.1007/s13143-014-0029-2.

Hong SY, Noh Y, and Dudhia J (2006) A new vertical diffusion package with an explicit treatment of entrainment processes. *Mon Weather Rev* 134: 2318–2341. doi:10.1175/mwr3199.1.

Hong SY and Pan HL (1998) Convective trigger function for a mass-flux cumulus parameterization scheme. *Mon Weather Rev* 126: 2599–2620. doi:10.1175/1520-0493(1998)126⟨2599:ctffam⟩2.0.co;2.

Hong SY, Park H, Cheong HB, Kim JEE, Koo MS, Jang J, Ham S, Hwang SO, Park BK, Chang EC, and Li H (2013) The global/regional integrated model system (GRIMs). *Asia-Pac J Atmos Sci* 49: 219–243. doi:10.1007/s13143-013-0023-0.

Hourdin F, Musat I, Grandpeix JY, Polcher J, Guichard F, Favot F, Marquet P, Boone A, Lafore JP, Redelsperger JL, Ruti PM, Dell'aquila A, Filiberti MA, Pham M, Doval TL, Traore AK, and Galle H (2010) AMMA-model intercomparison project. *Bull Amer Meteor Soc* 91: 95–104. doi:10.1175/2009bams2791.1.

Huang B, Banzon VF, Freeman E, Lawrimore J, Liu W, Peterson TC, Smith TM, Thorne PW, Woodruff SD, and Zhang HM (2015*a*) Extended reconstructed sea surface temperature version 4 (ERSST.v4). Part I: Upgrades and intercomparisons. *J Climate* 28: 911–930. doi:10.1175/jcli-d-14-00006.1.

Huang B, Polanski S, and Cubasch U (2015*b*) Assessment of precipitation climatology in an ensemble of CORDEX-East Asia regional climate simulations. *Clim Res* 64: 141–158. doi:10.3354/cr01302.

Huang DQ, Zhu J, Zhang YC, and Huang AN (2013) Uncertainties on the simulated summer precipitation over Eastern China from the CMIP5 models. *J Geophys Res D: Atmos* 118: 9035–9047. doi:10.1002/jgrd.50695.

Huffman GJ, Bolvin DT, Nelkin EJ, Wolff DB, Adler RF, Gu G, Hong Y, Bowman KP, and Stocker EF (2007) The TRMM multisatellite precipitation analysis (TMPA): Quasi-global, multiyear, combined-sensor precipitation estimates at fine scales. *J Hydrometeorol* 8: 38–55. doi:10.1175/jhm560.1.

Jacobsen I and Heise E (1982) A new economic method for the computation of the surface temperature in numerical models. *Beitr Phys Atmos* 55: 128–141.

Jiang P, Gautam MR, Zhu JT, and Yu ZB (2013*a*) How well do the GCMs/RCMs capture the multi-scale temporal variability of precipitation in the Southwestern United States? *J Hydrol* 479: 75–85.

Jiang XW, Yang S, Li YQ, Kumar A, Liu XW, Zuo ZY, and Jha B (2013*b*) Seasonal-to-interannual prediction of the asian summer monsoon in the ncep climate forecast system version 2. *Journal of Climate* 26: 3708–3727.

Jiang Z, Yang S, He J, Li J, and Liang J (2008) Interdecadal variations of East Asian summer monsoon northward propagation and influences on summer precipitation over East China. *Meteorol Atmos Phys* 100: 101–119. doi:10.1007/s00703-008-0298-3.

Jin EK, Kinter JL, Wang B, Park CK, Kang IS, Kirtman BP, Kug JS, Kumar A, Luo JJ, Schemm J, Shukla J, and Yamagata T (2008) Current status of ENSO prediction skill in coupled oceanatmosphere models. *Climate Dyn* 31: 647–664. doi:10.1007/s00382-008-0397-3.

Ju J, Qian C, and Cao J (2005) The intraseaonal oscillation of East Asian summer monsoon. *Chinese Journal of Atmospheric Sciences (in Chinese)* 29: 187–194.

Juang HMH, Hong SY, and Kanamitsu M (1997) The NCEP regional spectral model: An update. *Bull Amer Meteor Soc* 78: 2125–2143.

Juang HMH and Kanamitsu M (1994) The NMC nested regional spectral model. *Mon Weather Rev* 122: 3–26.

Kain JS and Fritsch JM (1990) A one-dimensional entraining/detraining plume model and its application in convective parameterization. *J Atmos Sci* 47: 2784–2802. doi:10.1175/1520-0469(1990)047⟨2784:aodepm⟩2.0.co;2.

Kalnay E, Kanamitsu M, Kistler R, Collins W, Deaven D, Gandin L, Iredell M, Saha S, White G, Woollen J, Zhu Y, Leetmaa A, Reynolds R, Chelliah M, Ebisuzaki W, Higgins W, Janowiak J, Mo KC, Ropelewski C, Wang J, Jenne R, and Joseph D (1996) The NCEP/NCAR 40-year reanalysis project. *Bull Amer Meteor Soc* 77: 437–471. doi:10.1175/1520-0477(1996)077⟨0437:tnyrp⟩2.0.co;2.

Kanamitsu M, Ebisuzaki W, Woollen J, Yang SK, Hnilo JJ, Fiorino M, and Potter GL (2002) NCEPDOE AMIP-II reanalysis (R-2). *Bull Amer Meteor Soc* 83: 1631–1643. doi:10.1175/bams-83-11-1631.

Kang IS, Lee JY, and Park CK (2004) Potential predictability of summer mean precipitation in a dynamical seasonal prediction system with systematic error correction. *J Climate* 17: 834–844. doi:10.1175/1520-0442(2004)017⟨0834:pposmp⟩2.0.co;2.

Kang IS and Shukla J (2006) *Dynamic seasonal prediction and predictability of the monsoon*, In *The Asian Monsoon*, (edited by Wang B), pp. 585–612. Springer Science & Business Media, Praxis, New York, NY, USA.

Khromov SP (1957) Die geographische verbreitung der monsune. *Petermanns Geographische Mitteilungen* 101: 234–237.

Kiehl JT, Hack JJ, Bonan GB, Boville BA, Briegleb BP, Williamson DL, and Rasch PJ (1996) Description of the NCAR community climate model (CCM3). *NACR Tech Note NCAR/TN-420+STR* p. 143.

Kim HM, Webster PJ, Curry JA, and Toma VE (2012) Asian summer monsoon prediction in ecmwf system 4 and ncep cfsv2 retrospective seasonal forecasts. *Climate Dynamics* 39: 2975–2991.

Kirtman B, Power S, Adedoyin J, Boer G, Bojariu R, Camilloni I, Doblas-Reyes F, Fiore A, Kimoto M, Meehl G, Prather M, Sarr A, Schör C, van Oldenborgh GJ, Vecchi G, and Wang H (2013) *Near-term Climate Change: Projections and Predictability*, In *Climate Change 2013: The Physical Science Basis. Contribution of Working Group I to the Fifth Assessment Report of the Intergovernmental Panel on Climate Change*, (edited by Stocker TF, Qin DH, Plattner GK, Tignor M, Allen SK, Boschung J, Nauels A, Xia Y, Bex V, and Midgley PM), book section 11, pp. 953–1028. Cambridge University Press, Cambridge, United Kingdom and New York, NY, USA.

Kistler R, Collins W, Saha S, White G, Woollen J, Kalnay E, Chelliah M, Ebisuzaki W, Kanamitsu M, Kousky V, van den Dool H, Jenne R, and Fiorino M (2001) The NCEP-NCAR 50year reanalysis: Monthly means CD-ROM and documentation. *Bull Amer Meteor Soc* 82: 247–267. doi:10.1175/1520-0477(2001)082⟨0247:tnnyrm⟩2.3.co;2.

Kobayashi S, Ota Y, Harada Y, Ebita A, Moriya M, Onoda H, Onogi K, Kamahori H, Kobayashi C, Endo H, Miyaoka K, and Takahashi K (2015) The JRA-55 reanalysis: General specifications and basic characteristics. *Journal of the Meteorological Society of Japan Ser II* 93: 5–48. doi:10.2151/jmsj.2015-001.

Laprise R (2008) Regional climate modelling. *J Comput Phys* 227: 3641–3666.

Lau KM and Wu HT (2001) Principal modes of rainfallSST variability of the asian summer monsoon: A reassessment of the monsoon-ENSO relationship. *J Climate* 14: 2880–2895. doi:10.1175/1520-0442(2001)014⟨2880:pmorsv⟩2.0.co;2.

Lau KM, Yang GJ, and Shen SH (1988) Seasonal and intraseasonal climatology of summer monsoon rainfall over East Asia. *Mon Weather Rev* 116: 18–37. doi: 10.1175/1520-0493(1988)116⟨0018:saicos⟩2.0.co;2.

Leduc M and Laprise R (2009) Regional climate model sensitivity to domain size. *Climate Dyn* 32: 833–854. doi:10.1007/s00382-008-0400-z.

Lee DK, Cha DH, Jin CS, and Choi SJ (2013*a*) A regional climate change simulation over East Asia. *Asia-Pac J Atmos Sci* 49: 655–664. doi:10.1007/s13143-013-0058-2.

Lee DK, Cha DH, and Kang HS (2004) Regional climate simulation of the 1998 summer flood over East Asia. *J Meteorolog Soc Jpn* 82: 1735–1753. doi:10.2151/jmsj.82.1735.

Lee DY, Ahn JB, and Ashok K (2013*b*) Improvement of multimodel ensemble seasonal prediction skills over East Asian summer monsoon region using a climate filter concept. *J Appl Meteor Climatol* 52: 1127–1138. doi:10.1175/jamc-d-12-0123.1.

Lee DY, Tam CY, and Park CK (2008*a*) Effects of multicumulus convective ensemble on East Asian summer monsoon rainfall simulation. *J Geophys Res* 113: D24111. doi: 10.1029/2008jd009847.

Lee E, Chase TN, and Rajagopalan B (2008*b*) Seasonal forecasting of East Asian summer monsoon based on oceanic heat sources. *Int J Climatol* 28: 667–678. doi:10.1002/joc.1551.

Lee JW and Hong SY (2014) Potential for added value to downscaled climate extremes over Korea by increased resolution of a regional climate model. *Theor Appl Climatol* 117: 667–677. doi:10.1007/s00704-013-1034-6.

Lee JW, Hong SY, Chang EC, Suh MS, and Kang HS (2014) Assessment of future climate change over East Asia due to the RCP scenarios downscaled by GRIMs-RMP. *Climate Dyn* 42: 733–747.

Lee JY and Wang B (2014) Future change of global monsoon in the CMIP5. *Climate Dyn* 42: 101–119. doi:10.1007/s00382-012-1564-0.

Lee JY, Wang B, Kang IS, Shukla J, Kumar A, Kug JS, Schemm JKE, Luo JJ, Yamagata T, Fu X, Alves O, Stern B, Rosati T, and Park CK (2010) How are seasonal prediction skills related to models' performance on mean state and annual cycle? *Climate Dyn* 35: 267–283. doi:10.1007/s00382-010-0857-4.

Lin R, Zhou T, and Qian Y (2014) Evaluation of global monsoon precipitation changes based on five reanalysis datasets. *J Climate* 27: 1271–1289. doi:10.1175/jcli-d-13-00215.1.

Lindsay R, Wensnahan M, Schweiger A, and Zhang J (2014) Evaluation of seven different atmospheric reanalysis products in the Arctic. *J Climate* 27: 2588–2606. doi:10.1175/jcli-d-13-00014.1.

Liu YQ, Giorgi F, and Washington WM (1994) Simulation of summer monsoon climate over East-Asia with an NCAR regional climate model. *Mon Weather Rev* 122: 2331–2348. doi:10.1175/1520-0493(1994)122⟨2331:Sosmco⟩2.0.Co;2.

Lock AP, Brown AR, Bush MR, Martin GM, and Smith RNB (2000) A new boundary layer mixing scheme. Part I: Scheme description and single-column model tests. *Mon Weather Rev* 128: 3187–3199. doi:10.1175/1520-0493(2000)128⟨3187:anblms⟩2.0.co;2.

Lorenz EN (1960) Maximum simplification of the dynamic equations. *Tellus* 12: 243–254.

Luo JJ, Masson S, Behera SK, and Yamagata T (2008) Extended ENSO predictions using a fully coupled oceanatmosphere model. *J Climate* 21: 84–93. doi:10.1175/2007jcli1412.1.

Lynn BH, Khain AP, Dudhia J, Rosenfeld D, Pokrovsky A, and Seifert A (2005) Spectral (bin) microphysics coupled with a mesoscale model (MM5). Part I: Model description and first results. *Mon Weather Rev* 133: 44–58. doi:10.1175/mwr-2840.1.

Magnusson L, Alonso-Balmaseda M, Corti S, Molteni F, and Stockdale T (2013) Evaluation of forecast strategies for seasonal and decadal forecasts in presence of systematic model errors. *Climate Dyn* 41: 2393–2409. doi:10.1007/s00382-012-1599-2.

Marotzke J, Müller WA, Vamborg FSE, Becker P, Cubasch U, Feldmann H, Kaspar F, Kottmeier C, Marini C, Polkova I, Prömmel K, Rust HW, Stammer D, Ulbrich U, Kadow C, Köhl A, Kröger J, Kruschke T, Pinto JG, Pohlmann H, Reyers M, Schröder M, Sienz F, Timmreck C, and Ziese M (2016) Miklip - a national research project on decadal climate prediction. *Bull Amer Meteor Soc* doi:10.1175/bams-d-15-00184.1,inpress.

Martin GM, Ringer MA, Pope VD, Jones A, Dearden C, and Hinton TJ (2006) The physical properties of the atmosphere in the new Hadley Centre global environmental model (HadGEM1). Part I: model description and global climatology. *J Climate* 19: 1274–1301. doi:10.1175/jcli3636.1.

Matei D, Pohlmann H, Jungclaus J, Mller W, Haak H, and Marotzke J (2012) Two tales of initializing decadal climate prediction experiments with the ECHAM5/MPI-OM model. *J Climate* 25: 8502–8523. doi:10.1175/jcli-d-11-00633.1.

Meehl G, Covey C, Delworth T, Latif M, McAvaney B, Mitchell J, Stouffer R, and Taylor K (2007) The WCRP CMIP3 multi-model dataset: a new era in climate change research. *Bull Amer Meteor Soc* 88: 1383–1394.

Meehl GA, Goddard L, Boer G, Burgman R, Branstator G, Cassou C, Corti S, Danabasoglu G, Doblas-Reyes F, Hawkins E, Karspeck A, Kimoto M, Kumar A, Matei D, Mignot J, Msadek R, Navarra A, Pohlmann H, Rienecker M, Rosati T, Schneider E, Smith D, Sutton R, Teng H, van Oldenborgh GJ, Vecchi G, and Yeager S (2014) Decadal climate prediction: An update from the trenches. *Bull Amer Meteor Soc* 95: 243–267. doi: 10.1175/bams-d-12-00241.1.

Meehl GA, Goddard L, Murphy J, Stouffer RJ, Boer G, Danabasoglu G, Dixon K, Giorgetta MA, Greene AM, Hawkins E, Hegerl G, Karoly D, Keenlyside N, Kimoto M, Kirtman B, Navarra A, Pulwarty R, Smith D, Stammer D, and Stockdale T (2009) Decadal prediction. *Bull Amer Meteor Soc* 90: 1467–1485. doi:10.1175/2009bams2778.1.

Meehl GA and Teng H (2012) Case studies for initialized decadal hindcasts and predictions for the Pacific region. *Geophys Res Lett* 39: 1544. doi:10.1029/2012gl053423.

Mitchell J, Karoly D, Hegerl G, Zwiers FW, Allen MR, Marengo J, *et al.* (2001) *Detection of Climate Change and Attribution of Causes*, In *Third Assessment Report of the Intergovernmental Panel on Climate Change.*, (edited by Houghton J, Griggs D, Noguer M, van der Linden P, Dai X, Maskell K, and Johnson C), p. 470. Cambridge University Press, New York.

Newman M, Sardeshmukh PD, and Bergman JW (2000) An assessment of the NCEP, NASA, and ECMWF reanalyses over the Tropical West Pacific warm pool. *Bull Amer Meteor Soc* 81: 41–48. doi:10.1175/1520-0477(2000)081⟨0041:aaotnn⟩2.3.co;2.

Nikulin G, Jones C, Giorgi F, Asrar G, Bchner M, Cerezo-Mota R, Christensen OB, Dqu M, Fernandez J, Hnsler A, van Meijgaard E, Samuelsson P, Sylla MB, and Sushama L (2012) Precipitation climatology in an ensemble of CORDEX-Africa regional climate simulations. *J Climate* 25: 6057–6078. doi:10.1175/jcli-d-11-00375.1.

Oh SG, Park JH, Lee SH, and Suh MS (2014) Assessment of the RegCM4 over East Asia and future precipitation change adapted to the RCP scenarios. *J Geophys Res D: Atmos* 119: 2913–2927. doi:10.1002/2013jd020693.

Onogi K, Tslttsui J, Koide H, Sakamoto M, Kobayashi S, Hatsushika H, Matsumoto T, Yamazaki N, Kaalhori H, Takahashi K, Kadokura S, Wada K, Kato K, Oyama R, Ose

T, Mannoji N, and Taira R (2007) The JRA-25 reanalysis. *J Meteorolog Soc Jpn* 85: 369–432.

Paeth H, Hall NMJ, Gaertner MA, Alonso MD, Moumouni S, Polcher J, Ruti PM, Fink AH, Gosset M, Lebel T, Gaye AT, Rowell DP, Moufouma-Okia W, Jacob D, Rockel B, Giorgi F, and Rummukainen M (2011) Progress in regional downscaling of west African precipitation. *Atmos Sci Lett* 12: 75–82. doi:10.1002/asl.306.

Pal JS, Small EE, and Eltahir EAB (2000) Simulation of regional-scale water and energy budgets: Representation of subgrid cloud and precipitation processes within RegCM. *J Geophys Res D: Atmos* 105: 29579–29594. doi:10.1029/2000jd900415.

Palmer TN, Alessandri A, Andersen U, Cantelaube P, Davey M, Delecluse P, Deque M, Diez E, Doblas-Reyes FJ, Feddersen H, Graham R, Gualdi S, Gueremy JF, Hagedorn R, Hoshen M, Keenlyside N, Latif M, Lazar A, Maisonnave E, Marletto V, Morse AP, Orfila B, Rogel P, Terres JM, and Thomson MC (2004) Development of a european multimodel ensemble system for seasonal-to-interannual prediction (demeter). *Bulletin of the American Meteorological Society* 85: 853–+.

Peterson TC and Vose RS (1997) An overview of the global historical climatology network temperature database. *Bull Amer Meteor Soc* 78: 2837–2849. doi:10.1175/1520-0477(1997)078⟨2837:Aootgh⟩2.0.Co;2.

Qian Y and Leung LR (2007) A long-term regional simulation and observations of the hydroclimate in China. *J Geophys Res* 112: D14104. doi:10.1029/2006jd008134.

Ramage C (1971) *Monsoon Meteorology*, vol. 15 of *International Geophysics Series*. CA: Academic Press, San Diego.

Rayner NA (2003) Global analyses of sea surface temperature, sea ice, and night marine air temperature since the late nineteenth century. *J Geophys Res* 108: 4407. doi:10.1029/2002jd002670.

Redelsperger JL, Thorncroft CD, Diedhiou A, Lebel T, Parker DJ, and Polcher J (2006) African monsoon multidisciplinary analysis - an international research project and field campaign. *Bull Amer Meteor Soc* 87: 1739–1746.

Reisner J, Rasmussen RM, and Bruintjes RT (1998) Explicit forecasting of supercooled liquid water in winter storms using the MM5 mesoscale model. *Quart J Roy Meteor Soc* 124: 1071–1107. doi:10.1002/qj.49712454804.

Rienecker MM, Suarez MJ, Gelaro R, Todling R, Bacmeister J, Liu E, Bosilovich MG, Schubert SD, Takacs L, Kim GK, Bloom S, Chen J, Collins D, Conaty A, da Silva A, Gu W, Joiner J, Koster RD, Lucchesi R, Molod A, Owens T, Pawson S, Pegion P, Redder CR, Reichle R, Robertson FR, Ruddick AG, Sienkiewicz M, and Woollen J (2011) MERRA: NASA's modern-era retrospective analysis for research and applications. *J Climate* 24: 3624–3648. doi:10.1175/jcli-d-11-00015.1.

Ritter B and Geleyn JF (1992) A comprehensive radiation scheme for numerical weather prediction models with potential applications in climate simulations. *Mon Weather Rev* 120: 303–325. doi:10.1175/1520-0493(1992)120⟨0303:acrsfn⟩2.0.co;2.

Rockel B, Will A, and Hense A (2008) The regional climate model COSMO-CLM (CCLM). *Meteorol Z* 17: 347–348. doi:10.1127/0941-2948/2008/0309.

Rummukainen M (2010) State-of-the-art with regional climate models. *Wiley Interdiscip Rev Clim Change* 1: 82–96. doi:10.1002/wcc.8.

Rummukainen M (2016) Added value in regional climate modeling. *Wiley Interdisciplinary Reviews-Climate Change* 7: 145–159. doi:10.1002/wcc.378.

Ruti PM, Williams JE, Hourdin F, Guichard F, Boone A, Van Velthoven P, Favot F, Musat I, Rummukainen M, Domnguez M, Gaertner M, Lafore JP, Losada T, Rodriguez de Fonseca MB, Polcher J, Giorgi F, Xue Y, Bouarar I, Law K, Josse B, Barret B, Yang X, Mari C, and Traore AK (2011) The West African climate system: a review of the AMMA model inter-comparison initiatives. *Atmos Sci Lett* 12: 116–122. doi:10.1002/asl.305.

Saha S, Moorthi S, Pan HL, Wu X, Wang J, Nadiga S, Tripp P, Kistler R, Woollen J, Behringer D, Liu H, Stokes D, Grumbine R, Gayno G, Wang J, Hou YT, Chuang HY, Juang HMH, Sela J, Iredell M, Treadon R, Kleist D, Van Delst P, Keyser D, Derber J, Ek M, Meng J, Wei H, Yang R, Lord S, Van Den Dool H, Kumar A, Wang W, Long C, Chelliah M, Xue Y, Huang B, Schemm JK, Ebisuzaki W, Lin R, Xie P, Chen M, Zhou S, Higgins W, Zou CZ, Liu Q, Chen Y, Han Y, Cucurull L, Reynolds RW, Rutledge G, and Goldberg M (2010) The NCEP climate forecast system reanalysis. *Bull Amer Meteor Soc* 91: 1015–1057. doi:10.1175/2010bams3001.1.

Saha S, Nadiga S, Thiaw C, Wang J, Wang W, Zhang Q, Van den Dool HM, Pan HL, Moorthi S, Behringer D, Stokes D, Peña M, Lord S, White G, Ebisuzaki W, Peng P, and Xie P (2006) The NCEP climate forecast system. *J Climate* 19: 3483–3517. doi:10.1175/jcli3812.1.

Schär C, Leuenberger D, Fuhrer O, Luthi D, and Girard C (2002) A new terrain-following vertical coordinate formulation for atmospheric prediction models. *Mon Weather Rev* 130: 2459–2480.

Schneider U, Becker A, Finger P, Meyer-Christoffer A, Ziese M, and Rudolf B (2014) GPCC's new land surface precipitation climatology based on quality-controlled in situ data and its role in quantifying the global water cycle. *Theor Appl Climatol* 115: 15–40. doi:10.1007/s00704-013-0860-x.

Shukla J (1998) Predictability in the midst of chaos: A scientific basis for climate forecasting. *Science* 282: 728–31.

Shukla J, Anderson J, Baumhefner D, Brankovic C, Chang Y, Kalnay E, Marx L, Palmer T, Paolino D, Ploshay J, Schubert S, Straus D, Suarez M, and Tribbia J (2000) Dynamical seasonal prediction. *Bulletin of the American Meteorological Society* 81: 2593–2606. doi:10.1175/1520-0477(2000)081⟨2593:Dsp⟩2.3.Co;2.

Simmons AJ, Willett KM, Jones PD, Thorne PW, and Dee DP (2010) Low-frequency variations in surface atmospheric humidity, temperature, and precipitation: Inferences from reanalyses and monthly gridded observational data sets. *J Geophys Res* 115: D01110. doi:10.1029/2009jd012442.

Smith DM, Cusack S, Colman AW, Folland CK, Harris GR, and Murphy JM (2007) Improved surface temperature prediction for the coming decade from a global climate model. *Science* 317: 796–9. doi:10.1126/science.1139540.

Smith DM, Eade R, and Pohlmann H (2013) A comparison of full-field and anomaly initialization for seasonal to decadal climate prediction. *Climate Dyn* 41: 3325–3338. doi:10.1007/s00382-013-1683-2.

Smith RK, Ulrich W, and Dietachmayer G (1990) A numerical study of tropical cyclone motion using a barotropic model. I: the role of vortex asymmetries. *Quart J Roy Meteor Soc* 116: 337–362. doi:10.1002/qj.49711649206.

Sohn SJ, Min YM, Lee JY, Tam CY, Kang IS, Wang B, Ahn JB, and Yamagata T (2012) Assessment of the long-lead probabilistic prediction for the Asian summer monsoon precipitation (1983-2011) based on the APCC multimodel system and a statistical model. *J Geophys Res D: Atmos* 117: D04102. doi:10.1029/2011jd016308.

Song F and Zhou T (2014) The climatology and interannual variability of East Asian summer monsoon in CMIP5 coupled models: Does air–sea coupling improve the simulations? *J Climate* 27: 8761–8777. doi:10.1175/jcli-d-14-00396.1.

Sperber KR, Annamalai H, Kang IS, Kitoh A, Moise A, Turner A, Wang B, and Zhou T (2013) The Asian summer monsoon: an intercomparison of CMIP5 vs. CMIP3 simulations of the late 20th century. *Climate Dyn* 41: 2711–2744. doi:10.1007/s00382-012-1607-6.

Sperber KR, Brankovic C, Deque M, Frederiksen CS, Graham R, Kitoh A, Kobayashi C, Palmer T, Puri K, Tennant W, and Volodin E (2001) Dynamical seasonal predictability of the asian summer monsoon. *Monthly Weather Review* 129: 2226–2248. doi:10.1175/1520-0493(2001)129⟨2226:Dspota⟩2.0.Co;2.

Staniforth A (1997) Regional modeling: A theoretical discussion. *Meteorol Atmos Phys* 63: 15–29. doi:10.1007/bf01025361.

Steiner AL, Pal JS, Rauscher SA, Bell JL, Diffenbaugh NS, Boone A, Sloan LC, and Giorgi F (2009) Land surface coupling in regional climate simulations of the West African monsoon. *Climate Dyn* 33: 869–892. doi:10.1007/s00382-009-0543-6.

Stephens GL, Li J, Wild M, Clayson CA, Loeb N, Kato S, L'Ecuyer T, Stackhouse PW, Lebsock M, and Andrews T (2012) An update on earth's energy balance in light of the latest global observations. *Nat Geosci* 5: 691–696. doi:10.1038/ngeo1580.

Stickler A, Brnnimann S, Valente MA, Bethke J, Sterin A, Jourdain S, Roucaute E, Vasquez MV, Reyes DA, Allan R, and Dee D (2014) ERA-CLIM: Historical surface and upper-air data for future reanalyses. *Bull Amer Meteor Soc* 95: 1419–1430. doi:10.1175/bams-d-13-00147.1.

Sylla MB, Giorgi F, Ruti PM, Calmanti S, and Dell'Aquila A (2011) The impact of deep convection on the West African summer monsoon climate: a regional climate model sensitivity study. *Quart J Roy Meteor Soc* 137: 1417–1430. doi:10.1002/qj.853.

Tao SY and Chen LX (1987) *A review of recent research on the East Asian summer monsoon in China*, In *Monsoon Meterology*, (edited by Chang CP and Krishnamurti TN), pp. 60–92. Oxford University Press, Oxford.

Tatebe H, Ishii M, Mochizuki T, Chikamoto Y, Sakamoto TT, Komuro Y, Mori M, Yasunaka S, Watanabe M, Ogochi K, Suzuki T, Nishimura T, and Kimoto M (2012) The initialization of the MIROC climate models with hydrographic data assimilation for decadal prediction. *J Meteorolog Soc Jpn* 90A: 275–294. doi:10.2151/jmsj.2012-A14.

Taylor KE (2001) Summarizing multiple aspects of model performance in a single diagram. *J Geophys Res D: Atmos* 106: 7183–7192. doi:10.1029/2000jd900719.

Taylor KE, Stouffer RJ, and Meehl GA (2012) An overview of CMIP5 and the experiment design. *Bull Amer Meteor Soc* 93: 485–498. doi:10.1175/bams-d-11-00094.1.

Tebaldi C and Knutti R (2007) The use of the multi-model ensemble in probabilistic climate projections. *Philosophical Transactions of the Royal Society a-Mathematical Physical and Engineering Sciences* 365: 2053–2075. doi:10.1098/rsta.2007.2076.

Tiedtke M (1989) A comprehensive mass flux scheme for cumulus parameterization in large-scale models. *Mon Weather Rev* 117: 1779–1800. doi:10.1175/1520-0493(1989)117⟨1779:acmfsf⟩2.0.co;2.

Trenberth KE, Fasullo JT, and Mackaro J (2011) Atmospheric moisture transports from ocean to land and global energy flows in reanalyses. *J Climate* 24: 4907–4924. doi:10.1175/2011jcli4171.1.

Trenberth KE and Guillemot CJ (1998) Evaluation of the atmospheric moisture and hydrological cycle in the NCEP/NCAR reanalyses. *Climate Dyn* 14: 213–231. doi:10.1007/s003820050219.

Trenberth KE, Stepaniak DP, and Caron JM (2000) The global monsoon as seen through the divergent atmospheric circulation. *J Climate* 13: 3969–3993. doi:10.1175/1520-0442(2000)013⟨3969:tgmast⟩2.0.co;2.

Turner AG and Annamalai H (2012) Climate change and the South Asian summer monsoon. *Nature Climate Change* 2: 587–595. doi:10.1038/nclimate1495.

Uppala SM, Kallberg PW, Simmons AJ, Andrae U, Bechtold VDC, Fiorino M, Gibson JK, Haseler J, Hernandez A, Kelly GA, Li X, Onogi K, Saarinen S, Sokka N, Allan RP, Andersson E, Arpe K, Balmaseda MA, Beljaars ACM, Berg LVD, Bidlot J, Bormann N, Caires S, Chevallier F, Dethof A, Dragosavac M, Fisher M, Fuentes M, Hagemann S, Hlm E, Hoskins BJ, Isaksen L, Janssen PAEM, Jenne R, McNally AP, Mahfouf JF, Morcrette JJ, Rayner NA, Saunders RW, Simon P, Sterl A, Trenberth KE, Untch A, Vasiljevic D, Viterbo P, and Woollen J (2005) The ERA-40 re-analysis. *Quart J Roy Meteor Soc* 131: 2961–3012. doi:10.1256/qj.04.176.

von Storch H, Langenberg H, and Feser F (2000) A spectral nudging technique for dynamical downscaling purposes. *Mon Weather Rev* 128: 3664–3673.

Wang A and Zeng X (2012) Evaluation of multireanalysis products with in situ observations over the Tibetan Plateau. *J Geophys Res D: Atmos* 117: D05102. doi: 10.1029/2011jd016553.

Wang B (2006) *The Asian Monsoon*. Springer Science & Business Media, Praxis, New York, NY, USA.

Wang B, Bao Q, Hoskins B, Wu G, and Liu Y (2008*a*) Tibetan Plateau warming and precipitation changes in East Asia. *Geophys Res Lett* 35: L14702. doi:10.1029/2008gl034330.

Wang B and Ding Q (2008) Global monsoon: Dominant mode of annual variation in the tropics. *Dyn Atmos Oceans* 44: 165–183. doi:10.1016/j.dynatmoce.2007.05.002.

Wang B, Ding Q, and Liu J (2012) *Concept of Global Monsoon*, In *The Global Monsoon System*, pp. 3–14. World Scientific, 2nd edn. doi:10.1142/9789814343411_0001.

Wang B, Ding QH, Fu XH, Kang IS, Jin K, Shukla J, and Doblas-Reyes F (2005) Fundamental challenge in simulation and prediction of summer monsoon rainfall. *Geophys Res Lett* 32: L15711. doi:10.1029/2005gl022734.

Wang B and Fan Z (1999) Choice of South Asian summer monsoon indices. *Bull Amer Meteor Soc* 80: 629–638. doi:10.1175/1520-0477(1999)080⟨0629:cosasm⟩2.0.co;2.

Wang B, Kang IS, and Lee JY (2004*a*) Ensemble simulations of AsianAustralian monsoon variability by 11 AGCMs. *J Climate* 17: 803–818. doi:10.1175/1520-0442(2004)017⟨0803: esoamv⟩2.0.co;2.

Wang B, Kim HJ, Kikuchi K, and Kitoh A (2011) Diagnostic metrics for evaluation of annual and diurnal cycles. *Climate Dyn* 37: 941–955. doi:10.1007/s00382-010-0877-0.

Wang B, Lee JY, Kang IS, Shukla J, Kug JS, Kumar A, Schemm J, Luo JJ, Yamagata T, and Park CK (2007) How accurately do coupled climate models predict the leading modes of Asian-Australian monsoon interannual variability? *Climate Dyn* 30: 605–619. doi:10.1007/s00382-007-0310-5.

Wang B, Lee JY, Kang IS, Shukla J, Park CK, Kumar A, Schemm J, Cocke S, Kug JS, Luo JJ, Zhou T, Wang B, Fu X, Yun WT, Alves O, Jin EK, Kinter J, Kirtman B, Krishnamurti T, Lau NC, Lau W, Liu P, Pegion P, Rosati T, Schubert S, Stern W, Suarez M, and Yamagata T (2009) Advance and prospectus of seasonal prediction: assessment of the APCC/CliPAS 14-model ensemble retrospective seasonal prediction (1980–2004). *Climate Dyn* 33: 93–117. doi:10.1007/s00382-008-0460-0.

Wang B, Lee JY, and Xiang BQ (2015) Asian summer monsoon rainfall predictability: a predictable mode analysis. *Climate Dyn* 44: 61–74. doi:10.1007/s00382-014-2218-1.

Wang B, Wu R, and Lau KM (2001) Interannual variability of the Asian summer monsoon: Contrasts between the indian and the Western North PacificEast Asian monsoons. *J Climate* 14: 4073–4090. doi:10.1175/1520-0442(2001)014⟨4073:ivotas⟩2.0.co;2.

Wang B, Wu R, and Li T (2003) Atmospherewarm ocean interaction and its impacts on AsianAustralian monsoon variation. *J Climate* 16: 1195–1211. doi:10.1175/1520-0442(2003)16⟨1195:aoiaii⟩2.0.co;2.

Wang B, Wu RG, and Fu XH (2000) Pacific-East Asian teleconnection: how does ENSO affect East Asian climate? *J Climate* 13: 1517–1536.

Wang B, Wu Z, Li J, Liu J, Chang CP, Ding Y, and Wu G (2008*b*) How to measure the strength of the East Asian summer monsoon. *J Climate* 21: 4449–4463. doi:10.1175/2008jcli2183.1.

Wang B, Xiang B, and Lee JY (2013*a*) Subtropical high predictability establishes a promising way for monsoon and tropical storm predictions. *Proc Natl Acad Sci USA* 110: 2718–22. doi:10.1073/pnas.1214626110.

Wang B and Xie X (1996) Low-frequency equatorial waves in vertically sheared zonal flow. Part I: Stable waves. *J Atmos Sci* 53: 449–467. doi:10.1175/1520-0469(1996)053⟨0449:lfewiv⟩2.0.co;2.

Wang D, Menz C, Simon T, Simmer C, and Ohlwein C (2013*b*) Regional dynamical downscaling with CCLM over East Asia. *Meteorol Atmos Phys* 121: 39–53. doi:10.1007/s00703-013-0250-z.

Wang Y, Leung LR, McGregor JL, Lee DK, Wang WC, Ding Y, and Kimura F (2004*b*) Regional climate modeling: Progress, challenges, and prospects. *J Meteorolog Soc Jpn* 82: 1599–1628. doi:10.2151/jmsj.82.1599.

Wilson DR and Ballard SP (1999) A microphysically based precipitation scheme for the UK meteorological office unified model. *Quart J Roy Meteor Soc* 125: 1607–1636.

Wu J, Gao XJ, Shi Y, and Filippo G (2011) Climate change simulation over Xinjiang region in 21st century by a high resolution RCM (in Chinese). *Journal of Glaciology and Geocrylogy (in Chinese)* 33: 479–487.

Wu R, Hu ZZ, and Kirtman BP (2003) Evolution of ENSO-related rainfall anomalies in East Asia. *J Climate* 16: 3742–3758. doi:10.1175/1520-0442(2003)016⟨3742:eoerai⟩2.0.co;2.

Wu T, Song L, Li W, Wang Z, Zhang H, Xin X, Zhang Y, Zhang L, Li J, Wu F, Liu Y, Zhang F, Shi X, Chu M, Zhang J, Fang Y, Wang F, Lu Y, Liu X, Wei M, Liu Q, Zhou W, Dong M, Zhao Q, Ji J, Li L, and Zhou M (2014) An overview of BCC climate system model development and application for climate change studies. *Acta Meteorologica Sinica* 28: 34–56. doi:10.1007/s13351-014-3041-7.

Wu Z, Wang B, Li J, and Jin FF (2009) An empirical seasonal prediction model of the East Asian summer monsoon using ENSO and NAO. *J Geophys Res* 114: D18120. doi:10.1029/2009jd011733.

Xiang B, Wang B, Yu W, and Xu S (2013) How can anomalous western North Pacific subtropical high intensify in late summer? *Geophys Res Lett* 40: 2349–2354. doi:10.1002/grl.50431.

Xiang B, Yu W, Li T, and Wang B (2011) The critical role of the boreal summer mean state in the development of the IOD. *Geophys Res Lett* 38: L02710. doi:10.1029/2010gl045851.

Xue Y, De Sales F, Lau WKM, Boone A, Feng J, Dirmeyer P, Guo Z, Kim KM, Kitoh A, Kumar V, Poccard-Leclercq I, Mahowald N, Moufouma-Okia W, Pegion P, Rowell DP, Schemm J, Schubert SD, Sealy A, Thiaw WM, Vintzileos A, Williams SF, and Wu MLC (2010) Intercomparison and analyses of the climatology of the west african monsoon in the West African monsoon modeling and evaluation project (WAMME) first model intercomparison experiment. *Climate Dyn* 35: 3–27. doi:10.1007/s00382-010-0778-2.

Yang S, Zhang ZQ, Kousky VE, Higgins RW, Yoo SH, Liang JY, and Fan Y (2008) Simulations and seasonal prediction of the asian summer monsoon in the ncep climate forecast system. *Journal of Climate* 21: 3755–3775. doi:10.1175/2008JCLI1961.1.

Yatagai A, Arakawa O, Kamiguchi K, Kawamoto H, Nodzu MI, and Hamada A (2009) A 44-year daily gridded precipitation dataset for Asia based on a dense network of rain gauges. *Sola* 5: 137–140. doi:10.2151/sola.2009-035.

Yi Y, Kimball JS, Jones LA, Reichle RH, and McDonald KC (2011) Evaluation of MERRA land surface estimates in preparation for the soil moisture active passive mission. *J Climate* 24: 3797–3816. doi:10.1175/2011jcli4034.1.

Yim SY, Wang B, and Xing W (2014) Prediction of early summer rainfall over south china by a physical-empirical model. *Climate Dynamics* 43: 1883–1891. doi:10.1007/s00382-013-2014-3.

Yu ET, Wang HJ, and Sun JQ (2010) A quick report on a dynamical downscaling simulation over China using the nested model. *Atmoshperic and Oceanic Science Letter* 3: 325–329.

Yun KS, Seo KH, and Ha KJ (2010) Interdecadal change in the relationship between ENSO and the intraseasonal oscillation in East Asia. *J Climate* 23: 3599–3612. doi:10.1175/2010jcli3431.1.

Zhang QY, Tao SY, and Cheng LT (2003) The inter-annual variability of east asian summer monsoon indices and its association with the pattern of general circulation over East Asia. *Acta Meteorologica Sinica* 61: 559–568.

Zhou T, Wu B, and Wang B (2009) How well do atmospheric general circulation models capture the leading modes of the interannual variability of the Asian–Australian monsoon? *J Climate* 22: 1159–1173. doi:10.1175/2008jcli2245.1.

Zhou TJ and Yu RC (2005) Atmospheric water vapor transport associated with typical anomalous summer rainfall patterns in China. *J Geophys Res* 110: D08104. doi:10.1029/2004jd005413.

Appendix A

Abbreviations

20CR	Twentieth Century Reanalysis
3D-Var	Three-Dimensional Variational data assimilation
4D-Var	Four-Dimensional Variational data assimilation
ACC	Anomaly Correlation Coefficient
AMSU-A	Advanced Microwave sounding Unit-A
AOGCMs	Coupled atmosphere-ocean general circulation models
APHRODITE	Asian Precipitation-Highly-Resolved Observational Data Integration Towards Evaluation of the Water Resources
BC	Boundary Condition
BOM	Bureau of Meteorology
CFSR	Climate Forecast System Re-analysis
CGCMs	Coupled General Circulation Models
CIRES	Cooperative Institute for Research Environmental Sciences
CMIP3	Coupled Model Inter-comparison Project phase 3
CMIP5	Coupled Model Inter-comparison Project phase 5
CORDEX	Coordinated Regional Climate Downscaling Experiment
CRU	Climatic Research Unit
DOE	Department of Energy
EASM	East Asian summer monsoon
EASMI	EASM index
ECMWF	European Centre for Medium Range Weather Forecasts
ENSO	El Niño-Southern Oscillation
EOF	Empirical orthogonal function
ERA-20C	ECMWFs first atmospheric re-analysis of the 20th century
ERA-40	ECMWF 45-year Reanalysis
ERA-Interim	ECMWF Interim Re-analysis
ERS	European Remote Sensing Satellite
ESA	European Space Agency

ESD	Ensemble Standard Deviation
ESMs	Earth System Models
ESRL	Earth System Research Laboratory
EUMETSAT	European Organisation for the Exploitation of Meteorological Satellites
GEOS	Goddard Earth Observing System
GMAO	Global Modeling and Assimilation Office
GPCC	Global Precipitation Climatology Centre
GPCP	Global Precipitation Climatology Project
HadISST	Hadley Centre Sea Ice and SST dataset
HadSLPr2r	extending Hadley Centres monthly historical mean sea level pressure dataset
ICOADS	International Comprehensive Ocean-Atmosphere Data Set
IFS	Integrated Forecasting System
IGRA	Integrated Global Radiosonde Archive
IOD	Indian Ocean Dipole
IPCC	Intergovernmental Panel on Climate Change
ISPD	International Surface Pressure Databank
ITCZ	Inter Tropical Convergence Zone
JMA	Japan Meteorological Agency
JRA-25	Japanese 25-year Reanalysis
JRA-55	Japanese 55-year Re-analysis
MERRA	Modern Era Retrospective-Analysis for Research and Applications
MPI	Max-Planck-Institut
MPI-ESM	Earth system model of MPI
MSU	Microwave Sounding Unit
NASA	National Aeronautics and Space Administration's Goddard Laboratory for Atmospheres
NCAR	National Center for Atmospheric Research
NCEP	National Centers for Environmental Predictions
NOAA	National Oceanic and Atmospheric Administration
NSD	Normalised Standard Dviations
PBL	Planetary Boundary Layer
PCC	Pattern Correlation Coefficient
PSD	Physical Sciences Division
RCMs	Regional Climate Models
RMSE	Root-Mean-Square-Error
SBUV	Solar Backscattered UltraViolet
SODA	Simple Ocean Data Assimilation
SSM/I	Special Sensing Microwave/Imager
SST	Sea Surface Temperature
SVD	Singular Value Decomposition
TIROS	Television Infrared Observation Satellite
TOVS	TIROS Operational Vertical Sounder
TRMM	Tropical Rainfall Measuring Mission

Appendix B

Methods

B.1 BIAS

BIAS, also called mean error, represents the mean value of deviations between comparison and verification values. BIAS is defined as follows:

$$BIAS = \left(\sum_{i=1}^{n} w_i D_i \right) / \sum_{i=1}^{n} w_i \qquad (B.1a)$$

$$D_i = F_i - A_i \qquad (B.1b)$$

$$w_i = \frac{1}{n} \, (or \; cos\emptyset_i, \; and \; so \; on) \qquad (B.1c)$$

where F_i, A_i, D_i represent comparison, verifying value, and the deviation between comparison and verifying value, respectively. Also, w_i indicates weighting coefficient, n is the number of samples, and $\emptyset_i$ is latitude. In general, observational values, initial values, or objective analyses are often used as the verifying values. When the comparison data is perfectly correct, called *perfect dataset*, BIAS is equal to zero.

In calculating the average in a wide region, *e.g.*, the Northern/Southern hemisphere, the average should be evaluated with the wighting coefficients, taking into account the differences of areas due to the latitudes. In this thesis, the equal weighting coefficient was employed due to the research is focusing on a regional scale. The other indices in Appendix B will be dealt with in the same manner.

B.2 Root Mean Square Error

Root-mean-square error (RMSE) is often used for indicating the accuracy of comparison, and its definition is:

$$RMSE = \sqrt{\sum_{i=1}^{n} w_i D_i^2} / \sqrt{\sum_{i=1}^{n} w_i} \tag{B.2}$$

where D_i represents the deviation between comparison and verifying value in Eq. (B.1b), w_i represents the weighting coefficient in Eq. (B.1c), and n is the number of samples. If RMSE is closer to zero, it means that the comparisons are closer to the verifying values.

B.3 Anomaly Correlation Coefficient

Anomaly Correlation Coefficient (ACC) is one of the most widely used measures in climate sciences, and is the correlation between anomalies of forecasts and those of verifying values with the reference values, such as climatological values (Drosdowsky and Zhang, 2003). ACC is defined by:

$$ACC = \frac{\sum_{i=1}^{n} w_i \left(f_i - \bar{f}\right)\left(a_i - \bar{a}\right)}{\sqrt{\sum_{i=1}^{n} w_i \left(f_i - \bar{f}\right)^2 \sum_{i=1}^{n} w_i \left(a_i - \bar{a}\right)^2}}, \ (-1 \leqslant ACC \leqslant 1) \tag{B.3a}$$

$$f_i = F_i - C_i, \ \bar{f} = \left(\sum_{i=1}^{n} w_i f_i\right) / \sum_{i=1}^{n} w_i \tag{B.3b}$$

$$a_i = A_i - C_i, \ \bar{a} = \left(\sum_{i=1}^{n} w_i a_i\right) / \sum_{i=1}^{n} w_i \tag{B.3c}$$

where n is the number of samples, and F_i, A_i, C_i represent comparison, verifying value, and reference value such as climatological value, respectively. Also, $\bar{f}$ is the mean of f_i, $\bar{a}$ is the mean of a_i, and w_i indicates the weighting coefficient in Eq. (B.1c). If the variation of anomalies of comparison dataset is perfectly coincident with that of the anomalies of verifying value, ACC will take 1 (the maximum value). Otherwise, if the variation is completely reversed, ACC is -1 (the minimum value).

B.4 Pattern Correlation Coefficient

The Pattern Correlation Coefficient (PCC) is used for pattern correlation studies. It is the Pearson product-moment coefficient of linear correlation between two variables that are respectively the values of the same variables at corresponding locations on two different patterns (Barnett and Schlesinger, 1987). There are two types of PCC, centred correlation and un-centred correlation, respectively. The centred (un-centred) statistic measures the similarity of two patterns after (without) removal of the global mean (Mitchell *et al.*, 2001). The centred PCC is defined by:

$$PCC_{centred} = \frac{\sum_{x=1}^{n}\sum_{y=1}^{m} w_{(x,y)}\left(F_{(x,y)}-\bar{f}\right)\left(A_{(x,y)}-\bar{a}\right)}{\sqrt{\sum_{x=1}^{n}\sum_{y=1}^{m} w_{(x,y)}\left(F_{(x,y)}-\bar{F}\right)^2 \sum_{x=1}^{n}\sum_{y=1}^{m} w_{(x,y)}\left(A_{(x,y)}-\bar{A}\right)^2}} \tag{B.4a}$$

$$\bar{F} = \left(\sum_{x=1}^{n}\sum_{y=1}^{m} w_{(x,y)}F_{(x,y)}\right) / \sum_{x=1}^{n}\sum_{y=1}^{m} w_{(x,y)} \tag{B.4b}$$

$$\bar{A} = \left(\sum_{x=1}^{n}\sum_{y=1}^{m} w_{(x,y)}A_{(x,y)}\right) / \sum_{x=1}^{n}\sum_{y=1}^{m} w_{(x,y)} \tag{B.4c}$$

and the un-centred PCC is defined as following:

$$PCC_{un-centred} = \frac{\sum_{x=1}^{n}\sum_{y=1}^{m} w_{(x,y)}F_{(x,y)}A_{(x,y)}}{\sqrt{\sum_{x=1}^{n}\sum_{y=1}^{m} w_{(x,y)}F_{(x,y)}^2 \sum_{x=1}^{n}\sum_{y=1}^{m} w_{(x,y)}A_{(x,y)}^2}} \tag{B.5}$$

where n and m are grids on longitude and latitude, respectively. $F_{(x,y)}$ and $A_{(x,y)}$ represent two dimensions comparison and validating value. Also, $\bar{F}$ is the mean of $F_{(x,y)}$, $\bar{A}$ is the mean of $A_{(x,y)}$, and $w_{(x,y)}$ indicates the weighting coefficient in Eq. (B.1c).

Acknowledgements

I would like to acknowledge all people who supported the creation of this thesis. In the first place, I would like to express my special appreciation and thanks my supervisor Prof. Dr. Ulrich Cubasch for his scientific advises and guidance, for his time, his interest and the continuous support throughout the last years. He gave me the opportunity to work on this thesis in the inspiring working environment of the Institute of Meteorology. Besides my supervisor, I gratefully acknowledge Dr. Stefan Polanski for fruitful discussions and the patience to answer all my technical and scientific questions. I would also like to express my gratitude to Dr. Bijan Fallah, Dr. Emmanuele Russo, Dr. Xu Zhou and Christopher Kadow for their help advises and comments, particularly on writing scientific texts.

I very much enjoyed being part of the Institute of Meteorology and the climate modelling group (AG Klimod) that always provided a friendly and inspiring working atmosphere. Thanks to all my Klimod-colleagues.

I would like to thank the dataset provider listed in Table 2.1, 3.1, 3.2, 5.2 of this thesis for producing and making their model output available. I am grateful to Dr. Delei Li from Helmholtz-Zentrum Geesthacht (HZG) for helping me to run the simulation in Chapter 4. I acknowledge the MiKlip project funded by the Federal Ministry of Education and Research and the German Climate Computing Centre (DKRZ) for providing the data services. Financial support for this thesis was provided by the China Scholarship Council (CSC) and the Center for International Cooperation, Freie Universität Berlin.

A special thanks to my family. Words cannot express how grateful I am to my girlfriend, my mother and my sister for supporting me spiritually throughout my life in general. I would also like to thank all of my friends who supported me in writing, and urged me to strive towards my goal.

Bo Huang
April 2017, Berlin